

SINGLE PARTICLE OPTICAL SIZING

Aggregation of polystyrene by salt and polymer



Promotor: dr. G. J. Fleeer, hoogleraar in de Fysische en Kolloïdchemie
Co-promotor: dr. M. A. Cohen Stuart, universitair hoofddocent

STELLINGEN

- I -

De conclusie van Heughebaert en medewerkers dat de vorming van octacalciumfosfaat uit oververzadigde oplossing verloopt volgens een polynucleair groeiemechanisme wordt niet door de experimentele resultaten gerechtvaardigd.

Heughebaert, J.C., Rooij de, J.F., and Nancollas, G.H., J. Crystal Growth, 76, 192 (1986).

- II -

Ten onrechte houden Flynn en medewerkers bij de meting van de coherente overdracht van magnetisatie door isotrope menging geen rekening met het Overhauser effect.

Flynn, P.F., Kintanar, A., Reid, B.R., and Drobny, G., Biochemistry, 27, 1191 (1988).

- III -

Bij de terughoudendheid die vele FT-NMR spectroscopisten tonen ten aanzien van nieuwe analysemethoden zoals Maximum Entropy Minimalisation en Linear Prediction vergeten zij dat ook de (Fast) Fourier Transformation benaderingen gebruikt.

Tang, J., Lin, C.P., Bowman, M.K., and Norris, J.R., J. Magn. Res. 62, 167 (1985).

NI, F., Scheraga, H.A., J. Magn. Res. 70, 506 (1986).

- IV -

Het is geen contradictie, dat pakkingen van bolvormige silicadeeltjes met gelijke volume fractie toch een verschil in permeabiliteit kunnen vertonen.

Danforth, S., and Velazquez, H., Mat. Res. Soc. Symp. Proc. 24, 239 (1984).

- V -

De toestand van geadsorbeerd eiwit is willekeurig.

Dijt, J., Ingenieursverslag Landbouwniversiteit Wageningen (1988).

- VI -

Door co-operatieve ordeningseffecten in het geconcentreerde regiem wordt het toepassingsgebied van de Mean-Field theorie voor polymeeradsorptie vooral voor sterke polymeren beperkt.

Fleer, G.J., Scheutjens, J.M.H.M., and Cohen Stuart, M.A., Conference Polymers in Colloidal Systems, Eindhoven (1987). Colloids and Surfaces, in press.

- VII -

Uit het vlokmodel gepresenteerd in dit proefschrift en uit het onderzoek van Cohen Stuart en Tawal kan geconcludeerd worden dat polymeren met een hoge adsorptie-energie effectievere vlokmiddelen zijn dan zwak adsorberende polymeren.

Cohen Stuart, M.A., and Tawal, H., Macromolecules, accepted.

Dit proefschrift

- VIII -

Persoonen met enig vermogen tot dramatische expressie zijn niet de onwaardigste.

voorjaar 1988, Parijs.

Proefschrift Eduard Pelssers

SINGLE PARTICLE OPTICAL SIZING

aggregation of polystyrene latices by salt and polymer

Wageningen, 6 mei 1988

PN000001, 1272

E. G. M. Pelssers

SINGLE PARTICLE OPTICAL SIZING

Aggregation of polystyrene latices by salt and polymer

Proefschrift

ter verkrijging van de graad van
doctor in de landbouwwetenschappen,
op gezag van de rector magnificus,
dr. C. C. Oosterlee,
in het openbaar te verdedigen
op vrijdag 6 mei 1988
des namiddags te twee uur in de aula
van de Landbouwniversiteit te Wageningen

**BIBLIOTHEEK
LANDBOUWUNIVERSITEIT
WAGENINGEN**

Omslagontwerp en fotografie: Gerrit Buurman

Aan mijn ouders

CONTENTS

CHAPTER 1. INTRODUCTION	1
1.1. Aggregation of colloidal dispersions	1
1.2. Static and Dynamic aspects	2
1.3. Measurement of aggregation	4
1.4. Aim and outline of this study	4
References	7
 Chapter 2. Methods for measuring aggregation and particle size	9
2.1. Introduction	9
2.2. Classical methods	9
2.2.1. Global methods	9
2.2.2. Turbidity	10
2.3. Multi particle detection	11
2.3.1. Static light scattering	11
2.3.3. Laser diffraction spectroscopy	11
2.3.3. Laser beat spectroscopy	13
2.3.4. Light scattering frequency analysis	13
2.4. Single particle detection	14
2.4.1. Microscopy	14
2.4.2. Coulter counter	14
2.4.3. Flow cytometry	15
2.4.4. Single Particle Optical Sizing (SPOS)	16
2.5. Performance of the various techniques	18
References	20
 CHAPTER 3. SINGLE PARTICLE LIGHT SCATTERING THEORY	25
3.1. Introduction	25
3.2. The Rayleigh and the Rayleigh-Gans-Debye theory	25
3.3. The Mie theory	27
3.4. Scattering by various spherical particles	27
3.4.1. Introduction	28
3.4.2. Polystyrene latex particles	28
3.4.3. Silica particles	30
3.4.4. Haematite particles	33

4.8.2. Fluorescent particles	79
4.8.3. Size distribution of fluorescent particles	79
4.8.4. Discussion	81
4.9. Conclusions	81
References	83

CHAPTER 5. PREPARATION OF POLYSTYRENE LATICES AND 87

THEIR COAGULATION BY SALT

5.1. Introduction	87
5.2. Synthesis	89
5.2.1. Introduction	89
5.2.2. Polymerization	89
5.2.3. Purification	90
5.2.4. Characterization	91
5.3. Coagulation	92
5.3.1. Introduction	92
5.3.2. Overview of literature data	92
5.3.3. Experimental	94
5.3.4. Results	96
5.3.5. Discussion	101
5.4. Concluding remarks	102
References	104

CHAPTER 6. EQUILIBRIUM AND NON-EQUILIBRIUM FLOCCULATION BY POLYMER 107

6.1. Introduction	107
6.2. Bridging flocculation	109
6.2.1. Dynamic aspects of flocculation	109
6.2.2. Equilibrium aspects of flocculation	111
6.3. Adsorbed amounts	111
6.3.1. Materials	112
6.3.2. Adsorption isotherms	113
6.4. Flocculation of a latex by polymer	116
6.4.1. Methods of mixing	116
6.4.2. Results	117
6.4.2.1. Influence of mixing methods	117
6.4.2.2. Flocculation as a function of the polymer dose	119

6.4.2.3. Flocculation as a function of the initial particle concentration	125
6.4.2.4. Flocculation as a function of time	131
6.4.2.5. Particle size distribution during flocculation	134
6.5. A new model for polymer flocculation	135
6.6. Estimation of the reconfiguration time	138
6.7. Concluding remarks	147
References	143
APPENDIX A	145
SUMMARY	151
SAMENVATTING	153
LEVENSLIOP	155
DANKWOORD	157

CHAPTER 1. INTRODUCTION

1.1 Aggregation of colloidal dispersions

There is considerable interest, both practical and fundamental, in the effect of salt and polymer on the stability of dispersions. Let us first introduce some terms encountered in stabilization and destabilization. The process of particles sticking together due to the compression of the double layer by salt is called **coagulation**. We will use the term **flocculation** for the destabilization of dispersions by (small amounts of) polymer. The most widely accepted mechanism in this case is bridging of different particles by stretches of polymer. Sometimes some salt is needed to induce flocculation by polymers. This action of salt is often referred to as **sensitization**. When excess polymer is added, the polymer may have a stabilizing effect. This phenomenon, whereby the particles are protected against salt-induced aggregation by extended layers of polymer, is commonly denoted as **protection** or **steric stabilization**.

Coagulation, flocculation, sensitization and protection of dispersions are interrelated phenomena that are widely applied in a variety of industrial processes, both in aqueous and in non-aqueous media. For example, flocculation and coagulation play an important role in water treatment, paper making, mineral processing and sludge dewatering [1]. Protection, for example, is essential in paint production, magnetic tapes and food technology.

In these practical applications, often a complex mixture of salt and different types of polymer is used. Due to this complexity, usually the mechanisms of these processes are only poorly understood. Consequently, in most cases trial and error methods are applied to find the best operating conditions. A fundamental knowledge about the mechanism could contribute to optimize these processes, could stimulate the design of new and more effective polymers, and could help to develop new (mixing) methods for flocculation or stabilization of dispersions. To gain such fundamental knowledge, experiments with well-defined colloidal model systems and relatively simple homopolymers, preferably homodisperse, are necessary.

A polymer molecule can be considered as a string of repeating units, which in solution form a coil that assumes a more or less globular shape (random coil). When such a coil comes into contact with a particle surface, the structure is changed. Immediately after attachment, the polymer is still in an extended

conformation, but the ensuing reconformation process leads ultimately to an equilibrium conformation with loops and tails protruding into solution. These processes are schematically illustrated in Fig. 1.

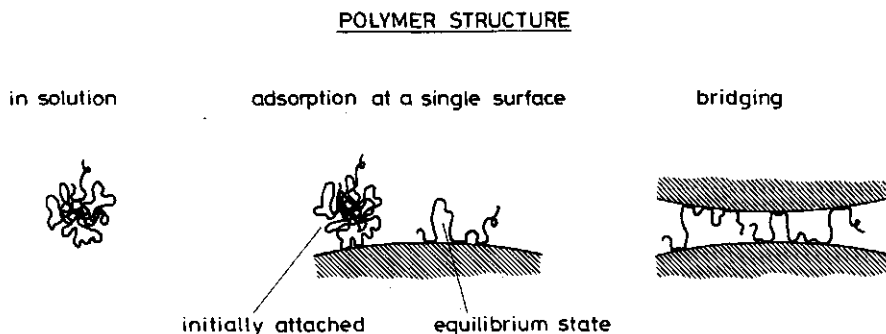


Figure 1. Polymer structure in solution and at interfaces.

When a polymer molecule adsorbs simultaneously onto two particles, a bridge between the particles is created. If the number of such polymer bonds is high enough **bridging flocculation** may take place, see fig. 1. Although in practice this is probably the most widely occurring mechanism for destabilization [2], other mechanisms are possible [3].

As already illustrated in Fig. 1, both equilibrium ("static") and kinetic ("dynamic") aspects play an important role in bridging flocculation. We discuss these aspects in more detail in the following section, both for salt-induced coagulation and for flocculation by polymer.

1.2 Static and dynamic aspects

The most comprehensive theory for the electrostatic interactions between particles in equilibrium is due to Deryaguin and Landau [4], Verwey and Overbeek [5], commonly referred to as the DLVO-theory. This theory combines the concepts of Van der Waals attraction and double layer repulsion between colloidal particles into a framework which allows a quantitative description of many stability phenomena. Although some experimental facts [6,8] cannot be explained with the theory, the general agreement between theory and experiments is rather good [9].

For the stability in the presence of polymer that is in equilibrium with the particles, a fairly comprehensive theoretical model has been recently proposed by Scheutjens and Fleer (SF) [10]. With this theory, the free energy as a function of the separation between two flat surfaces can be calculated for various molecular weights and adsorbed amounts. Also the fraction of polymer in bridges, loops, tails and trains (two dimensional sequences in direct contact with the surface) can be computed. The model distinguishes between **full equilibrium** (where the polymer can desorb and diffuse away during particle approach) and **restricted equilibrium** (where the amount of polymer is constant because there is no time for the polymer to leave the gap between the particles). The main features of the theory, especially for the conditions of restricted equilibrium, have been corroborated by experimental observations, such as direct force measurements between mica surfaces in polymer solutions [11]. Hence, also for stability in the presence of polymers, a first understanding of the equilibrium aspects is now emerging.

In the above theories dynamic aspects of particle-particle encounters and polymer reformation during aggregation are not considered. The DLVO-theory assumes a completely relaxed double layer during particle encounters. For the case of Brownian motion of the particles this seems not unreasonable [12]. Recently a first attempt to incorporate the double layer relaxation in the DLVO-model has been described [13].

The SF-theory assumes that the polymer between the plates is in local equilibrium within the gap between the plates. A theory accounting for non-equilibrium conformation is still far away. Also experimentally, only little information is available about the relaxation of polymers during adsorption. Preliminary data on the reformation of polymer after the initial attachment have been reported [14].

These dynamic aspects of polymer conformations must be reflected in the mechanism of bridging flocculation. Gregory [15] introduced two limiting cases, which he denoted as **equilibrium flocculation** and **non-equilibrium flocculation**. In equilibrium flocculation the adsorbed polymers are completely relaxed before the particles collide, whereas during non-equilibrium flocculation bridging is due to non-relaxed, extended polymer molecules. While equilibrium flocculation could perhaps be interpreted on the basis of interactions predicted by the Scheutjens Fleer theory, for non-equilibrium flocculation no suitable theory exists.

As discussed above the DLVO and the SF theory predict the free energy of

interaction between the particles and can describe under what conditions a dispersion is stable or unstable. They do not give information about the kinetics of the particle collision process and the evolution of the aggregation in time. Such a kinetic theory is available in the Von Smoluchowski-Fuchs theory [16,17] or newer variations thereof [18].

As we will show in this study, equilibrium flocculation can be adequately described with the Von Smoluchowski-Fuchs theory, whereas non-equilibrium flocculation obeys quite different kinetics.

1.3 Measurement of aggregation

Until very recently, the available techniques for the study of aggregation gave only global information. The signals detected by these techniques give some indication for the overall degree of aggregation, but provide no unambiguous information about the size and distribution of the various aggregates. Examples of these techniques are turbidity, light scattering and sedimentation. From turbidity or light scattering measurements the initial rate of the total process can be obtained, but one has to make assumptions about the scattering of aggregates.

With sedimentation, the major criterion for quantitative analysis is that the Stokes law should apply; however it is doubtful whether this is always the case. Moreover, the Stokes radius of aggregates is not very well defined.

Recently, sophisticated equipment has become available in which very quickly the number and size of various aggregates can be monitored. We denote this technique as Single Particle Optical Sizing (SPOS).

In this technique, the particles pass one-by-one through a tiny, illuminated volume and the small flash of light that each of them emits, is recorded. Since the intensity of a flash can be related to the size of the corresponding particle, a particle size distribution is obtained directly. Several authors have described equipment based on this principle [19-28]. However, the reliability and particle size resolution are critically dependent on the apparatus design. Therefore we decided to construct our own instrument, thereby introducing several alterations that increase the accuracy and reliability of the SPOS-technique.

1.4 Aim and outline of this study

The central purpose of this study is to improve our fundamental understanding of the colloidal aggregation process, in particular polymer induced flocculation, by means of new experimental techniques. We describe in this thesis some major improvements of the SPOS technique which lead to an instrument with a considerably better performance. One is a special optical arrangement which gives an elliptically shaped detection volume. The other is a refined hydrodynamic focusing which helps to project the particles accurately through the detection volume.

With the help of this new apparatus it proved possible to study the aggregation process and its kinetics in great detail, giving some surprising new results.

In chapter 2 we discuss the available methods for studying aggregation. We distinguish between classical methods (such as turbidity and sedimentation), multi particle methods (for example laser beat spectroscopy and laser diffraction spectroscopy, and single particle methods (Coulter counter, electron microscopy and SPOS). Our analysis shows that the SPOS technique has many advantages: it is fast and reliable and the information obtained about e.g., aggregation is very detailed.

The small light flash which is the basic event in the SPOS technique is usually a pulse of scattered light. In chapter 3 we therefore present the basic light scattering theory, focusing on numerical results obtained with the Mie theory. We applied this theory to various colloidal model systems, such as latex, silica and haematite. From these results we are able to estimate the particle size range for which the SPOS should work, and to choose proper operating conditions. In particular, we show that the detection angle should be chosen small in order to obtain unambiguous information on particle size and particle size distribution.

In chapter 4 the design of the SPOS is described. The instrument consists of an optical, a flow and an electronic system, and we discuss the main features of each of these. The novel feature of the optical system is the elliptical focus. We explain the optical set-up needed for this focus, and its advantages over other arrangements. The central part of our flow system is the efficient hydrodynamic focus. We discuss the construction of the flow cell and we pay much attention to the shear and extension forces which particles undergo during passage through the cell. We present arguments which show that the hydrodynamic forces are small as compared to the binding strength between particles in aggregates so that break-up of aggregates may be neglected for

most purposes. We also show that orthokinetic (shear induced) aggregation is of minor importance in the instrument.

Experimental tests show that our instrument is a powerful tool to study aggregation. We find that the instrument can distinguish (and count) aggregates up to heptaplets, independent of the degree of aggregation. This is a great advantage since it means that our SPOS can be used not only in the initial stages of aggregation but can follow the process much longer.

In chapter 5 we investigate the coagulation of polystyrene latex by salt (KNO_3). We obtain the aggregate size distribution as a function of time, and, from this, we determine not only the rate constant of the overall process, but also the separate rate constants of the first few coagulation steps. This enables us to check the primary assumption of the Von Smoluchowski theory which states that all these rate constants are the same.

In chapter 6 we use the SPOS method to study the aggregation induced by polymer. We obtain results showing, at first sight, puzzling dependencies on initial particle concentration and polymer molecular weight, indicating that the aggregation process is rather complicated and often does not follow Von Smoluchowski-kinetics. However, by taking dynamical aspects of polymer attachment and reformation into account, we were able to analyse the data quite consistently. We show that it is necessary to distinguish between flocculation due to relaxed polymers (equilibrium flocculation) and that due to non-relaxed polymers (non-equilibrium flocculation).

Under some conditions, both mechanisms occur simultaneously. We therefore propose a new model for polymer induced flocculation which incorporates these two mechanisms and show that it can satisfactorily account for nearly all the data obtained in this study. The new model is visualized and summarized in two illustrative schemes (Fig. 18 and 19 of Chapter 6).

References

1. Kuz'kin, S.K., and Nebera, V.P., Synthetic Flocculants in De-watering Processes, Moscow (1963) (Trans. Nat. Lending Library, Boston, G.B., 1966).
2. Kitchener, J.A., Br. Polym. J. 4, 217 (1972).
3. Napper, D.H., Polymeric Stabilization of Colloidal Dispersions, p. 17, Academic Press, New York (1983).
4. Deryaguin, B.V., Trans. Faraday Soc. 36, 203, 730 (1940).
Deryaguin, B.V., and Landau, L.D., Acta Physicochim. 14, 633 (1941).
5. Verwey, E.J., and Overbeek, J.Th.G., Theory of the stability Lyophobic Colloids, Elsevier, Amsterdam (1984).
6. Penners, N.H.G., and Koopal, L.K., Colloids and Surfaces 28, 67 (1987).
7. Reerink, H., and Overbeek, J.Th.G., Discuss. Faraday Soc. 18, 74 (1954).
8. Ottewill, R.H., and Shaw, J.N., Discuss. Faraday Soc. 42, 154 (1966).
9. Overbeek, J.Th.G., J. Colloid Interfaces Sci. 58, 408 (1977).
10. Scheutjens, J.M.H.M., and Fleer, G.J., Macromolecules 18, 1882 (1985).
11. Klein, J., and Luckham, P.F., Nature (London) 308, 836 (1984).
12. Lyklema, J., Pure and Appl. Chem, 52, 1221 (1980).
13. Dukhin, S.S., and Lyklema, J., Langmuir 3, 94 (1987).
14. Cohen Stuart, M.A., and Tamai, H., accepted Macromolecules.
15. Gregory, J., and Sheiham, I., Br. Polym. J. 6, 47 (1974).
16. Von Smoluchowski, M., Phys. Z. 17, 557, 585 (1916).
Von Smoluchowski, M., Z. Phys. Chem. 92, 129 (1917).
17. Fuchs, N., Z. Phys., 89, 736 (1934).
18. Ziff, R.M., in "Kinetics of Aggregation and Gelation" (F. Family and D.P. Landau, Ed), p.191, North Holland, Amsterdam (1984).
19. Bowen, M.S., Broide, M.L., and Cohen, R.J., J. Colloid Interface Sci. 105, 605 (1985).
20. Cummins, P.G., Smith, A.L., Staples, E.J., and Thompson, L.G., in "Solid Liquid Separation" (J. Gregory, Ed), p. 161, Ellis Horwood Ltd, Chichester, 1984.
21. Buske, N., Gedan, H., Lichtenfeld, H., Katz, W., and Sonntag, H., Colloid Polym. Sci. 258, 1303 (1980).
22. Walsh, D.J., Anderson, J., Parker, A., and Dix, M.J., Colloid Polym. Sci. 259, 1003 (1981).

23. Beyer, M.S., J. Colloid Interface Sci. 118, 137 (1987).
24. Mc.Padyen, P., and Smith, A.L., J. Colloid Interface Sci. 45, 573 (1973).
25. Davidson, J.A., Collins, E.A., and Haller, S., J. Polym. Sci. Part C. 35, 235 (1971).
26. Rehn, B., in "Particle size analysis 1981"(N.G. Stanley, Ed), p. 415, Wiley Heyden LTD (1982).
27. Umhauer, H., Chem.-Ing.-Tech. 52, 55 (1980).
28. Bartholdi, M., Salzman, G.L., Hiebert, R.D., and Kerker, M., Appl. Optics. 19, 1573 (1980).

CHAPTER 2. METHODS FOR MEASURING AGGREGATION AND PARTICLE SIZE

2.1. Introduction

Several techniques are available for studying aggregation in colloidal dispersions. Some of these give only global information, others give detailed information on particle or floc size distribution. In this chapter a review is given of these techniques, with their own specific features. By comparison one can decide which technique satisfies the experimental criteria the best. The discussion is limited to methods designed for liquid dispersions.

When investigating unstable systems one usually compares measurements before and after some arbitrarily chosen time. However, a few kinetic studies have also been reported [1-13], i.e., where measurements are made continuously as a function of time. It is our opinion that rate constants provide the best fundamental basis for comparing the effects of various additives and additive concentrations.

We choose to divide the methods in three categories namely: classical methods, multi-particle scattering and single particle detection. In the classical techniques a global property of the dispersion is measured, which is some measure of aggregation. In the multi-particle scattering techniques, an average particle size can be measured and some information about the particle size distribution can be obtained. Single particle detection methods yield detailed information about the particle size distribution, even if this distribution consists of discrete fractions. In the next chapters, a detailed discussion will be given of the Single Particle Optical Sizer (SPOS), a technique which yields rapidly and reliably complete particle size distributions. In the study of salt- or polymer induced aggregation this technique yields, at present, more information than any other technique.

2.2. Classical methods

2.2.1. Global methods

Under some conditions, a flocculating system will gradually subside, leaving a clear boundary line above the flocs. The rate of change of the boundary height with time is an empirical measure of the flocculation kinetics [14-17]. Stable

dispersions tend to sediment into close packed cakes of small volume, aggregating systems settle with large sediment volumes. Measurement of the sediment volume after some fixed time can be used to compare degrees of aggregation [18]. Some caution is needed [12]: in many cases the final sediment volume is determined by the floc packing characteristics rather than by the rate of aggregation in the dispersion. Both settling rate and sediment volume can be followed by eye or with a laser sedimentometer [19].

Various forms of gravitational (for large particles) and centrifugal (for small particles) sedimentometers have been described [20]. The major criterion for quantitative analysis is that the Stokes law should apply; however for most aggregating systems, it is doubtful whether this is the case. A Joyce-Loebl disk centrifuge is sometimes used to analyse the size distribution of a mixture of stable colloid particles [21].

Rheological properties depend strongly on the state of aggregation [22]. Attempts have been made to relate rheological parameters to the degree of dispersion [23], but the results are highly specific to the particular systems.

Although not widely used, electrical conductivity and dielectric constant measurements can yield information on the state of dispersion [24-26].

For large flocs, simple sieving techniques using fine mesh sieves can be used. An alternative is the method of La Mer [27,28] who used the flocs themselves as filter bed. The filtrate is then re-passed through this filter bed. In general, the larger the degree of flocculation, the shorter the refiltration time. Several attempts were made to quantify this effect [27-30] but these attempts were also criticized [31-33].

2.2.2. Turbidity

A widely used procedure is to monitor the turbidity of a flocculating system as a function of time. One of the problems is that the turbidity may not increase monotonously with the degree of aggregation and this makes the interpretation difficult [22]. By monitoring the turbidity in the initial stages of aggregation one can obtain a rate constant for the aggregation process [3,11-13]. The stopped flow technique is often used for this approach [3,13,14,34]. Turbidity measurements are only possible in a limited range of particle concentrations, depending on the size and refractive index of the particles.

A rather new technique is based on the fluctuations occurring in the turbidity signal. The number of particles in the detection volume is not constant in time but fluctuates due to Brownian motion. As a result, the turbidity intensity fluctuates around the average value. When a dispersion starts aggregating, the average number of particles decreases. The frequency of the fluctuations will thereby decrease, while the relative amplitude increases. Gregory and Eisenlauer [35,36] both developed a instrument to measure these fluctuations in a rather simple way. The technique is especially sensitive to the onset of aggregation. The physical background is discussed by Gregory [35].

2.3. Multi-particle detection

2.3.1. Static light scattering

From the total intensity scattered by a dispersion, an average particle size can be determined provided the Rayleigh-Gans-Debye approximation is valid (see section 3.2). For example, the upper limit for polystyrene latex particles in water is about 25 nm radius and for silica particles in cyclohexane this is about 500 nm. The lower limit is approximately 1 to 10 nm, depending on concentration and refractive index of the particles.

Walstra [37] applied small angle light scattering to emulsions, and measured the scattered intensity as a function of wavelength at 1.5° detection angle. These data were successfully fitted on calculated Mie scattering profiles as function of particle size and with a presupposed Gaussian particle size distribution (e.g. a log-normal distribution). An average radius and a standard deviation could be obtained. This technique has been called fat droplet size analysis or spectroturbidimetry. The latter term is somewhat misleading because not turbidity but small angle light scattering is measured. The size range that can be dealt with is 0.2 to 15 μm diameter for paraffin oil in water.

Lips and Willis [38] used small angle light scattering to determine the initial rate of coagulation of coagulating latex dispersions.

2.3.2. Laser diffraction spectroscopy

In this technique, the particles move across a spatially filtered and expanded

low power laser beam (figure 1). All particles will scatter the incident light but big particles contribute more to the scattering at small angles. Originally this technique was designed for rather large particles, in this case the diffraction theory of light can be applied to analyse the angular distributed scattering intensity. The scattered light is imaged by a optical lens on an array of radially placed detectors. The focusing action of the lens makes the scattering pattern on the detectors independent of the position and velocity of the particles.

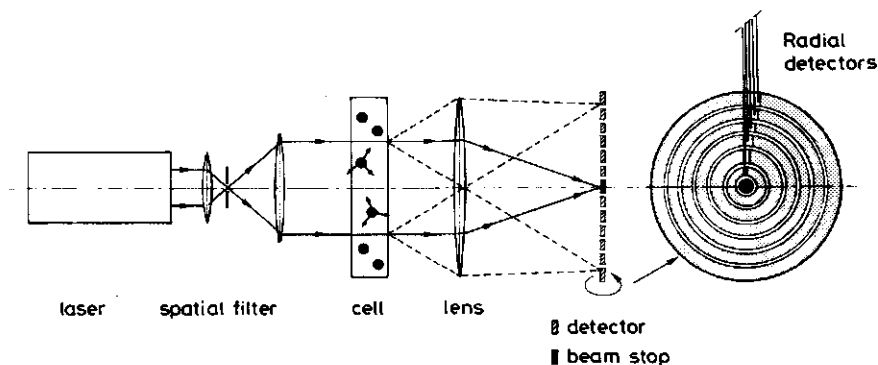


Figure 1. Optical set up and detection area of a laser diffraction apparatus. The detectors are shown both from the side and in the front (right).

The light scattering energy $E_{\theta,r}$ of a single spherical particle, with size r , imaged on one detector can be calculated with the Mie-theory. This energy depends on the scattering angle θ between detector and particle. For N particles of the same size, the total scattered energy is N times $E_{\theta,r}$. For a sample with several different particle sizes, with N_r particles in size class r , the total scattered energy can be written as: $E_{\theta}^T = \sum_r N_r E_{\theta,r}$ [39,40].

The resolution in size is determined by the number of detectors. For each class $E_{\theta,r}$ is calculated a priori. For a particular instrument (Malvern2600) the scattered energy (E_{θ}^T) is simultaneously measured at 30 scattering angles separately with 30 detectors all with different θ . This enables to construct 30 equations with 30 unknown numbers of particles in each size class. The lower limit for polystyrene particles in water is approximately 3 μm in diameter [41]. Non-spherical particles will cause an error in the distribution.

2.3.3. Laser beat spectroscopy

Laser beat spectroscopy has been used to characterize the particle sizes of a variety of monodisperse and polydisperse colloidal dispersions. The technique makes use of the random fluctuations in the scattered intensity due to particles undergoing Brownian motion [42,43]. Commercial instruments can measure sizes between 0.001 and 5 μm in diameter, again depending on the refractive index. From the autocorrelation function of the scattered intensity one can obtain an average particle size and sometimes a standard deviation. A bimodal distribution can be distinguished provided the two sizes are well separated from each other [44]. If the particle/solvent contrast is very low, even dispersions of 60% volume fraction can be measured [45].

Heterodyne detection (mixing of incident and scattered light) is reported by Ross [46]. This author constructed a fibre-optic Doppler anemometer and claimed higher sensitivity and larger dynamic range than with homodyne detection (only light scattering). The incident light is radiated through the fibre into the dispersion. The scattered light and the reflection of the incident light at the tip of the fibre is collected by a detector.

2.3.4. Light scattering frequency analysis

In this technique, a dispersion flowing in a tube passes a narrow laser beam (thickness $<$ particle size) and gives rise to light scattering. At fixed velocity of the flow, each particle will yield a light scattering flash with a duration which is a function of its size. If many particles pass the laser beam simultaneously, the detector measures the superposition of many such flashes. This scattered intensity as function of time can be Fourier transformed into a power spectrum $I(f)$ where f is the frequency [47]. The frequency is simply related to the diameter, d , of the particles by $d = v/2f$ where v is the dispersion velocity. In this way, a size spectrum $I(d)$ can be obtained. Since the passage time changes due to random forward and backward movements of the particles, Brownian motion will broaden this distribution. A difficult problem is to derive the number of particles corresponding to the intensity $I(d)$ of the power spectrum. For spherical particles, the Mie theory can be used to do this. However, for other shapes especially when orientation effects come into play (e.g. for fibres) this becomes extremely difficult.

Nevertheless, Wagberg [48] designed an apparatus based on this principle and measured the backscattering of flowing flocculating fibres and claimed to determine some average particle size.

2.4. Single particle detection

2.4.1. Microscopy

With optical or electron microscopy the size of individual particles in the appropriate size range can be determined so that in principle particle size distributions can be obtained. By recording data on tape or photographs, experiments can be done as a function of time. Data analysis is time consuming, but image processing equipment can speed this up. Care has to be taken to distinguish between merely overlapping particles and real aggregates, and to ensure that a sufficiently representative field is counted. A major problem with electron microscopy is particle aggregation or de-aggregation during evaporation of the solvent on the grid. Some particles will melt in the electron beam, for example polymethylmethacrylate particles [49]. Nevertheless, electron microscopy has found increasing use in studying floc structure [50-52]. Optical microscopy can only measure particles $> 1 \mu\text{m}$ in radius.

2.4.2. Coulter counter

A Coulter counter is able to detect and size particles individually by changes in electrical conductance when they pass a very narrow orifice [53]. In figure (2) a schematical representation of a Coulter counter is given.

The particles emerge from a capillary and are hydrodynamically focused into a narrow dispersion stream passing an orifice. At any particle passage, the conductance between the electrodes is changed considerably. If the concentration of particles is not too high (10^6 - 10^7 particles/ cm^3), they can be detected individually. A Coulter counter can count 10^4 particles per minute, but the particles have to be larger than $0.5 \mu\text{m}$ - $1 \mu\text{m}$ in radius. With a multichannel analyzer it is also possible to obtain a particle size distribution. Coulter counters require the presence of an electrolyte to provide sufficient electrical conductivity; this can influence the state of dispersion. Another factor is the possible disruption of aggregates in the

elongational flow field just before the orifice. For particles with a high refractive index the Coulter counter could have an advantage over single particle sizers based on light scattering. A review of the technique is given by Kachel [54]. Coagulation studies with this apparatus were done among others by Matthews and Rhodes [55].

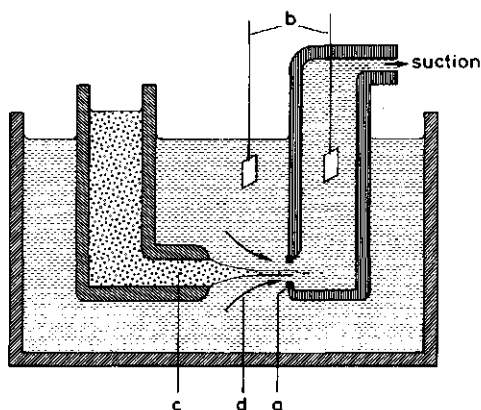


Figure 2. Coulter counter cell. a/ orifice (diameter 30-100 μm), b/ electrodes, c/ dispersion flow, d/ water flow.

2.4.3. Flow cytometry

In a flow cytometer biological cells are detected and sized individually by fluorescence or light scattering detection [56,57]. The instrument operates in a way analogous to a Single Particle Optical Sizer, but some important differences should be mentioned. The count rate is as high as 10^5 particles per minute and usually particles larger than $1\ \mu\text{m}$ in radius are employed. As a rule, no effort is made to remove small dust particles from the carrier water and, hence, the signal to noise ratio is very poor for small particles. A high count rate is possible by using a high flow rate, but this introduces high shear forces which probably cause disruption of aggregates [58].

By staining the cells with a fluorescent dye (which often binds specifically to DNA or other cell material), specific properties of the individual cells can be determined. By means of an Argon laser the dye molecules in the cells

can be excited and the resulting fluorescence is detected through a cut-off filter which blocks the scattered light. With different dyes and detectors it is even possible to detect the fluorescence at several wavelengths as well as normal light scattering simultaneously [59,60]. Often these instruments are equipped with a cell sorter, which makes it possible not only to detect the cells but also to separate and collect them. After detection, the flow carrying the cells is separated in droplets by a piezo electric transducer. Depending on the signals due to the cell, the detection system activates an electrical droplet charger as the cell arrives at the droplet formation break-off point. This causes a charge on the droplet which is subsequently deflected into a collection vessel by a static electric field.

In principle, such an instrument could be used to separate doublets from an aggregating system. However, given the count rate of 10^5 min^{-1} it would take 70 days of continuous operation to collect 10^9 doublets out of a dispersion with 10% doublets.

2.4.4. Single Particle Optical Sizing (SPOS)

In this paragraph we shortly describe a modified flow ultramicroscope which can be used for measuring particle number concentration and size distribution in colloidal dispersions. A detailed description is given in chapter 4. With this instrument it is possible to distinguish between aggregates varying in size between two and seven primary particles. Size distributions can be measured in the range of 0.1 to 5 μm (diameter) for particles of spherical and other simple shapes. The technique consists of measuring the light scattered by individual particles as they pass through a laser-illuminated volume. The dispersion stream is hydrodynamically focused and carries the particles through an optically focused laser beam. Each particle produces a flash of scattered light which is detected by a photomultiplier. The pulses are displayed in the form of a frequency distribution of pulse heights. Insofar as pulse height can be related to particle size, a size distribution can be obtained.

For spheres and simply shaped particles, the relationship between particle size and scattered light intensity is known through the Mie theory [61]. In general, the scattered intensity does not increase monotonously with particle size at all detection angles. However, by using a small detection angle one can in many cases obtain a monotonous increase in scattering cross section

with size. At small angles, the interference effects of light scattered from different parts of relative large particles are less pronounced. Particle concentrations that can be handled are 10^7 to 10^8 particles per cm^3 ; a typical count rate is 5000 particles per minute. It is also possible to count and size particles with fluorescence, but then fluorescent groups must be incorporated in the particles.

Five other single particle sizers based on small angle laser light scattering have now been reported [58,62-65]. In some of the older instruments light scattering detection around 90° was used [66,67], which decreases the resolution of the instrument considerably (see section 3.4.1.).

Beyer [65] measured the scattered light intensity at three angles (10, 20 and 40 degrees) and used the ratio of the intensities (I_{40}/I_{20} , I_{20}/I_{10}) to classify the size. This principle is described by Hodgkinson [68] and applied by Gravatt [69] for aerosols. For polystyrene particles in water a measurable size range of $0.2 \mu\text{m}$ - $1 \mu\text{m}$ in diameter was claimed.

The optics of the several single particle optical sizers differ in details. For example, we used a spatial filter and a combination of cylindrical and spherical lenses, Cummins et al [62] used only a diaphragm and a spherical lens and Buske et al [63] employed a spatial filter, a diaphragm and a tilted lens.

Oscillations in the scattered intensity as a function of particle size can be partially damped by using a large detection aperture but also by using polychromatic light (see section 3.4.2.). Rehn and Umhauer [70,71] both constructed a single particle sizer based on polychromatic light. Rehn reported a minimum size of $0.8 \mu\text{m}$ in diameter for latex in water. Neither author used hydrodynamic focusing; the detection volume was defined by the cross-sectional volume of the laser beam and the "view" of the photomultiplier. The advantage of this could be that shear forces in the instrument are very weak but a "border error" effect [66,70] in the detection volume limits the particle concentration to 10^5 particles per cm^3 (with 5% coincidence error, see section 4.4.2.).

Bartholdi [72] constructed a single particle laser light scattering instrument which simultaneously detects scattering at 60 different angles. Hence not only the size of the particles but also the angular light scattering distribution of each particle could be measured. Unfortunately, only measurements on monodisperse particles were reported by this author. It is questionable whether this technique could also be used for a coagulating system.

2.5. Performance of the various techniques

From literature data we can obtain characteristics of the methods described in this chapter. Such characteristics are collected in table 1. Some techniques can actually measure a discrete size distribution, other techniques can just measure an average size and (by some fitting procedure) a standard deviation. Table 1 indicates also whether the technique is capable of determining the rate constant of an aggregation process. The ranges in particle size and concentrations are given and finally the level of de-aggregation forces in the instrument (divided in three classes) is estimated. De-aggregation forces can be hydrodynamic forces in the instrument or other forces, for example due to the evaporation in an electron microscope. Large forces can change the size distribution of aggregates. This is an important factor in judging the suitability of an instrument for aggregation studies.

Table 1. Comparison of several methods for measuring aggregation and particle size.

Method	Distribution	rate constant	diameter ¹	concentration ² (cm ⁻³)	forces ³	references
Optical microscopy	discrete	no	> 2 μ m	-	medium	-
Electron microscopy	discrete	no	> 1 nm	-	high	[49]
Coulter counter	discrete	yes	> 1 μ m	10 ⁷	medium	[54]
Flow cytometry	discrete	no	> 2 μ m	10 ⁷ - 10 ⁸	high	[56]
SPOS(monochromatic)	discrete	yes	0.2 - 2 μ m	10 ⁷ - 10 ⁸	medium	[2]
SPOS(polychromatic)	unknown	unknown	0.8 - 5 μ m	10 ⁵	unknown	[70]
Diffraction spectr.	limited resolution	no	3 - 550 μ m	10 ⁴ (d=10 μ m)	low	[41]
Static light scatt.	no	no	2 - 480 nm	10 ⁸ (d=0.7 μ m)	low	-
Laser beat spectr.	standard deviation	no	2 - 5000 nm	10 ⁸ (d=0.7 μ m)	low	[42]
Frequency analysis	no	no	> 40 μ m	unknown	medium	[48]
Turbidity	no	yes	0.09 - 0.5 μ m	10 ⁹ (d=0.3 μ m)	low	[3]
Fluct. of turbidity	no	no	unknown	10 ⁹ (d=0.9 μ m)	low	[35]
Disk centrifuge	limited resolution	no	< 2 μ m	unknown	high	[21]
Spectroturbidimetry	no	no	0.2 - 15 μ m	10 ⁹ (d=1 μ m)	low	[37]

1 The indicated size refers to polystyrene particles, except for the spectroturbidimetry (emulsion of paraffin oil in water)

1,2 Particle diameter and concentration are only indications.

3 Low forces: no de-aggregation of flocs. Medium forces: no de-aggregation observed but possibly weakly bound flocs could de-aggregate. High forces: de-aggregation observed.

References

1. Cahill, J., Cummins, P.G., Staples, E.J., and Thompson, L.G., Colloids Surf. 18, 189, (1986).
2. Cahill, J., Cummins, P.G., Staples, E.J., and Thompson, L., J. Colloid Interface Sci. 117, 406 (1987).
3. Lichtenbelt, J., thesis, State University Utrecht, The Netherlands, (1974).
4. Gedan, H., Lichtenfeld, H., Sonntag, H., and Krug, H., Colloids Surf. 11, 199 (1984).
5. Sonntag, H., Shilov, V., Gedan, H., Lichtenfeld, H., and Dürr, C., Colloids Surf. 20, 303 (1986).
6. Bowen, S.M., Broide, M.L., and Cohen, R.J., J. Colloid Interface Sci. 105, 617 (1985).
7. Gregory, J., J. Colloid Interface Sci. 42, 448 (1973).
8. Sarkar, N., Teot, A.S., J. Colloid Interface Sci. 43, 370 (1973).
9. Reerink, H., and Overbeek, J.Th.G., Discuss. Faraday Soc. 18, 74 (1954).
10. Ottewill, R.H., and Sirs, J.A., Bulletin of the Photoelectric Spectrometry Group. 10, 262 (1957).
11. Ottewill, R.H., and Shaw, J.N., Discuss. Faraday Soc. 42, 154 (1966).
12. Fleer, G.J., thesis, Agricultural University Wageningen, The Netherlands, (1971).
13. Uriarte, F.A., thesis, Univ. Carnegie Mellon; Diss.Abstr. 32, 1541 (1971).
14. La Mer, V.K., Smellie, R.H., and Lee, P.K., J. Colloid Sci. 12, 230 (1957).
15. Gaudin, A.M., Fuerstenau, M.C., and Mitchell, S.R., Mining Eng. (New York). 11, 613 (1959).
16. Michaels, A.S., and Bolger, J.C., Ind. Eng. Chem. Fund. 1, 24 (1962).
17. Killman, E., and Eisenlauer., in "The effect of polymer on dispersion properties"(Th.F.Tadros, ed), p. 221, Academic Press, London, (1982).
18. Wolff, R., Koll. Z. 150, 71 (1957).
19. Killmann, E., Wild, Th., Gütling, N., and Maier, H., Colloids Surfaces. 18, 241 (1986).
20. Bell, S.H., and Crawl, V.T., "Dispersions of Powders in Liquids", 2nd ed., p. 267, (1973).
21. Oppenheimer, L.E., J. Colloid Interface Sci. 92, 350, (1983).

22. Vincent, B., *Advances in Colloid and Interface Science*. 4, 193 (1974).
23. Michaels, A.S., and Bolger, J.C., *Ind. Eng. Chem. Fund.* 1, 153 (1962).
24. Hanai, T., and Sherman, P., (ed.), "Emulsion Science", p. 353, Academic Press, New York, (1968).
25. Lord Rayleigh., *Phil. Mag.* 34, 481 (1892).
26. Runge, I., *Z. Tech. Phys.* 6, 61 (1925).
27. La Mer, V.K., and Healy, T.W., *Rev. Pure Appl. Chem.* 13, 112 (1963).
28. La Mer, V.K., Smellie, R.H., and Lee, P.K., *J. Colloid Sci.* 12, 506 (1957).
29. Carman, P.C., *J. Soc. Chem. Ind.* 57, 225 (1938); 58, 1 (1939) ; 69, 134 (1950).
30. Kozeny, J., *Ber. Wien. Akad.* 136a, 271 (1927).
31. Slater, R.W., and Kitchener, J.A., *Discuss. Faraday Soc.* 42, 267 (1966).
32. Shyluk, W.G., and Smith, R.W., *J. Polym. Sci. Part A2.* 7, 27 (1969).
33. Dollimore, D., and Horridge, T.A., *Powder Technol.* 5, 111 (1972).
34. Scheer van der, A., Tanke, M.A., and Smolders, C.A., *Faraday Discuss. Chem. Soc.* 65, 264 (1978).
35. Gregory, J., Nelson, D.W., *Colloids Surf.* 18, 175 (1986).
36. Ditter, W., Eisenlauer, J., and Horn, D., in "The effect of polymer on dispersion properties"(Th.F.Tadros, ed), p. 323, Academic Press, London, (1982).
37. Walstra, P., *Brit. J. Appl. Phys.* 15, 1545 (1964).
Walstra, P., *J. Colloid Interface Sci.* 27, 493 (1968).
38. Lips, A., and Willis, E.J., *J. Chem. Soc. Faraday I.* 69, 226 (1973).
39. Cornillault, J., *Appl. Optics.* 11, 265 (1972).
40. Boer de, G.J., Weerd de, C., Thoenes, D., and Goossens, H.W.J., *Part. Charact.* 4, 14 (1987).
41. Boer de, G.B.J., thesis, Technical University Eindhoven, The Netherlands, (1987).
42. Clark, N.A., Lunacek, J.H., and Benedek, G.B., *Am. J. Phys.* 28, 5 (1970).
43. Thompson, D.S., *J. Phys. Chem.* 25, (1971).
44. Muriel, C., Cambon, S., Leclerc, D., and Dodds, J., *Anal. Chem.* 58, 86 (1986).
45. Philipse, A., thesis, State University Utrecht, The Netherlands, (1987).
46. Ross, D.A., Dhadwal, H.S., and Dyott, R.B., *J. Colloid Interface Sci.* 64, 533 (1978).

47. Norman, B., Wahren, D., Svensk Papperstidning. 20, 807 (1972).
48. Wagberg, L., Svensk Papperstidning. 6, R49 (1985).
49. Fitch, R.M., and Tsai, C.H., in "Polymer Colloids" (R.M. Fitch, ed), p. 76, Plenum Press, New York, 1971.
50. Audsley, A., and Farsley, A., Nature. 208, 753 (1965).
51. Friedman, B.A., Dugan, P.R., Pfister, R.H., and Remsen, C.C., J. Bacteriol. 98, 1328 (1969).
52. Ries, H.E., and Meyers, B.L., J. Appl. Polym. Sci. 15, 2023 (1971).
53. Spielman, L., and Goren, S.L., J. Colloid Interface Sci. 26, 175 (1968).
54. Kachel, V., and Menke, E., in "Flow Cytometry and Sorting" (M.R.Melamed, ed), p. 41, Wiley, New York, 1979.
55. Matthews, B.A., and Rhodes, C.T., J. Colloid Interface Sci. 32, 332 (1970).
56. Steinkamp, J.A., Rev. Sci. Instrum. 55, 1375 (1984).
57. Steen, H.B., Lindmo, T., and Sørensen, O., Flow Cytometry IV, p 31, Universitetsforlaget (1980).
58. Bowen, M.S., Broide, M.L., and Cohen, R.J., J. Colloid Interface Sci. 105, 605 (1985).
59. Super, B.S., in "Flow Cytometry and Sorting"(M.R.Melamed, ed), p 639, Wiley, New York, (1979).
60. Fulwyler, M.L., McDonald, C.W., and Haynes, J.L., in "Flow Cytometry and Sorting"(M.R.Melamed, ed), p 653, Wiley, New York, (1979).
61. Mie, G., Ann. Physik. 25, 377 (1908).
Debye, P., Ann. Physik. 30, 57 (1909).
62. Cummins, P.G., Smith, A.L., Staples, E.J., and Thompson, L.G., in "Solid Liquid Separation" (J. Gregory, ed), p. 161, Ellis Horwood ltd, Chichester, 1984.
63. Buske, N., Gedan, H., Lichtenfeld, H., Katz, W., and Sonntag, H., Colloid Polym. Sci. 258, 1303 (1980).
64. Walsh, D.J., Anderson, J., Parker, A., and Dix, M.J., Colloid Polym. Sci. 259, 1003 (1981).
65. Beyer, M.S., J. Colloid Interface Sci. 118, 137 (1987).
66. Mcfadyen, P., and Smith, A.L., J. Colloid Interface Sci. 45, 573 (1973).
67. Davidson, J.A., Collins, E.A., and Haller, S., J. Ploym. Sci. Part C. 35, 235 (1971).
68. Hodkinson, R., Appl.Optics. 5, 839 (1966).
69. Gravatt, C.C., J. Air Pollut. Control Assoc. 23, 1035 (1973).

70. Rehn, B., in "Particle size analysis 1981"(N.G.Stanley, ed), p. 415, Wiley Heyden LTD, (1982).
71. Umhauer, H., Chem.-Ing.-Tech. 52, 55 (1980).
72. Bartholdi, M., Salzman, G.L., Hiebert, R.D., and Kerker, M., Appl. Optics. 19, 1573 (1980).

CHAPTER 3. SINGLE PARTICLE LIGHT SCATTERING THEORY

3.1. Introduction

Single Particle Optical Sizers can operate in two detection modes, viz. fluorescence or light scattering mode. The theory of fluorescence will be discussed briefly in section 4.8. In this chapter we treat the theory of light scattering by single particles. The aim is to correlate the intensity of the detected light flash to the size of the particles, depending on the detection angle and the aperture of the photomultiplier. This will enable us to formulate optimum operating conditions of a single particle optical sizer for various types of particles.

In this chapter we will briefly discuss three light scattering theories : Rayleigh, Rayleigh-Gans-Debye (RGD) and Mie theory. Every theory has its own range of validity, the Mie theory being the most general. The theory will be applied to three commonly used colloidal systems: polystyrene in water, silica in various solvents and haematite in water.

In light scattering theory, three important parameters occur:

The propagation constant $k = 2\pi/\lambda$

The wave vector $h = 2k\sin(\theta/2)$

The complex refractive index $m = n + ik$

Here λ is the wavelength in the medium, θ is the scattering angle and n and κ are the real and the imaginary part, respectively, of the refractive index of the particle. The imaginary part accounts for the light absorption.

3.2. The Rayleigh and the Rayleigh-Gans-Debye theory

The basic premise of the Rayleigh theory is, because the particle is small compared to the wavelength, that the electromagnetic field is uniform over the extent of one particle. Therefore the upper limit of the particle size for which the Rayleigh theory is presumed to be valid is generally set at $b/\lambda < 0.05$, where b is the longest distance through the particle. A more detailed discussion of the range of validity is given by Kerker[1a]. Rayleigh [2] derived a formula for the light scattering of a particle that does not adsorb light ($\kappa = 0$). If $b/\lambda < 0.05$ the particle shape is irrelevant, for larger particles the extended theory, known as the Rayleigh-Gans-Debye (RGD) theory,

introduces a form factor $p(h)$ which depends on the shape. For unpolarized light with the incident light of unit intensity:

$$I_s(h) = \frac{9\pi^2}{2r^2} \left[\frac{n^2 - n_0^2}{n^2 + 2n_0^2} \right]^2 \frac{V^2}{\lambda^4} (1 + \cos^2\theta) p(h) \quad (1)$$

where $I_s(h)$ is the intensity of scattering at wavevector h (i.e., at angle θ), and r is the distance between the detector and the particle. The parameters n and n_0 are the refractive indices of particle and medium, respectively, and V is the volume of the particle. The form factor $p(h)$ accounts for the interference of the scattered light inside a particle. In the Rayleigh regime $p(h)=1$, in the RGD regime $p(h)$ is smaller than unity and an oscillating function of h . Equation (1) is only valid if the imaginary part of the refractive index is negligible compared to the real part.

The main features of the Rayleigh theory are now apparent: the light intensity decreases as the fourth power of the wavelength and is proportional to the square of the particle volume. The scattering intensity is independent of the shape of the particles.

In the Rayleigh-Gans-Debye approximation particles of arbitrary shape are subdivided into small volume elements. Each element is treated as a scatterer according to the Rayleigh theory. The amplitude function is the result of interference of the scattered waves of each of the scatterers and is obtained by vectorial summation [1b,3,4]. The fundamental approximations in the RGD theory are that the "phase shift" corresponding to any point in the particle is negligible : $2kb \cdot \text{abs}[n/n_0 - 1] \ll 1$ and that reflection of the incident beam at the particles is negligible : $\text{abs}[n/n_0 - 1] \ll 1$. For a more detailed validity range we refer to Kerker (1b).

The form factor $p(h)$ can be evaluated for a variety of particle shapes. Rayleigh [1c] gave the result for a homogeneous sphere with radius a :

$$p(h) = \left\{ \frac{3}{(ha)^3} [\sin(ha) - (ha)\cos(ha)] \right\}^2 \quad (2)$$

This form factor will have zeros for those values of ha where $\tan(ha) = ha$. The first three minima are positioned at $ha = 4.4935$, 7.7252 and 10.9041 . An

example of the dependence of $p(h)$ is given in figure 4, below. From experimentally determined minima it is, in principle, possible to calculate the radius of the particles.

For aggregates the derivation of $p(h)$ is much more complicated: not only can the shape vary considerably (see also figure 7, below), but also the orientation in space can be different. One relatively simple situation is that of a doublet of homogeneous spheres. For that case the form factor can be written as [1d]:

$$p_d(h) = \frac{1}{2} p_s(h) \left[1 + \frac{\sin(2ha)}{2ha} \right] \quad (3)$$

where $p_d(h)$ is the form factor of a doublet and $p_s(h)$ that of a singlet, given by eq. (2).

3.3. The Mie theory

Lorentz, Debye and Mie contributed to a more general scattering theory [1e], but we shall adapt the most commonly used term: the Mie theory. Mie [5] was the first to derive the exact solution for the scattering of a homogeneous sphere of arbitrary size and arbitrary complex refractive index. In contrast with the Rayleigh-Gans-Debye approximation, the Mie theory takes into account the adsorption of the light (the imaginary part of the refractive index). If the particles have a high refractive index difference with the medium (due to the real or imaginary part) then the particles are highly reflective. The equations derived by Mie are written in terms of Bessel, Hankel and Legendre functions, and we do not give them here but we refer to Kerker [1e]. For the computations, we used a computer program published by Bohren and Huffman [3b]. Computer programs for coated spheres and for infinite cylinders are also published in the same reference.

An exact solution for the scattering of aggregates of arbitrary size and arbitrary complex refractive index is very complex. Levine et al and Lipps et al [6,7] attacked this problem with approximations only valid for small particles.

3.4. Scattering by various spherical particles

3.4.1. Introduction

Three model systems frequently used in colloid chemistry are latex, silica and haematite particles. They can be prepared as homodisperse spheres of various sizes. We used the Mie theory to calculate the light scattering intensity for these model particles as function of size, wavelength, scattering angle and aperture (size) of the detector. These calculations give information about the applicability of the Single Particle Optical Sizer to measure these model systems.

The imaginary part of the refractive index for latex and silica particles is negligible, but for haematite particles this is not the case.

3.4.2. Polystyrene latex particles

We calculated the light scattering intensity as function of particle radius for different detection angle increments, see figure 1a-d. In figure 1a, we represent the light scattering intensity for the case that the photomultiplier receives the light scattered between 5° and 6° . We denote this as the aperture of the detector. It is obvious from the figure that in this case the light scattering intensity has a one-to-one relation with particle size: the scattered intensity can be unambiguously related to size. The curve in figure 1a can be fitted to the following equation (with less than 1 % error):

$$I_{5-6} = \beta V^{1.83} \quad (4)$$

where I_{5-6} is the total scattered intensity between 5 and 6 degrees, β is a constant and V is the volume of the particles. According to the Rayleigh theory (valid for $a < 0.03 \mu\text{m}$ in this case) the intensity is proportional to V^2 . Apparently, the interference in larger particles leads to an exponent which is, for polystyrene in water, slightly smaller.

In figure 1b-c we show the light intensity as a function of particle size at higher detection angles and an aperture of 1° . In figure 1d the effect of the aperture is shown: the (average) scattering angle is the same as in figure 1b but the aperture is larger (20°). It can be seen clearly that in these cases

the one-to-one relation between intensity and size is lost. One measured intensity may correspond to different particle sizes and therefore the intensity does not unambiguously characterise the particle size. Note that the light scattering intensity at small angles is much higher than at high detection angle. Comparison of figure 1d with figure 1b shows that the oscillations in intensity as a function of size are still present but less pronounced. Also at a 20° aperture no complete one-to-one relation between intensity and size is obtained.

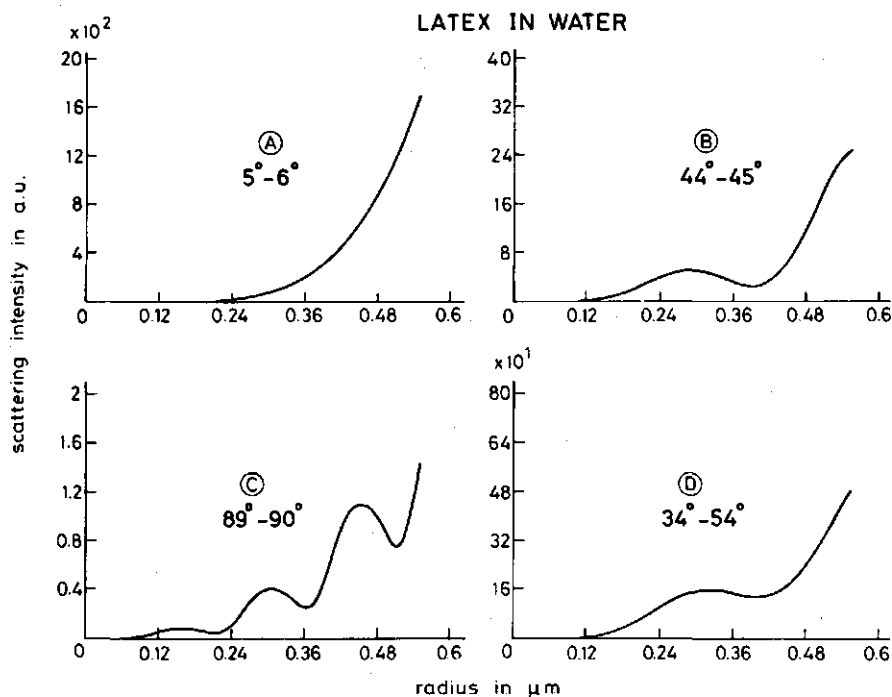


Figure 1. Light scattering intensity of polystyrene particles in water, calculated with the Mie theory. The scattering intensity is given in arbitrary units (the same for all diagrams) and the wavelength is 632.8 nm. $n=1.608$, $k=0$, $n_0=1.332$. The detection aperture is (A) $5^\circ-6^\circ$ (B) $44^\circ-45^\circ$ (C) $89^\circ-90^\circ$ and (D) $34^\circ-54^\circ$.

Figure 2 represents the light scattering intensity at a detection aperture $5-6^\circ$ with an extended particle size range. Up to $1.1 \mu\text{m}$ in diameter the simple

equation (4) holds, and up to 2 μm in diameter the intensity has a one-to-one relation with particle size. Also the range from 2.7 to 4 μm in diameter would be suitable for unambiguous interpretation.

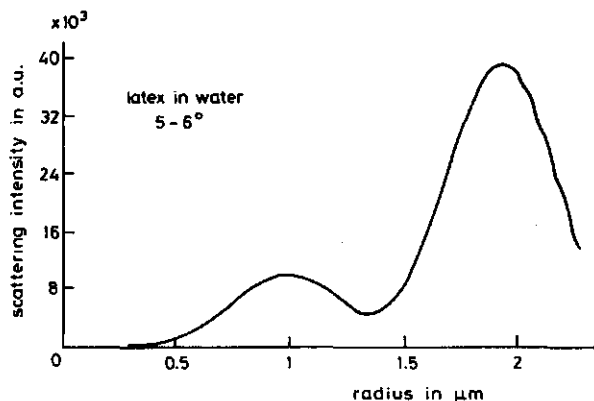


Figure 2. Light scattering intensity of polystyrene particles in water over a larger size range, calculated with the Mie theory. Parameters as in figure 1, detection aperture $5-6^\circ$.

3.4.3. Silica particles

Three common dispersion media for silica particles are water, ethanol and cyclohexane. Therefore we calculated the light scattering intensity as a function of particle size for these solvents. The results are presented in figure 3. The calculations were done for a aperture of $5-6^\circ$. From figure 3, we may conclude that the ranges of the one-to-one relation between light scattering intensity and particle size are different for the three fluids. The upper limit of the measurable particle size range corresponds with the first maximum in the curves, above this limit one intensity can be related to different particle sizes. In water, ethanol and cyclohexane these limits are 1.7 μm , 2.0 μm and 2.3 μm , respectively.

It is interesting to compare the predictions of the RGD and Mie theory. To that end, we calculated with both models the angular distribution of the scattered light intensity for three different silica particle sizes in

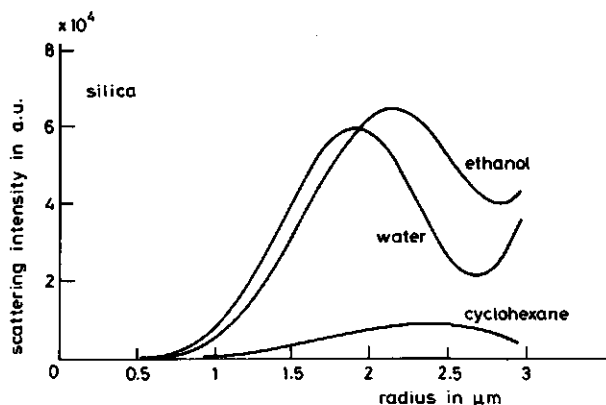


Figure 3. Light scattering intensity of silica particles in water, ethanol and cyclohexane, calculated with the Mie theory. The scattering intensity is given in arbitrary units (the same as in fig. 1 and 2) and the wavelength is 632.8 nm. $n=1.440$, $\kappa=0$. The refractive indices n_0 of the solvents are 1.332 (water), 1.361 (ethanol) and 1.421 (cyclohexane). Detection aperture is $5-6^\circ$.

ethanol. By normalizing the intensity to one at wavevector zero, we obtained the form factors, shown in figure 4a-c. The deviation of the form factor calculated with the RGD-approximation from that obtained with the Mie theory is more pronounced at higher wavelengths. Nevertheless the RGD-approximation can be used for these silica particles at low wavevectors. For higher values of h the oscillations predicted by the Mie theory are smoother than those in the RGD-approximation.

Note that figure 4a is reproduced in the initial part of figure 4b and 4c; the only difference is a scaling factor (proportional to a^2) in the abscissa axis. Similarly figure 4b corresponds to the left hand part of figure 4c.

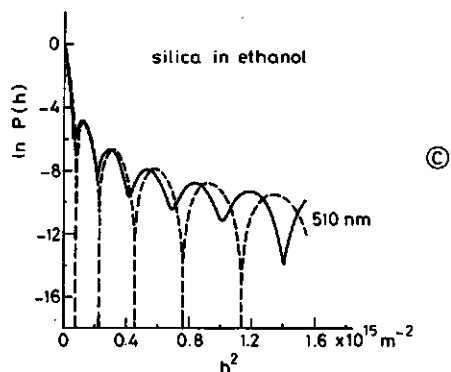
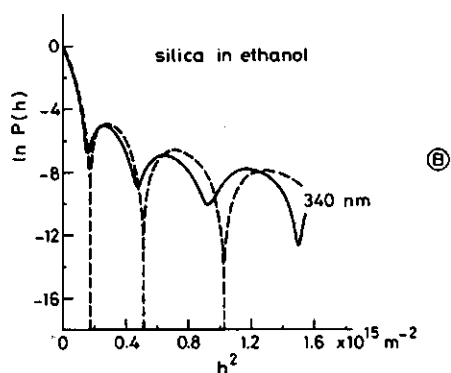
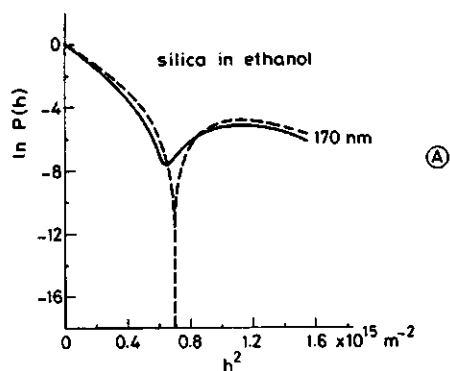


Figure 4. Form factors of silica in ethanol as a function of the square of the wavevector, for three different particles sizes: 170 nm(A), 340 nm(B) and 510 nm(C), as calculated with the Mie theory (-----) and the RGD-approximation (- - -). $n=1.444$, $\kappa=0$, $n_0=1.368$. The detection aperture is $5-6^\circ$ and the wavelength 436 nm.

3.4.4. Haematite particles

In contradistinction to latex and silica, haematite has a nonzero absorption coefficient. The real and imaginary parts of the refractive index for haematite as a function of wavelength are given in figure 5. We have adopted the data for the imaginary part as reported by Kerker [9]. Unfortunately some discrepancy exist in the literature about the value of this parameter [9,10]. Some caution is needed with the notation: Kerker defines the complex refractive index as $m = n(1-i\kappa^*)$, whereas we use $m = n+i\kappa$, following Bohren et al [3]. So $\kappa^* = -\kappa/n$.

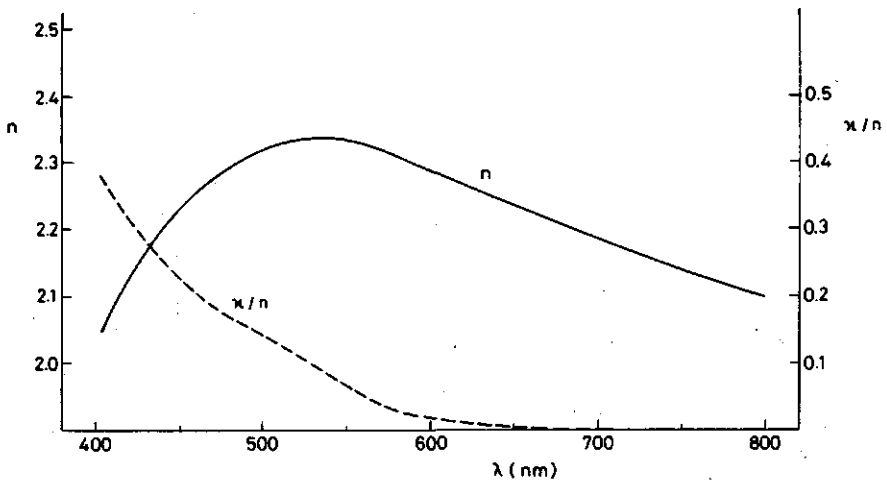
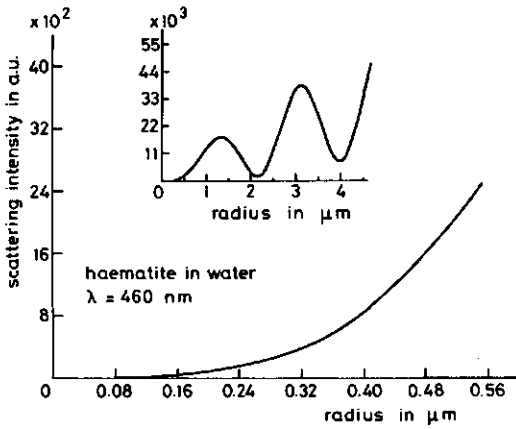
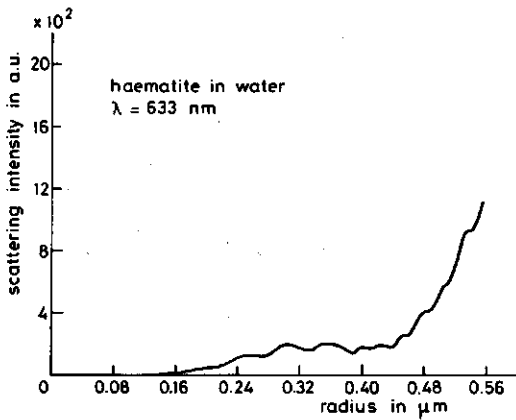


Figure 5. The real part n and the imaginary part κ of the complex refractive index $m = n+i\kappa$ of haematite particles versus wavelength. Instead of κ the ratio κ/n is plotted. The data were taken from reference [9].

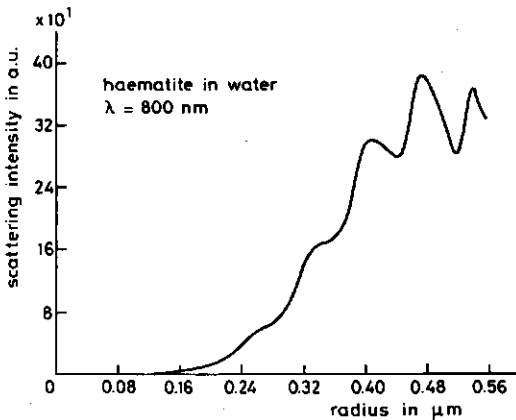
For haematite in water, the light scattering intensity as a function of particle size was calculated at three different wavelengths, see figure 6a-c. Figure 6a applies to 460 nm, the principle wavelength of an Argon ion laser. In the inset of figure 6a an extended particle size range (up to $a = 4.6 \mu\text{m}$) is shown. It can be concluded that at 460 nm the one-to-one relation between scattered intensity and size holds up to a diameter of $2.7 \mu\text{m}$. Alternative measurable particle size ranges are: 2.7 to $4.3 \mu\text{m}$ in diameter and 4.3 to $6.4 \mu\text{m}$ in diameter.



(A)



(B)



(C)

Figure 6. Light scattering intensity of haematite particles in water, calculated with the Mie theory at three different wavelengths. The main figures cover the size range 0 - 0.56 μm in radius, in the inset of fig.6a this range is extended to 4.6 μm . The scattering intensity is given in arbitrary units and the detection aperture is $5-6^\circ$. (A) $\lambda=460 \text{ nm}$, $n=2.24$, $\kappa=0.45$ and $n_0=1.338$ (B) $\lambda=633 \text{ nm}$, $n=2.24$, $\kappa=0.02$ and $n_0=1.332$ (C) $\lambda=800 \text{ nm}$, $n=2.10$, $\kappa=0$ and $n_0=1.328$.

In figure 6b, the wavelength of a Helium-Neon laser (633 nm) is used. In this case the measurable size range is much smaller than at a wavelength of 460 nm. As a special case it is very likely that one can distinguish doublets from singlets with particle diameter of $0.44 \mu\text{m}$.

At a wavelength of 800 nm (solid state laser) one could measure a particle size unambiguously up to $0.82 \mu\text{m}$ in diameter, see figure 6c.

3.5. Scattering by aggregates

So far, we have only discussed results for spherical particles. However, in many cases a single particle optical sizer is used for studying aggregation processes. The shape and orientation of aggregates may be very complex. Some possibilities for aggregates of four spheres (tetraplets) are given in figure 7.

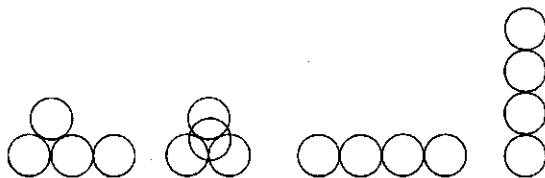


Figure 7. Different conformations and orientations of a tetraplet

A general theory like that of Mie is not available for aggregates. In the RGD-approximation, only very simple cases have been treated (see eq.(3)). Although the validity of the Rayleigh-Gans-Debye theory does not cover all situations, we use this theory for some qualitative discussion.

The form factor accounts for the shape effects of the particles on the angular light scattering distribution. Aggregates can have different spatial arrangements and different orientations in the detection volume. In general, the form factor for a particular aggregate is unknown. However, at zero detection angle the form factor is always unity. Although in this case no information on the shape is available, the volume of an aggregate can be measured. The light scattering in the RGD theory at zero angle depends only on the volume to the second power. Since measuring at zero angle is impossible we

measure at a detection aperture 5 to 6°. Experimentally we can show that still a clear distinction is possible between aggregates containing different numbers of singlets (section 4.6.3.). Apparently the form factor has not a large effect on the scattering intensity at this detection aperture. To gain information both on size and shape one would have to measure simultaneously at different angles [8], but analysis of the data could be very difficult.

3.6. Conclusions

The lower and upper limit of the particle size ranges that can be studied with a Single Particle Optical Sizer are presented in table 1.

The upper limits in table 1 are derived from figures 1-6. The lowest lower limit for each particle type is determined by the interference of dust particles in our present SPOS instrument. The light intensity of the dust particles was determined experimentally at a wavelength 633 nm. The optical properties of the dust particles are unknown, therefore we are not able to calculate the intensity of the dust particles at other wavelengths. Hence the lower size limit at these wavelengths can not be calculated, but should be determined experimentally.

Apart from the size ranges indicated in table 1, occasionally measurements could be done for larger particles within a rather limited size range. As discussed above for latex in water at 633 nm the diameter ranges 2.0 - 2.7 μm (intensity monotonously decreasing with increasing a) and 2.7 - 4.0 μm (increasing intensity) could be used (figure 2). Similarly, for haematite in water measurements would be possible in the ranges 2.7 - 4.3 μm and 4.3 - 6.3 μm (figure 6). However, in these cases one should be sure that the initial particles and any aggregates formed are precisely in these ranges.

Table 1. Particle size ranges.

particle	medium	wavelength in nm	particle diameter in μm	
			low	high
latex	water	633	0.2	2.0
silica	water	633	0.26	3.6
silica	ethanol	633	0.42	4.0
silica	cyclohex.	633	0.50	4.8
haematite	water	633	0.14	0.26
haematite	water	460		2.7
haematite	water	800		0.82

References

1. Kerker, M., "The scattering of light and other electromagnetic radiation", (a) p. 31, (b) p. 414, (c) p. 417, (d) p. 446, (e) p. 39, Academic Press, New York, 1969.
2. Lord Rayleigh., Phil. Mag. 41, p 107,274,447, (1871).
Lord Rayleigh., Phil. Mag. 12, p 81 (1881).
3. Bohren, C.F., and Huffman, D.R., "Absorption and Scattering of Light by Small Particles", (a) p. 158, (b) p. 475, John Wiley & Sons, New York, (1983).
4. Hulst van der, H.C., "Light Scattering by Small Particles"(Dover ed), p. 85, Dover publications Inc, New York, (1981). First ed. (1957).
5. Mie, G., Ann. Physik. 25, 377 (1908).
Debye, P., Ann. Physik. 30, 57 (1909).
6. Levine, S., and Oloafe, G.O., J. Colloid Interface Sci. 27, 442 (1968).
7. Lips, A., and Levine, S., J. Colloid Interface Sci. 33, 455 (1970).
8. Bartholdi, M., Salzman, G.L., Hiebert, R.D., and Kerker, M., Appl. Optics. 19, 1573 (1980).
9. Kerker, M., Scheiner, P., Cooke, D.D., and Kratochvil, J.P., J. Colloid Interface Sci. 71, 176 (1979).
10. Gehlen, K.V., and Piller, H., N. Jahrbuch Mineral. Monatshefte. 4, 97 (1965).
Forsterling, C., N. Jahrbuch Min. Geol. Beilageband. 25, 344 (1908).

CHAPTER 4. THE SINGLE PARTICLE OPTICAL SIZER

4.1 Introduction

The instrument is based on detection of light scattering by single particles under a small angle. In this chapter we will first discuss the general outline of the instrument, followed by a detailed treatment of the optical, flow and electronic system. Furthermore, the effects of hydrodynamic forces in the instrument on aggregating systems are discussed. Orthokinetic and de-aggregation effects can be induced by these forces. We will show that aggregates bound by Van der Waals forces or by "polymer bridging" forces, are not disrupted by the hydrodynamic forces in the instrument. Some test experiments are described, whereby the size distribution of stable latex particles is explicitly considered. For unstable systems, the instrument can resolve aggregates containing up to seven singlet units. Finally, we discuss some preliminary experiments with fluorescent particles, using the instrument in fluorescent detection mode.

4.2. General description

A plan of the apparatus is depicted schematically in figure 1. Basically, it is a flow ultramicroscope in which light scattering by individual particles is detected.

Light from a Helium-Neon laser is passed through a spatial filter in order to create a homogeneous light beam without any local intensity variations. Subsequently, this beam is focused into an elliptical focus by a special lens system. Particles of a dispersion are injected into a stream of flowing water and hydrodynamically focused so as to pass individually through the laser focus. During passage the particles give rise to flashes of scattered light which are detected at a small angle by a detection system. Low angle detection is advantageous as explained in chapter 3. All the particles have to receive the same incident laser intensity because otherwise particles of the same size could give light scattering flashes of different intensity. An elliptical laser focus is especially suitable for a homogeneous incident light intensity in a small detection volume. The detection volume is determined by the intersection of the dispersion stream and the laser focus. As will be seen

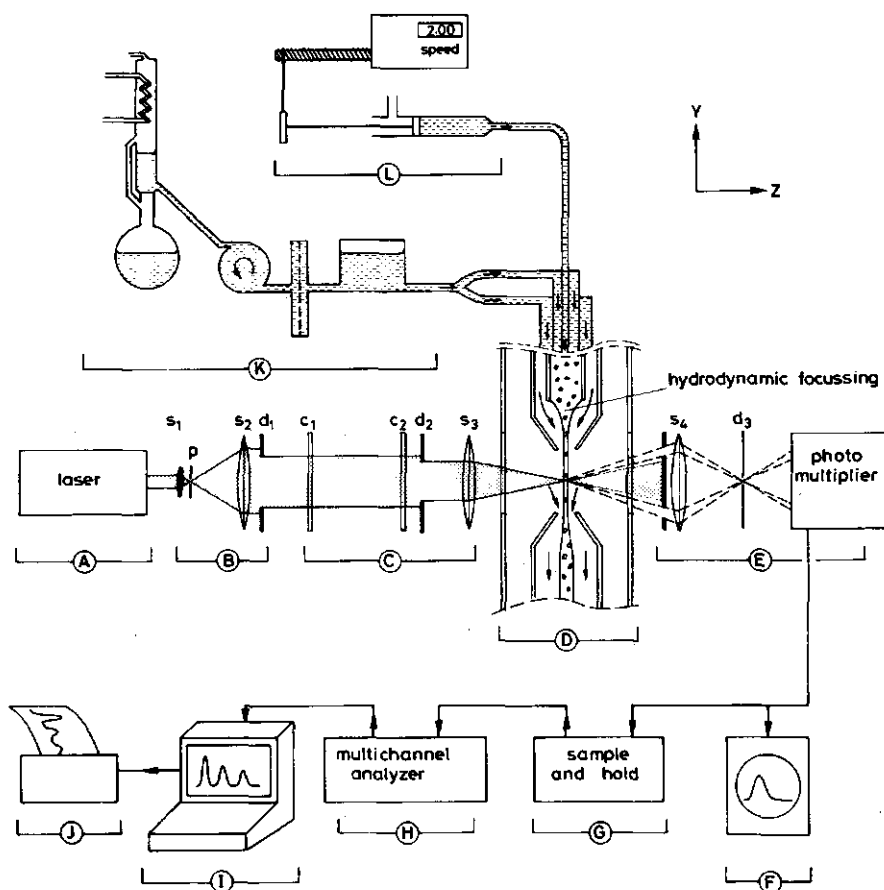


Figure 1. A schematic diagram of the single particle optical sizer. (A) laser, (B) spatial filter, (C) focusing lens system, (D) flow cell, (E) detection system, (F) oscilloscope, (G) sample and hold, (H) multichannel analyzer, (I) microcomputer, (J) printer, (K) water pretreatment, (L) dispersion injector.

from coincidence statistics, a small detection volume is critical for the measurement of individual particles. If a coincidence error of 0.5% - defined as the probability of finding two particles instead of one in the scattering volume - is allowed, the maximum particle concentration N_{\max} is given by:

$$N_{\max} = 0.01/V \quad (1)$$

where V is the detection volume. This relation will be derived in sec. 4.4.2. The hydrodynamic focus must be a stable laminar flow, otherwise the particles will deviate from the laser focus and cause erroneous light scattering signals. Reynolds numbers, which are a measure for laminar or turbulent flow, are evaluated for the flow system. Furthermore, a detailed description is given of the cell and water pretreatment. It is essential to avoid dust in both sample and in the water flow.

The detected light scattering flashes are visualized on an oscilloscope, which helps adjusting the particle stream with respect to the laser focus. Simultaneously, these flashes are electronically processed as a sequence of pulse heights. Each signal is processed by a peak catcher (indicated as a sample and hold in the figure) and stored according to its intensity in one of the 2048 channels of a multichannel analyzer. The peak catcher is a pulse shaper which transforms the pulses in such a way that they can be accepted by the multichannel analyzer.

4.3. The optical system

In this section we will discuss the optical components: laser, spatial filter, optical focus and detection system. The optical set up is mounted in micro- and macrobank components of Spindler U.Hoyer. The whole instrument is carried by four vibration dampers (T-073, Physik Instrumente).

4.3.1. Laser

The light source is a 10 mwatt linearly polarized TEM_{00} Helium-Neon laser (Spectra Physics model 106-1). The beam diameter (at $1/e^2$ of the maximum intensity) is 0.68 mm and the beam divergence angle is 1.2 mrad. The wavelength is 632.8 nm.

4.3.2. Spatial filter

The laser intensity profile over a cross-section perpendicular to the laser beam has a Gaussian shape. Small irregularities of the mirrors of the laser cause local intensity variations of this profile. To minimise these variations

the laser light is led first through a spatial filter (Spindler U.Hoyer ,040148), which transforms the laser beam into a wider beam of more homogeneous intensity. A spherical lens (s_1 , focal length 10 mm) focuses the beam on a pinhole p ($d=20\mu\text{m}$) which transmits an interference pattern. The beam diameter D of the zero order interference after the second lens (s_2 , focal length 100 mm) can be calculated with [1]:

$$D = 4\lambda f / \pi d_p \quad (2)$$

where λ is the wavelength of the light, f the focal length of the second lens and d_p the diameter of the pinhole. This equation gives $D=4.03$ mm for our set-up. However, equation (2) is only valid for the case of a Gaussian beam of infinite extension. In all practical cases the Gaussian beam is truncated, i.e. the outer edges of the beam will be cut off. The effect of the truncation will modify the interference pattern somewhat [2]. Higher order interference is blocked by a diaphragm d_1 ($d=4$ mm).

4.3.3. The optical focus

4.3.3.1. The focus shape

For optimum detection it is required that all the particles experience the same incident light intensity and that the detection volume is as small as possible. A focus with an elliptical cross-section satisfies both criteria very well. The particle stream is along the short axis of the ellipse, giving a small detection volume. Perpendicular to the particle stream, the elliptical cross-section of the laser focus is wide and therefore a flat intensity distribution is present in this direction. The ellipse is 30 by 250 μm (section 4.3.3.2.) and the focused particle stream is 5.7 μm in diameter (section 4.4.3.). A circular laser focus cannot optimally satisfy both criteria simultaneously.

In the propagation direction of the laser, the light distribution in the detection volume is also uniform. That this is the case and how the optical focus is created, is explained in the next section.

4.3.3.2. The focus lens system

The laser beam, which is expanded by the spatial filter, passes through two cylindrical lenses (c_1 and c_2 , both with focal length 40 mm), one diaphragm ($d_2=1.6\text{mm}$) and one spherical lens (s_3 , focal length 30 mm) to create the elliptical focus, see figure 2.

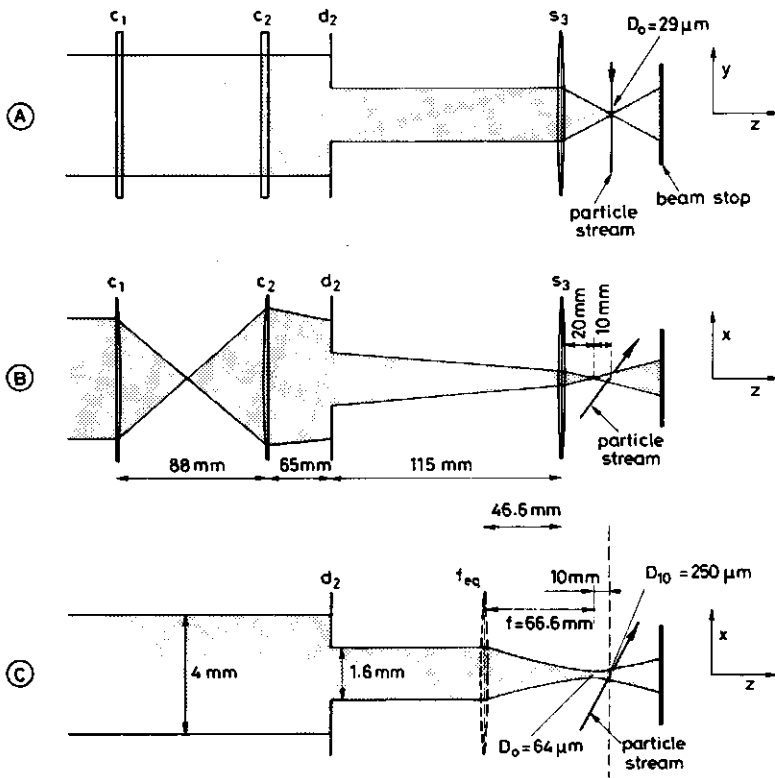


Figure 2. The system of focusing lenses. A/ light rays in the yz -plane, view perpendicular to the particle stream. B/ xz -plane, view parallel to the particle stream. C/ xz -plane, with the lens system is replaced by the equivalent lens.

In this figure the z -axis is the optical axis and the y -axis is along the direction of the particle flow. Both cylindrical lenses deflect the laser beam

in the xz -plane. The distance between these lenses is somewhat larger than two times their focal distance, therefore the light beam is converged in the xz plane. In the yz -plane the laser beam is still parallel after the two cylindrical lenses, therefore the position of the focus in the yz -plane created by the spherical lens s_3 is shifted with respect to the focus position in the xz -plane. A cross section of the laser beam at the intersection with the particle stream yields an elliptical focus spot. Although the lenses are coated to yield a minimum reflection at 633 nm (1.2% reflection), remaining reflections have to be blocked by the diaphragm d_2 ($d=1.6\text{mm}$). The diameter of the diaphragm is smaller than the diameter of the laser beam, therefore interference effects are created. However, because the diameter of the diaphragm is relatively large with respect to the wavelength this effect is very small.

We designed this particular lens system because by small variations of the position of the lenses, one can achieve many different focus shapes and sizes. In this flexible set-up one can easily optimise the size and shape of the laser focus.

In order to assure an uniform incident light intensity in the focus one has to determine the position and the size of the focus. The position of the focus can be obtained from the combination rule for thin lenses and the size of the focus is calculated from an equation for the cross-section of a Gaussian light beam.

Position of the focus in the xz and yz plane.

By the fair assumption that this lens system can be treated as a thin lens system we can use a standard relation (3) for the calculation of the resulting focal distance in the xz -plane for a combination of three lenses. In the yz -plane, the light is not deflected by the cylindrical lenses and the focus position is only determined by the spherical lens s_3 .

In general, two thin lenses i and j with focal length f_i and f_j , respectively, at mutual separation t give the same result as one lens with focal length f placed at a distance A to the left of the second lens j . According to elementary optics [3], f and A are given by:

$$f = f_1 f_j / (f_1 + f_j - t) \quad A = tf/f_1 \quad t < f_1 + f_j \quad (3)$$

$$f = -f_1 f_j / (f_1 + f_j - t) \quad A = -tf/f_1 + 2f \quad t > f_1 + f_j$$

We use a distance $t=88$ mm between the two cylindrical lenses, giving for this combination an equivalent lens with focal distance $f=200$ mm and positioned right from c_2 ($A=-40$ mm) in the xz -plane. Applying eq.(3) once more for this equivalent lens and s_3 , we find a new equivalent lens replacing c_1 , c_2 and s_3 in the xz -plane. This lens has a focal distance of $f=66.6$ mm and is positioned left from s_3 ($A=46.6$ mm), see figure 2. Hence, the position of the focus in the xz -plane is $66.6-46.6=20$ mm to the right of s_3 , which is 10 mm left of the focus in the xy -plane.

Size of the focus at the intersection with the particle stream

A Gaussian light beam converged by a lens has a diameter D which is given by [1]:

$$\left(\frac{D}{D_0}\right)^2 = 1 + (\alpha \lambda z / n D_0)^2 \quad (4)$$

where D is the diameter of the laser beam at position z , D_0 the diameter at position $z=0$ (focus), λ the wavelength in vacuum and n the refractive index of the medium; α is a numerical constant which is $4/\pi$ for a Gaussian light beam. For an uniform light beam $\alpha=2.44$. For the truncated Gaussian light beam, in our set-up, the value of α will be close to 2.44. For large z one can neglect the term 1 in the right hand side of equation (4). If z equals the focal distance f , then D equals the diameter of the diaphragm d_2 and equation (4) reduces to:

$$D_0 = \alpha f / n d_2 \quad (5)$$

With the help of these equations, we obtain the dimensions of the laser beam at the intersection with the dispersion stream as follows. From equation (5),

we calculate, with the focal distance of s_3 ($f=30$ mm), $D_0(yz)$ as $29\text{ }\mu\text{m}$. Similarly, with the focal distance of the equivalent lens ($f=66.7$ mm) we obtain $D_0(xz)=64\text{ }\mu\text{m}$, see figure 2a+c. The particle stream is situated at the yz -focus and 10 mm from the xz -focus. The width of the laser beam at this position in the xz -plane is calculated from equation (4) with $z=10$ mm: $250\text{ }\mu\text{m}$. Hence, the elliptical focus is $29\text{ }\mu\text{m}$ wide in the y -direction, along the particle stream, and $250\text{ }\mu\text{m}$ wide in the x -direction, perpendicular to it. The particle stream has a diameter of $5.7\text{ }\mu\text{m}$ (see section 4.4.3.) and is situated in the middle of the laser beam, therefore the light intensity change in the particle stream in the x -direction is very small ($<0.4\%$).

In the z -direction (optical axis) the light intensity is inversely proportional to the cross-sectional area of the laser beam. The particle stream is situated between $z=9997.15$ and $z=10002.85\text{ }\mu\text{m}$ (from the focus in the xz -plane). Substituting these values in equation (4) shows that the variation in beam diameter over the particle stream is very small ($<0.04\%$). We can conclude that the variation in the incident light intensity in the detection volume is negligible.

Lens aberrations are of minor importance. For a monochromatic laser beam incident along the axis of the lens, the most important aberration is the spherical aberration [2]. Spherical aberrations become larger when the focal length of the lens becomes shorter. The physics of the aberration are rather complex [4], but with reasonable assumptions one can estimate that the aberration is at most 1% in our set up [5].

With the help of a light microscope we determined experimentally the focus size in the yz -plane: $30 \pm 3\text{ }\mu\text{m}$. This value is in excellent agreement with the value of $29\text{ }\mu\text{m}$ calculated above.

In the above calculations, the shift of the optical focus due to refraction by the cell window and the water in the cell was disregarded. This shift of 3.3 mm to the right was simply taken into account by moving the flow cell over the same distance. The cell windows have anti-reflection coatings optimised for wavelength 633 nm (1.2% reflection).

4.3.4. The detection optics

In figure 3 the detection optics are presented schematically. The beam stop allows only the light scattered at $5-6$ degrees to pass, intercepting the scattering under all other angles. A microscope objective s_4 images the

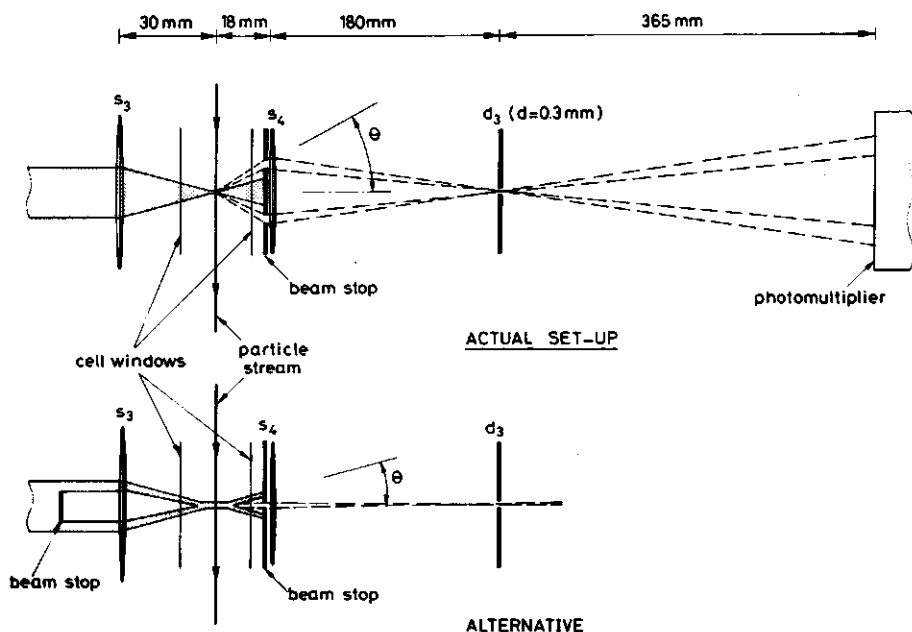


Figure 3. The actual detection system and a possible alternative. In the actual set-up the minimum detection angle is somewhat larger than in the alternative set-up.

scattered light (created in the focus) on the diaphragm d_3 ($d=0.3$ mm). Reflections from the cell windows are imaged as a blurred circle around the hole of diaphragm d_3 . These reflections are effectively blocked by this diaphragm, which is an essential step to enhance the signal to noise ratio.

The cell and beam stop thicknesses determine the working distance of the objective. We used an objective with working distance 13 mm and focal length 18 mm (Melles Griot 04oas013). Higher detection angles would worsen the measurable particle size range (see section 3.4.). It might be possible to use smaller angles, but the incident laser beam could decrease the signal to noise ratio.

Although we used only the detection system discussed above, other options could be considered. One alternative is to block the central part of the incident laser beam (lower part of figure 3), but then the intensity in the

focus would be smaller and inhomogeneities in intensity caused by diffraction at the edge of the beam stop would occur. The detection angle in this case is smaller, compare the detection angles in the top and bottom parts of figure 3. For particles with a high refractive index relative to the solvent, this alternative could be useful. Another option is to use a focusing lens with a larger focal distance. This makes it possible to use a lower detection angle but also increases the detection volume. A consequence would be a decrease of the maximum measurable particle concentration.

The scattered light is detected by a red sensitive photomultiplier (Thorn Emi, 9658b), which is placed at such a distance of the diaphragm d_3 that the sensitive area of the photomultiplier is optimally used. For detection of incoherent light (fluorescence) a cut-off filter is placed between diaphragm d_3 and the photomultiplier.

Visual inspection is possible with a microscope (magnification 30x) which is placed perpendicular to the particle stream and the laser beam. The microscope is very useful in adjusting the cell with respect to the laser beam.

4.4. The flow system

4.4.1. Introduction

According to the very principle of single particle sizing, the particles have to pass one by one through the laser focus. First we derive from coincidence statistics how the maximum permissible particle concentration for single particle detection depends on the detection volume. Then we describe how a small detection volume is obtained by means of a very narrow particle stream. A stable laminar flow is created by injecting the particle dispersion into a faster flowing water stream, called inner flow: a hydrodynamic focusing occurs. Around this inner flow, an outer water flow is present which makes it possible to place the cell windows relatively far away from the detection volume. By this geometrical separation, laser reflections on the cell window can be eliminated in the detection system (section 4.3.4.). Moreover, contamination of the cell windows by dispersion particles is avoided. Dust particles in the inner and outer flow are removed by water pretreatment. Below we will describe subsequently the coincidence statistics, the flow cell and the water pretreatment.

4.4.2. Coincidence statistics

The laser beam and the particle stream cross each other. The detection volume is defined as the illuminated volume of the particle stream. The particles are distributed in the detection volume by chance and since the mean particle number $\langle n \rangle$ in the volume is small, the probability P_n that n particles are simultaneously present in a given volume can be described by a Poisson distribution:

$$P_n = \frac{\langle n \rangle^n}{n!} \exp(-\langle n \rangle) \quad (6)$$

If a coincidence error of 0.5% is allowed - defined as the probability of finding two particles instead of one particle in the detection volume - then the ratio $P_2/P_1=0.005$. Coincidence of three or more particles can be neglected completely if $P_2/P_1=0.005$. With this value of P_2/P_1 we find $\langle n \rangle_{\max}=0.01$. Hence, the maximum particle concentration N_{\max} is given by $N_{\max}=0.01/V$, where V is the detection volume. The detection volume equals the laser focus thickness times the cross-sectional area of the particle stream. The laser beam is 30 μm along the dispersion stream (section 4.3.3.2.) and the diameter of the particle stream is 5.7 μm (section 4.4.3.) so the detection volume is $7 \cdot 10^{-10} \text{ cm}^3$ corresponding to $N_{\max} = 1.5 \cdot 10^7 \text{ cm}^{-3}$.

The theoretical lower limit for the detection volume is obtained from the intersection of a particle stream of $\approx 1 \mu\text{m}^2$ cross-section (in a narrower stream the particles would not fit in) and a laser beam thickness of 1 μm , of the order of wavelength. With this lower limit of V the maximum particle concentration would be 10^{10} cm^{-3} , about 600 times higher than in our instrument. In practice, such a low detection volume cannot be obtained because other restrictions, which depend on detection angle and hydrodynamic forces, are not satisfied.

4.4.3. The flow cell

We modified a flow cell used by Cahill et al [6]. In turn, these authors improved a flow cell described by Herschberger [7]. A 10 μl syringe (hamilton80lrnel3) is motordriven to inject the dispersion into the cell. The

Figure 4. The flow cell. (a) capillary, (b) not-lock, (c) capillary support, (d) circular cross-section, (e) nozzle (circular cross-section), (f) microscope objective, (g) squared cross-section. The lower inset shows the exit of the upper nozzle in more detail, the upper inset gives an enlarged view of the capillary exit.

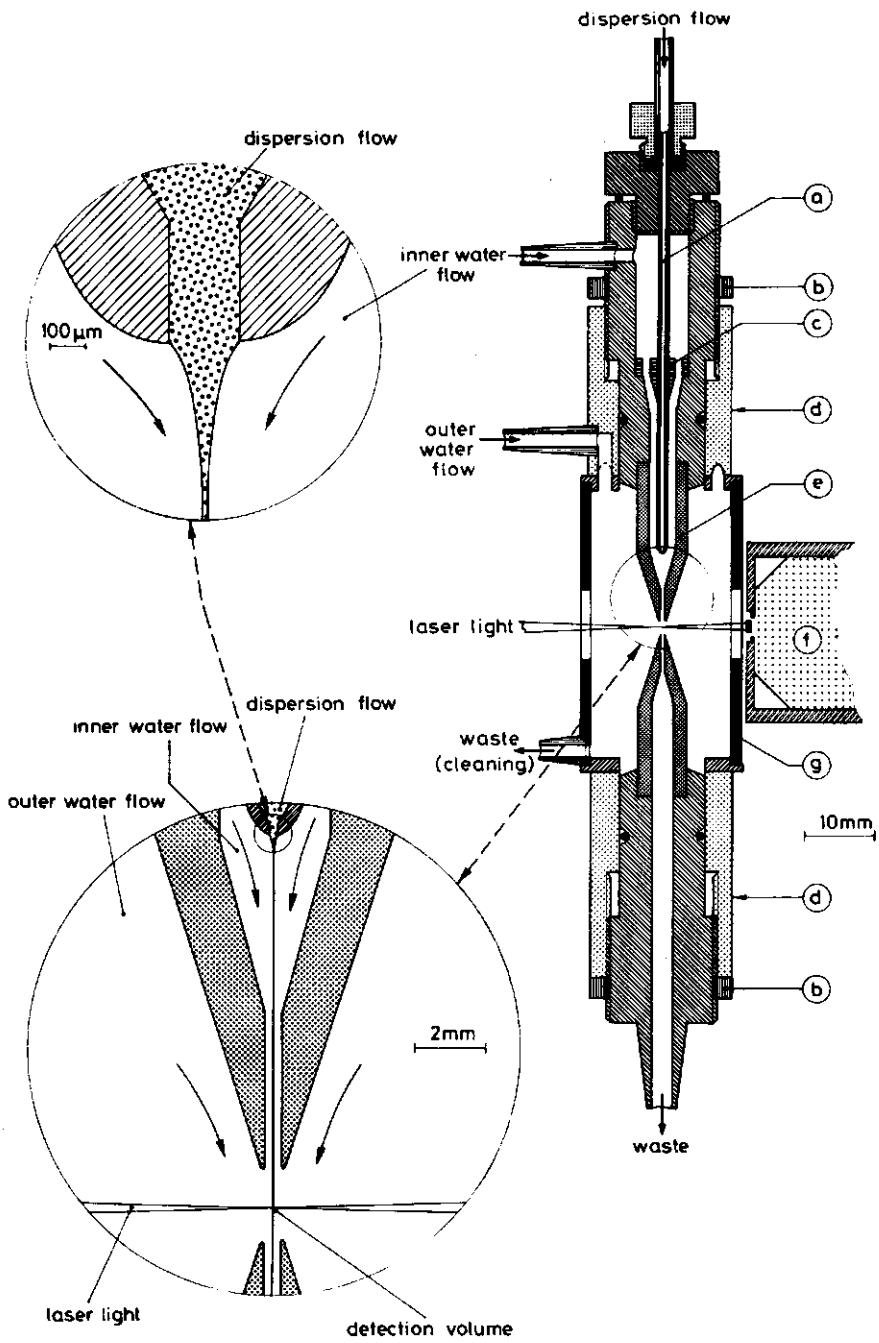
syringe is equipped with an inlet which allows filling if the plunger is in the drawback position. A Teflon tube (10 cm long, $d=0.75\text{mm}$) connects the syringe with the capillary in the cell. The flow cell construction is shown in figure 4. To the right a cross-section of the cell is shown. The dispersion enters the inner water flow through the capillary ($d=0.75\text{mm}$) which ends in a tip ($d=0.2\text{mm}$). The tip is shown in detail in the upper inset. The function of the inner flow is to narrow the dispersion stream. Because the inner flow is much faster than the dispersion velocity, the dispersion is hydrodynamically focused by extensional and shear forces. Subsequently, the inner flow is accelerated by the upper conical nozzle which provides an additional hydrodynamic focusing of the dispersion stream. The tip of the nozzle ($d=0.5\text{mm}$) is shown in detail in the lower inset. At this position the inner flow enters the outer flow. The function of the outer flow is to avoid contamination of the cell windows and to enable the separation of reflections from the scattered light of the particles. The lower nozzle functions as the outlet and stabilizes the dispersion stream spatially, because all flows are forced to leave the cell through this nozzle.

In earlier cell models, no outer flow was present [8], resulting in a rather poor signal to noise ratio. Gedan [9] used a flow cell with the cell windows some distance away from the detection volume but without outer flow. This author could distinguish aggregates up to triplets.

The flow must be laminar in order to be spatially stable. Generally, flow behaviour (laminar or turbulent) is determined by the Reynolds number Re , which is defined as:

$$Re = \frac{2F\rho}{\eta\pi R} \quad (7)$$

where F is the flux, η the viscosity, ρ the density of the fluid and R the



radius of the tube. The flow is laminar if the Reynolds number is smaller than 2100 [10a]. For tube flow, an entrance length is required to build up a fully developed parabolic velocity profile in the tube. The maximum entrance length L_e is given by: $L_e = 0.07 R Re$ [10a, 11-13]. Just before entering the outer flow, the inner flow passes the exit of the upper nozzle; this exit is a tube with radius 0.25 mm and length 5 mm. With $F = 5.3 \cdot 10^{-2} \text{ cm}^3/\text{s}$ the Reynolds number is calculated as 135 and the entrance length becomes 2.4 mm. Hence a fully developed parabolic laminar flow is established in the exit part of the upper nozzle.

We can now calculate the radius of the dispersion stream in the exit of the nozzle, which is important for the calculations of the shear forces (section 4.6.2.). The velocity of a laminar parabolic flow in the tube centre is two times the mean velocity and is given by $2F/\pi R^2$. The flux of the dispersion ($3.05 \cdot 10^{-6} \text{ cm}^3/\text{s}$) is very small with respect to the inner water flux and the dispersion is therefore entirely situated at the centre of the inner flow. The average velocity of the dispersion will almost equal the velocity in the tube centre which is 54 cm/s. By taking the ratio of flux and velocity, we calculate for the radius of the dispersion stream in the upper nozzle 1.34 μm . The flux of the outer flow is the same as that of the inner flow, but its cross-section (perpendicular to the flow direction) is much larger, hence its velocity will be smaller. As the inner flow, containing the dispersion stream, enters the outer flow, the cross-section of the inner flow starts to expand. Rapidly this expansion will change into contraction because all three flows have to enter the lower nozzle (see also figure 6, below). The distance between the nozzles is 2 mm and that is not enough to give a fully developed velocity distribution between the nozzles. Hence it is very difficult to derive the velocity and surface cross-section of the particle stream in the focus exactly from hydrodynamic considerations.

Fortunately we are able to measure the pulse time of a scattered light flash with an oscilloscope. The experimental value is $225 \cdot 10^{-6} \text{ s}$. This pulse time is equivalent with the time a particle needs to travel through the laser focus. The detection volume equals Ft , where F is the dispersion flux and t the pulse time. As discussed in section 4.3.3.2., the thickness of the laser focus is 30 μm so the velocity of the particles in the focus is 13.3 cm/s and the radius of the dispersion flow in the laser focus is 2.7 μm . The expansion of the dispersion flow from 1.34 μm radius in the upper nozzle to 2.7 μm radius in

the focus is further discussed in section 4.6.2., where we will discuss the hydrodynamic forces in the cell.

4.4.4. Water pretreatment

It is essential to avoid dust contamination in the cell. Dust particles in the same size range as that of the particles lower the resolution of the instrument. The light scattering of a particle is different from that of a particle plus a dust particle. Therefore, the particle size distribution is artificially broadened by the dust.

Before entering the cell, the water is distilled and on-line filtered through a 0.05 μm Millipore filter ($d=47\text{mm}$). The used plunger pump (M-pump, Metering Pumps Ltd, London) causes a pulsating volume transport. A damping vessel and a capillary ($l=1\text{m}$, $d=0.75\text{mm}$) are placed between the filter and the flow cell to give a smooth flux.

Distilling and filtering are both necessary. Small air bubbles in the colloidal size range do not disappear by filtering alone.

4.5. Data acquisition

The hardware

As described in section 4.2., each flash of scattered light corresponds to one particle and is detected by the photomultiplier. The signal from the photomultiplier is transformed from current to voltage and amplified 1000 times. The connection between photomultiplier and amplifying circuit is as short as possible to minimize the noise. The amplified signal passes a high frequency cut-off filter ($f_c=10\text{ kHz}$) and is fed into a "sample and hold" circuit and simultaneously into an oscilloscope. With the help of the signal on the scope, the flow cell can be positioned so as to yield an optimal signal. The "sample and hold" transforms the time base of each pulse ($225\mu\text{s}$) to a smaller time base ($7\mu\text{s}$) which can be accepted correctly by the multichannel analyzer (pca2048, The Nucleus). The analyzer collects the pulses and classifies them according to height. The analyzer has a 11 bits analog to digital converter, so 2048 levels are available in the pulse height range. The analyzer is incorporated in a ms-dos compatible microcomputer (m24 olivetti) and the number of pulses as a function of pulse height can be displayed.

The "sample and hold" circuit was designed and constructed in our workshop by Mr. Wegh. A detailed description is provided in appendix A.

The software

A machine language programme, which is delivered with the multichannel analyzer, makes it possible to activate the analyzer. This programme was incorporated in a user programme. This programme can automatically activate and deactivate several times during arbitrarily chosen time intervals. The measured size distribution is displayed during data collection and stored on disk. The contents of specified channels can be added (for example to get the number of singlets, doublets etc.). An important feature is the dead time correction. While a pulse is being processed another pulse cannot be accepted by the electronics and is lost. The relation between the true total number of pulses C^* and the dead time τ is given by [8]:

$$C^* = \frac{C}{1 - \frac{C\tau}{\Delta t}} \quad (8)$$

where C is the total observed number of pulses in all channels in time interval Δt . In our set-up, $\tau=0.7$ ms. The content of each channel is corrected by multiplying with C^*/C .

Further options are the calculation of the standard deviation of the particle size distribution and the computation of the rate constant of the total aggregation process if the particle size distribution is followed in time. With the microcomputer it is also possible to display the number of particles as a function of time. Graphs can be scaled and printed as desired. Copies of the program are available on request.

The same data, i.e., the number of particles as a function of time, can be transferred to a VAX 8700 computer to calculate the rate constants for the different aggregation steps.

4.6 Effects of shear on aggregating systems

4.6.1. Introduction

Shear and extension forces in the flow cell are inevitable if a hydrodynamic focus is created. However, these hydrodynamic forces should not influence the particle size distribution before monitoring, otherwise an incorrect size distribution will be measured for aggregating systems.

In this section, we address two questions. First, is it possible that the hydrodynamic forces break up the aggregates? Second, is there a substantial speed-up of the aggregation process by these forces? In order to answer these questions, we will subsequently give a detailed description of the hydrodynamic forces in the instrument (4.6.2.), the binding forces in different types of aggregates (4.6.3.), and the orthokinetic effect in the instrument (4.6.4.). Experimentally, we studied the influence of the hydrodynamic forces on the size distribution by variation of the flow rate in the instrument (4.7.3.).

4.6.2. Shear and extension forces

The maximum hydrodynamic force F_h between two "touching" spheres in linear flow, for two equal spheres with radius a , is given by Goren [14]:

$$F_h = 6\pi\eta a^2 G h(R) \quad (9)$$

where η is the dynamic viscosity of the solvent and G is the shear rate. The hydrodynamic factor $h(R)$ is 2.04 for spheres of equal size. This equation is valid in the creep flow regime where inertial terms may be neglected, which is the case in our system. The spheres can be either individual particles or aggregates.

Apart from shear forces, there are extension forces in the instrument. The dispersion stream is elongated by the faster flowing inner water flow (4.4.3.). Cahill et al [15] calculated the extension force by replacing, in relation (9), the shear rate by the extension rate. The hydrodynamic factor $h(R)$ is unknown under the conditions of extensional flow, but for the present purpose it is assumed to be the same as for shear. For the calculation of the hydrodynamic forces, we have to evaluate first the shear and extension rates.

Shear rates

We begin with a general discussion of the shear rates in a tube and in an

annulus. Subsequently, we apply the models to our particular flow cell.

In figure 5, the velocity distribution and shear rate for a flow in an annulus of outer radius R and inner radius κR are sketched. For a laminar Poisseuille flow, the shear rate $G(r)$ at radial distance r is given by [10b]:

$$G(r) = \frac{dV(r)}{dr} = - \frac{\Delta p R}{2\eta L} \left[\left(\frac{r}{R} \right) - \lambda^2 \left(\frac{R}{r} \right) \right] \quad (10)$$

where $V(r)$ is the flow velocity and Δp the pressure difference between the entrance and the exit. The factor L is the length of the annulus and η the dynamic viscosity of the fluid. The parameter λ is defined by $\lambda^2 = \frac{1}{2}(1-\kappa^2)/\ln(1/\kappa)$.

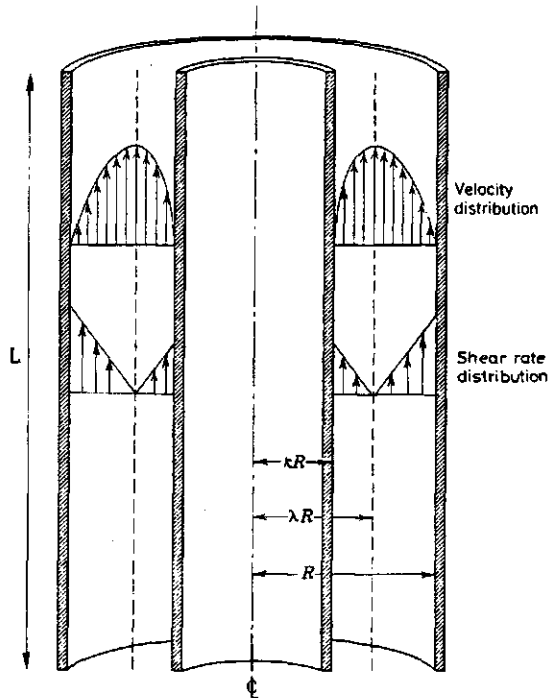


Figure 5. Flow in an annulus.

The factor $\Delta p R / 2 \eta L$ can be calculated from the mean velocity $\langle V \rangle$ of the flow:

$$\langle V \rangle = \frac{F}{\pi R^2 (1 - \kappa^2)} = \frac{\Delta p R}{2 \eta L} * \frac{R}{4} * \left[\frac{1 - \kappa^4}{1 - \kappa^2} - \frac{1 - \kappa^2}{\ln(\frac{1}{\kappa})} \right] \quad (11)$$

where F is the volume rate (flux).

Edge effects at the entrance of the annulus are ignored. In the limiting case that κ goes to zero, equation (10) and (11) reduce to those for a laminar Poisseuille flow in a tube of radius R :

$$G(r) = \frac{dV(r)}{dr} = \frac{2V(0)r}{R^2} = \frac{4Fr}{\pi R^4} \quad (12)$$

where $V(0)$ is the flow speed at the central axis.

The mean shear rate $\langle G \rangle$ in the inner part of the tube, between the central axis and radial distance r , is given by:

$$\langle G \rangle = \frac{\int_0^r G(r) r dr}{\int_0^r r dr} \quad (13)$$

In figure 6 a schematical representation of the injection of the dispersion into the inner water flow is shown. As stated before (4.4.3.) the flux of the dispersion flow is $3.05 \cdot 10^{-6} \text{ cm}^3/\text{sec}$ and the flux of the inner flow is $5.3 \cdot 10^{-2} \text{ cm}^3/\text{sec}$. We can now calculate the shear rates of the dispersion stream at different positions in the cell. The maximum shear rate of the dispersion flow in the capillary, just before entering the inner flow, equals 3.9 sec^{-1} (eq.12) and the average shear rate at this position is 2.6 sec^{-1} (eq. 13). The shear rate of the inner flow at the outer wall of the capillary is 61.6 sec^{-1} (eq. 10,11). As seen in section 4.4.3. the diameter of the dispersion stream, in the exit of the upper nozzle is $2.7 \text{ }\mu\text{m}$. The maximum shear rate of the dispersion at this position is 23.1 sec^{-1} (eq.12) and the average shear rate is 15.4 sec^{-1} (eq.13). At the intersection with the laser beam the flow diameter is expanded by a factor of two and the maximum shear rate at this position will be somewhat lower than 23.1 sec^{-1} . If the capillary

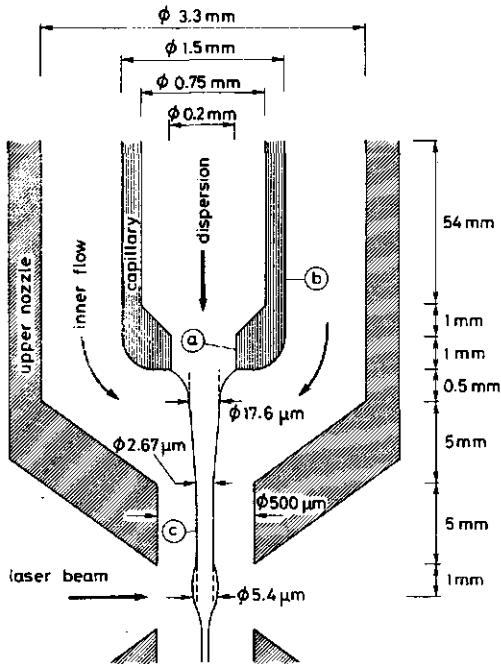


Figure 6. Schematic representation of the hydrodynamic focus. The horizontal dimensions are expanded as compared with the vertical distances. The maximum shear rates G are: (a) 3.9 s^{-1} , (b) 61.6 s^{-1} and (c) 23.1 s^{-1} .

wall is thin, the maximum shear rate rises almost immediately from 3.9 sec^{-1} to 61.6 sec^{-1} and then drops to about 23.1 sec^{-1} . For a capillary with thicker walls the initial rise will be less.

Extension rates

In figure 6 one can see that the diameter of the dispersion stream decreases non-linearly when it enters the inner flow. After this extension the inner water flow plus the dispersion flow enter the converging part of the nozzle and the diameter of the dispersion flow decreases linearly.

We consider first the extension due to injection of the dispersion flow into a faster flowing inner water flow and then the extension caused by the converging nozzle.

Non-linear decrease of the flow profile

The non-linear decrease of the flow profile of the dispersion can in principle be calculated with the help of the Navier-Stokes equation. The solution of this equation is possible but involves tedious algebra and numerical methods. Therefore, we determined the flow profile experimentally. In a perspex copy of the flow cell, the flow profile of a black-ink dispersion was photographed with the help of a microscope. The radius $r(h)$ of the dispersion flow as function of distance h (counting from the exit of the capillary) could be fitted with:

$$r(h) = C_1 \exp(-C_2 h) + C_3 \quad (14)$$

where the constants giving the best fit turned out to be $C_1 = 98.6 \mu\text{m}$, $C_2 = 1.667 \cdot 10^{-2} \mu\text{m}^{-1}$ and $C_3 = 8.85 \mu\text{m}$.

From the flux of the dispersion F one can easily derive the average speed of the dispersion $\langle V \rangle$ at distance h as $\langle V \rangle = F / \pi r(h)^2$, where $r(h)$ is given by equation (14). Because the radial velocity variation is small compared to the velocity variation in the flow direction, only the average velocity, with respect to the radial direction, is considered. The extension rate γ can be obtained by differentiating the speed of the dispersion $\langle V \rangle$ with respect to h :

$$\gamma = \frac{d \langle V \rangle}{dh} = \frac{-2F}{\pi r(h)^3} * \frac{dr(h)}{dh} \quad (15)$$

The derivative $dr(h)/dh$ equals $-C_1 C_2 \exp(-C_2 h)$, according to equation (14). In figure 7 the radius, velocity and extension rate of the dispersion flow in the non linear part are presented as function of the distance h .

Linear decrease of the flow profile

For the calculation of the extension rate in the converging nozzle, we adapt the procedure used by Cahill et al [15]. The cross-section $A(h)$ of the inner

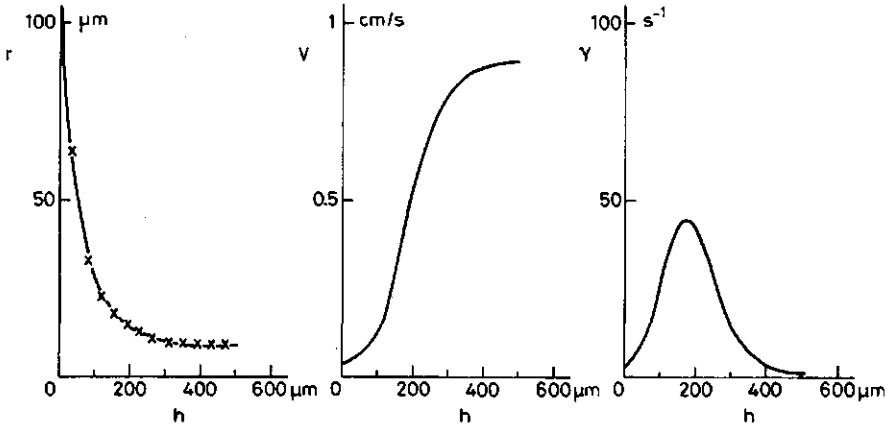


Figure 7. Radius, velocity and extension rate of the dispersion due to the acceleration of the dispersion by the faster flowing inner water flow, as a function of the distance in the flow direction (counted from the capillary exit).

flow in the nozzle is a function of the distance h . In this case the reference point of h is the height where the nozzle starts to converge, $h=0$:

$$A(h) = \pi(R - yh)^2 \quad (16)$$

Here R is the maximum nozzle radius (0.165cm) and $y=(R - R')/H$, where R' is the minimum nozzle radius (0.025cm) and H the nozzle length (0.5 cm). The mean velocity of the fluid passing through a cross-section is given simply as $\langle V \rangle = F/A(h)$. F is now the flux of the inner flow.

The velocity $V(0)$ at the symmetry axis of the nozzle is twice the mean velocity, if the Poisseuille flow is maintained. Because the flux of the dispersion is very small with respect to the flux of the inner water flow, the trajectory of the particles coincides almost with the central axis of the nozzle. The extension rate γ along this axis is obtained by differentiating $V(0)$ with respect to h :

$$\gamma = \frac{dV(0)}{dh} = \frac{4Fy}{\pi(R - yh)^3} \quad (17)$$

In figure 8a we present the radius of the inner flow and extension rate of the dispersion as a function of the distance h along the direction of the flow. One can see that the extension rate increases from 1.4 sec^{-1} to 1210 sec^{-1} and drops to zero in the exit of the upper nozzle. A much lower extension rate would occur if the shape of the upper nozzle would be adjusted. Figure 8b gives an example for $R(h) = [1/(ah+b)]^{1/2}$ where $a = (1/R^2 - 1/R^2)/H$ and $b = 1/R^2$. Another modification could be to increase the length H of the nozzle, this would also decrease the maximum extension rate.

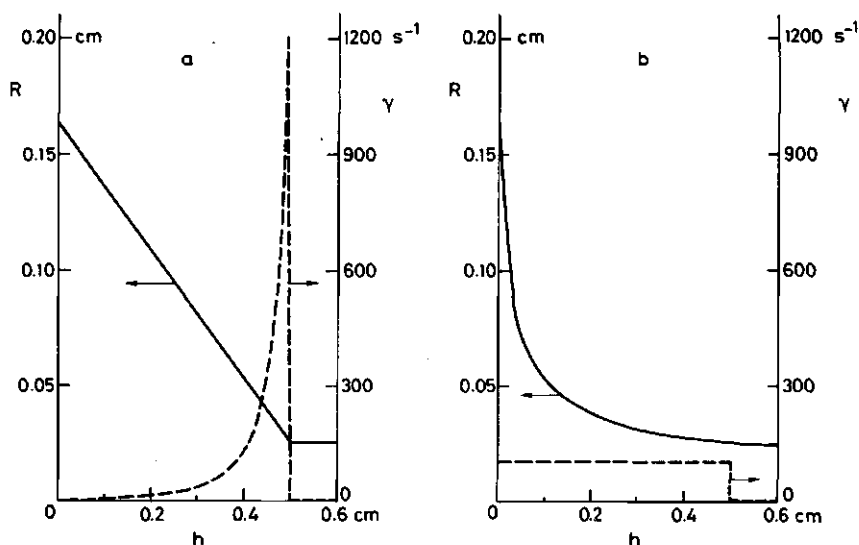


Figure 8. Radius of the nozzle and extension rate of the dispersion due to the acceleration in the nozzle, as a function of the distance in the flow direction (counted from the upper arrows in fig. 6). a/ "linear" nozzle as used in our present apparatus. b/ "inverse square root" nozzle (see text).

The hydrodynamic force

A small variation of the inner flow volume rate (flux) or a small variation in the construction of the nozzle can change the shear and extension rate considerably. Nevertheless we expect values for these rates of the same order of magnitude. In our experimental set-up, shear rates are smaller than extension rates. The biggest calculated rate is the extension rate in the nozzle: 1210 sec^{-1} . The average rate is approximately a factor of ten smaller. The hydrodynamic force acting on a doublet is calculated with equation 9 after replacing G by γ . In table 1 we present estimates of the hydrodynamic forces on doublets for different particle sizes.

table 1. hydrodynamic force

particle radius	maximum force in pN	average force in pN
220 nm	2.3	0.2
250 nm	2.9	0.3
340 nm	5.4	0.5
1000 nm	46.5	4.7

4.6.3. Binding forces

4.6.3.1. Introduction

Binding forces of aggregates depend on size, charge, material, solvent, salt concentration, polymer addition, surface modification, ageing effects and temperature. We will apply some models to estimate the binding force in an aggregate. For aggregates in which the electrostatic interactions play a dominant role, we use the DLVO theory [16,17] and compare the results with a model of Firth and Hunter [18] based on the Bingham yield relation of Gillespie [19]. For particles that flocculate by a polymer bridging mechanism, we use some results of the Scheutjens-Fleer theory [20]. Limited information is available about the direct measurement of the binding forces between particles. Some results of Visser [21] and Mühle [22] will be discussed.

4.6.3.2. DLVO-type interactions

The DLVO-theory [16,17] describes the interaction between particles as a combination of Van der Waals attraction and electrostatic double layer repulsion. For the former we use an equation due to Hamaker [23], valid for short separations. For the latter we modified an expression given by Wiese and Healy [24] by incorporating a Stern layer with thickness Δ . Combining the two results, we may write for two equal spheres with radius a at separation h :

$$V_I = -\frac{Aa}{12h} + 2\pi\epsilon_0\epsilon_r(a+\Delta)\psi^2 \ln\{1 + \exp[-\kappa(h-2\Delta)]\} \quad (18)$$

In equation (18), A is the Hamaker constant, ϵ_0 is the permittivity of vacuum, ϵ_r the relative dielectric constant of the medium, Δ the Stern layer thickness, ψ the Stern potential and κ the reciprocal Debye length. The repulsive term of Equation (18) is valid for $h \ll a$, $\kappa a > 10$ and $\psi < 60$ mV, with the premise that the potential is constant during particle approach. Other authors derived modifications, e.g., for unequal spheres [23,24], for constant charge [25,26], for particles with an adsorbed layer [27] and for surface potentials greater than 60 mV but only at large particle separation [28]. Theoretically, the distance of closest approach between particles can reduce to zero. However, in recent years evidence on reptitization has supported the idea that many coagulating particles remain separated by a finite distance [29]. Several reasons for such a minimum separation have been suggested [30-32].

We will use equation (18) to calculate the interaction free energy for polystyrene spheres in an electrolyte solution. The binding force (F_I) can be calculated by differentiating equation (18) with respect to h . We used a Hamaker constant of $7 \cdot 10^{-21}$ J [33], a particle radius of 340 nm and a temperature of 293° K. If ψ_d and Δ are known, the binding energy and force at any electrolyte concentration can be found. Unfortunately these parameters are not known accurately and only estimates can be made.

The double layer repulsion is suppressed by the presence of salt ions. We assume that the Stern layer thickness equals the radius of a potassium ion. Unfortunately, it is unknown to which extent the ion is hydrated in the Stern layer, therefore we used an average between the crystal and fully hydrated radius: 0.2 nm [34].

One could take the zeta-potential for an estimation of the Stern-potential. However, Norde [35] found that the Stern-potential at the critical coagulation concentration (0.17 mol/l in his case) was smaller than the zeta-potential. Therefore we adopted the following procedure. Firstly, we assumed the same critical coagulation concentration as Norde and calculated for two Sternlayer thicknesses (0.2 and 0.4 nm) the Stern-potential at the critical coagulation concentration from eq.(18), $dV_I/dh=0$ and $V_I=0$. We found $\psi_d=-17.8$ mV ($\Delta=0.2$ nm) and $\psi_d=-14.3$ mV ($\Delta=0.4$ nm).

Secondly, we calculated the minimum in the interaction energy with equation (18) for these two data sets and found 7.9 and 7.5 kT, respectively. We concluded that the choice of the Sternlayer thickness is not very critical for the value of the minimum energy.

Thirdly, we used $\psi_d=-17.8$ mV, $\Delta=0.2$ nm and an electrolyte concentration of 0.5 M (at this concentration most experiments were carried out) to calculate both the binding energy and the binding force. Obviously, the Stern-potential will be lower at 0.5 M than at critical coagulation conditions, and therefore we will certainly not overestimate the energy and the force. We found $V_{\min}=-34$ kT units and $F_{\min}=-660$ pN.

Effects of surface roughness and inhomogeneous charge distribution of the particles are not incorporated in this calculation but these effects will probably play a minor role in our estimation. It is quite possible that latex particles behave more like particles with constant charge at particle approach, but also this effect does not change the order of magnitude of the binding forces [36].

Firth and Hunter [18] modified an equation of Gillespie [19] which relates the Bingham yield stress τ_b to the energy to separate a doublet of spherical flocs. The Bingham yield stress can be experimentally determined from the shear stress dependence on the shear rate [37]. With their model they calculated for polymethylmethacrylate particles with radius 220 nm, at an ionic strength of 0.2 M, a binding energy and a binding force of 53 kT units and 470 pN, respectively. They also derived from this model the distance of closest approach: 0.5 nm. These results are of the same order of magnitude as our estimates from the DLVO theory.

4.6.3.3. Polymer bridging interactions

Scheutjens and Fleer [20] developed a lattice theory for the adsorption of polymers at interfaces. This theory can also be applied for interaction between particles. Scheutjens and Fleer [38] calculated the interaction free energy per lattice site between two polymer-covered plates. This energy is given in terms of kT units per lattice site and depends on the adsorbed amount of polymer, which is expressed in equivalent monolayers.

In figure 9 we show some theoretical results of Scheutjens and Fleer.

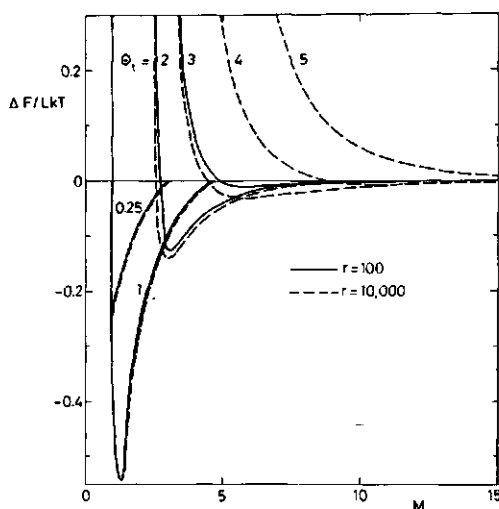


Figure 9. The energy per lattice site in kT units, due to polymer addition, as a function of the separation distance between the plates. The figure is taken from ref [38]. Curves are given for various adsorbed amounts θ , expressed in equivalent monolayers, and for two chain lengths r . Adsorption energy 1 kT per segment, Flory Huggins parameter $\chi=0.5$.

As can be seen, the interaction free energy is strongly dependent on the amount of polymer adsorbed. The molecular weight of the polymer has little influence on the interaction energy (compare a polymer of 100 segments and one of 10000 segments) provided that the adsorbed amounts are the same. The free energy per lattice site for two plates can easily be transformed to the force between two spheres using the Derjaguin method [39]. According to this

approximation, the force between two spheres with radius a at small separation h equals the free energy between two plates at the same h multiplied by $\frac{1}{2}\pi a$.

In order to use theoretical results for practical systems we have to scale these results on reality, i.e., an estimate has to be made of the size of a lattice cell. A reasonable assumption is to set the edge a lattice cell equal to the length of a statistical chain element of the polymer. With this information the interaction energy per unit area can be derived. From the volume of a lattice cell and the volume of a monomer unit, one can estimate the number of monomers in one statistical element so that an adsorbed amount can be converted to weight per unit area.

In our experiments (chapter 6) we studied the effect of Poly(ethylene) oxide adsorption on the stability of latices. Kato and Nahamura [40] give a value of 0.6 nm for the statistical segment length of Poly(ethylene) oxide. From the specific volume of PEO [41] the volume of a monomer is calculated as 0.061 nm³, hence 3.5 monomer units will fill one cubic lattice cell. Therefore, the area per lattice site is 0.36 nm² and one equivalent monolayer corresponds to 0.7 mg/m². In section 6.3. we found similar adsorption amounts for our systems used in experiment. The minimum in the interaction free energy, at an adsorption of one equivalent monolayer, is -0.55 kT units per lattice site. This corresponds to $6.3 \cdot 10^{-3}$ J/m², which represents a binding force of 3350 pN for spheres with radius 340 nm.

Several assumptions had to be made to scale theoretical results to make them applicable to our experimental system, but we expect that our estimates have the right order of magnitude. These results are valid for non-charged particles, in the case of charged particles, Van der Waals and electrical double layer interactions have to be added to find the total binding force.

4.6.3.4. Direct measurement of adhesion forces

Another approach to estimate binding forces is to interpret directly measured adhesion forces. Both Visser [21] and Mühle [22] used a centrifugal method to determine the adhesion force of spherical particles on a flat surface.

Mühle studied glass beads of 9-27 μ m in diameter adhered on glass or mica. This author found that the adhesion force between particles and surface increased a factor of ten by addition of polymer (hydrolyzed polyacryl amide). Furthermore he concluded that the adhesion force for hydrophobic glass beads is a factor of ten higher than of hydrophilic glass beads on these hydrophilic

surfaces. Unfortunately no smaller particles were investigated.

Visser studied smaller polystyrene latex spheres on a flat surface of cellophane. For particles of $0.5\ \mu\text{m}$ in diameter in a $0.1\ \text{M}$ NaCl solution (pH 6), this author found a adhesion force of $450\ \text{pN}$. From geometrical considerations it can be shown that the adhesion force between two spheres is half the adhesion force between a sphere and a flat surface. On the other hand, the Hamaker constant for polystyrene/cellophane in water is approximately half of that for polystyrene/polystyrene in water. Both effects will compensate each other, therefore a value of $450\ \text{pN}$ is a reasonable value for the binding force between two spheres of $0.5\ \mu\text{m}$ in diameter.

4.6.4. Comparison of hydrodynamic and binding forces

Unfortunately, data from experiment and theory are far from complete, and it is therefore impossible to obtain the hydrodynamic and binding forces accurately. Nevertheless an order of magnitude could be estimated and a summary is given in table 2.

table 2. Comparison of the maximum hydrodynamic force $F_{h,\text{max}}$ and the binding force F_b .

particle	radius	$F_{h,\text{max}}$	F_b	binding mechanism	basis for estimate
PMMA	220 nm	2 pN	470 pN	Van der Waals	FH theory [18]
PS	250 nm	3 pN	450 pN	DLVO-type	Visser exp [21]
PS	340 nm	5 pN	660 pN	DLVO-type	section 4.6.3.2.
PS	340 nm	5 pN	3350 pN	polymer bridg.	SF theory [38]
PS	1000 nm	47 pN	9900 pN	polymer bridg.	SF theory [38]

Abbreviations: PMMA polymethylmethacrylate, PS polystyrene

FH Firth-Hunter, SF Scheutjens-Fleer

The DLVO type binding forces in colloidal latex aggregates, without steric repulsion, are two orders of magnitude higher then the maximum hydrodynamic force in the instrument. Binding forces caused by a polymer bridging mechanism are even stronger than the DLVO binding forces, provided an optimum dosage of polymer is added.

The calculated maximum hydrodynamic force is approximately a factor of ten higher than the average value in the instrument. This maximum force is only experienced during a very short time interval. Therefore even aggregates with small binding forces, of the order of magnitude of the maximum hydrodynamic force, might very well resist de-aggregation in the instrument. The value of the hydrodynamic energy dissipation could give more detailed information about the break-up of flocs. For the present purpose, such an analysis is not necessary.

Cahill et al [15] calculated the hydrodynamic force due to the extension rate in the nozzle of a similar particle sizer, for spheres of 1 μm in diameter. They concluded on the basis of the DLVO theory that for strong aggregation (in absence of steric repulsion) no de-aggregation of doublets occurs. However, for weakly bound doublets (with steric repulsion) it might be possible to get some break-up of flocs.

4.6.5. Orthokinetic aggregation

Hydrodynamic forces can have two effects on an aggregation process: the break-up of flocs or an extra speed-up of the aggregation process. In the previous sections, the hydrodynamic forces in the instrument were compared with the binding forces. In this section we will discuss the acceleration of the aggregation in the instrument.

Hydrodynamic forces can bring particles faster together than the Brownian motion of the particles. The aggregation caused by an external force field (shear flow, gravitation, etc.) is called orthokinetic aggregation. Aggregation due to Brownian motion only is denoted as perikinetik aggregation. Before dealing with orthokinetic aggregation, we will make some comments on the aggregation kinetics in the instrument. A particle size distribution can be measured with the single particle optical sizer in typically 60 seconds. If one wants to know the particle size distribution at a certain time, one has to be sure that in the measuring interval the distribution does not change. If the reaction conditions do not satisfy this criterion then one has to dilute the samples before measuring.

Orthokinetic aggregation in Poisseuille flow has been treated by Higashitani et al [42] and by Gregory [43]. In the following, we will use the equations of Gregory and will apply his analysis for flow in the single particle optical sizer. Gregory considered particles without Brownian motion, hence perikinetik

effects are excluded. He derived the degree of orthokinetic aggregation (N/N_0) as a function of the radial position r in a Poisseuille tube flow with tube length L :

$$\frac{N}{N_0} = \exp\left\{-\frac{8\alpha_0 \phi L}{\pi R} \left[\frac{(r/R)}{1 - (r/R)^2}\right]\right\} \quad (19)$$

where N is the remaining singlet particle concentration and N_0 the initial particle concentration. The factor α_0 is the orthokinetic capture efficiency, ϕ the volume fraction of the particles and R is the tube diameter. This expression is based on a number of simplifying assumptions and is applicable only in the early stages of the aggregation process, when the majority of the particles are still single. Nevertheless equation (19) is useful for a semi-quantitative discussion.

In our instrument we also have a dispersion in nearly parallel flow, but the velocity is not constant because the dispersion stream converges. We assume the flow in the nozzle to be still a Poisseuille laminar flow (see figure 6). Let us consider a small volume element of the flowing system, see figure 10. In this figure a part of the dispersion flow and one volume element is shown. The volume element is a "ring" with thickness dr in radial direction and length dl in the direction of the flow. Equation (19) is used for each volume element after replacing L by dl . We considered the flow of the dispersion starting at the entrance of the capillary and ending at the intersection with the laser beam. After this intersection, we are not interested any more in orthokinetic effects because the particle distribution is monitored at this point.

At each position in the cell the number of volume elements in radial direction is the same. In order to calculate the total orthokinetic effect in the cell, we first multiply the orthokinetic effect of all volume elements with the same value (r/R) :

$$\left[\frac{N}{N_0}\right]_{(r/R),L} = \pi \left[\frac{N}{N_0}\right]_{(r/R),dl} \quad (20)$$

where $[N/N_0]_{(r/R),dl}$ is the orthokinetic effect of one volume element at position l . The factor $[N/N_0]_{(r/R),L}$ is the cumulative orthokinetic effect of

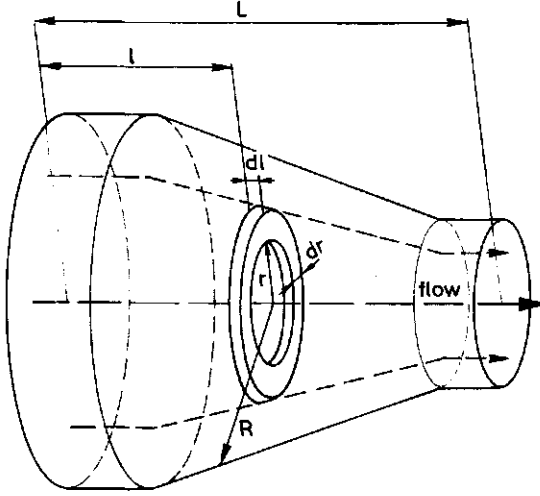


Figure 10. A part of the dispersion flow in the nozzle with one ring-shaped volume element shown. The left hand side end is the exit of the capillary, the right hand side end is at the intersection with the laser beam.

all volume elements at a radial position with the same value of (r/R) .

Secondly, we have to calculate the flow-weighted average of the orthokinetic effect in radial direction [45] to obtain the total orthokinetic effect N/N_0 at the intersection with the laser beam. In general, the velocity of the dispersion stream is largest in the centre of the stream and here more particles will pass per unit time than at the edge of the stream. Therefore one has to use a flow-weighted average.

$$\left[\frac{N}{N_0}\right] = \frac{\int_0^{R_d} \left[\frac{N}{N_0}\right](r/R), L 2\pi r v_d dr}{\int_0^{R_d} 2\pi r v_d dr} \quad (21)$$

In equation (21) R_d equals the radius of the dispersion beam at the intersection with the laser beam. As mentioned in section 4.6.2. the velocity

of the dispersion V_d equals the velocity $V(0)$ at the centre of the flow. $V(0)$ is independent of r and therefore, in our special case the volume-weighted average equals the radius-weighted average.

Until now we did not discuss the value of the orthokinetic capture efficiency α_0 . Van de Ven and Mason (44) give a semi-empirical formula for α_0 . For non-Brownian particles in the absence of any electrical repulsion :

$$\alpha_0 = f\left(\frac{A}{36\pi\eta G(r)a}\right)^{0.18} \quad (22)$$

where A is the Hamaker constant, η the viscosity of the fluid, $G(r)$ the shear rate and a the particle radius. Numerical values for the function f have been given by Van de Ven and Mason. The shear rate can be calculated with equation (12).

For the present numerical calculations we used the following values: $f=0.91$, $A=7*10^{-21}$ J, $\eta=10^{-3}$ Nsm⁻², $\phi=5*10^{-6}$ and $a=3.4*10^{-7}$ m. The geometrical properties of the cell are indicated in figure 6. In two small parts of the flow profile we have to simplify the flow profile according to the dashed lines in figure 6. Without these simplifications, we are not able to use the equations (19-21). The dashed curves yield a larger orthokinetic effect than the real flow profile hence we will not underestimate the effect.

The total orthokinetic effect is calculated to be $[N/N_0]=0.975$. The calculation is only valid in the initial stages of aggregation, but as the aggregation carries on, the volume fraction and the orthokinetic capture efficiency both decrease so the orthokinetic effect will also be smaller. We assumed laminar Poisseuille flow in all regions, which is correct except for the converging parts of the flow. Here the flow will be more a plug flow but this will certainly not enhance the orthokinetic effect.

From our computation above we may thus conclude that orthokinetic effects are of minor importance, we estimate an effect of 2-3% in the instrument and an additional effect of 2-3% by mixing, diluting and injecting. Orthokinetic effects are also discussed by Gedon [9] but only based on the average shear rate. He did not detect any difference between the coagulation rate of particles different in size (radius 0.15 and 0.25 μ m). This would not be the case with a significant degree of orthokinetic coagulation.

In section 4.7.3. we give experimental evidence which also supports the view

that the particle size distribution of an aggregating system is not affected by the hydrodynamic forces.

4.7 Test of the instrument

4.7.1. Introduction

In this section we show a few examples of particle size distributions in stable and aggregating latex dispersions. More detailed information about the effect of salt or polymer addition is presented in the next chapters.

We will verify experimentally the dependence of the light scattering intensity on particle size, as discussed in section 3.4.2, and obtain a simple power law. An similar equation is found for aggregates.

Moreover, we compare particle sizes determined with SPOS with results obtained by electron microscopy and laser beat spectroscopy. The width of the particle size distribution of monodisperse latices, determined with SPOS, is also compared with results obtained with a Coulter counter, with electron microscopy and with Flow cytometry.

Coincidence effects and dust correction will be discussed briefly.

Finally the flow rate of the inner water flow is varied by a factor of four to study the effect of the hydrodynamic forces in the instrument on the studied aggregation processes.

4.7.2. Stable systems

In figure 11, two particle size distributions of a mixture of latices are shown. In figure 11a five distinct peaks occur, each corresponding to a monodisperse latex. The horizontal axis is proportional to the light scattering intensity and the number of particles can be derived from the surface area under each peak. In figure 11b, some overlap of peaks occurs; this is due to the width of the particle size distribution of the individual samples and not due to the resolution of the instrument, which is much better. In figure 12 we plotted the light scattering intensity of the particles as a function of size (as determined from electron microscopy) on a double logarithmic scale. The slope of the fitted line is 5.52 within 3% error. This corresponds to $I \sim \nu^{1.84}$, which is in very good agreement with the theory ($I \sim \nu^{1.81}$, section 3.4.2.).

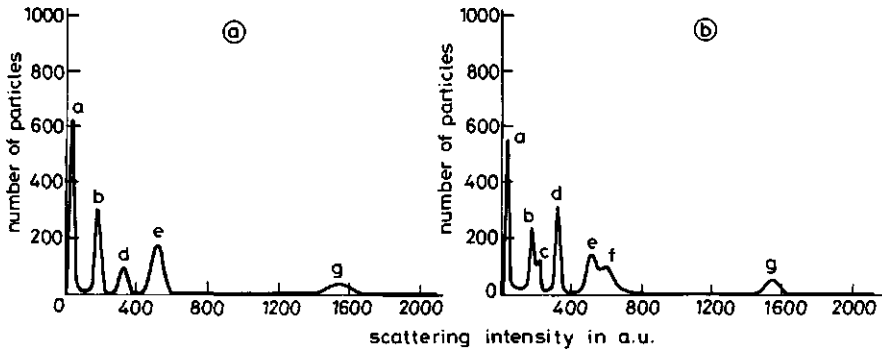


Figure 11. Particle size distribution of various latices. The used latices and diameters are: (a) VG17A $d=460$ nm, (b) F70 $d=602$ nm, (c) C1N2 $d=633$ nm, (d) VD27A $d=672$ nm, (e) B703 $d=721$ nm, (f) VD23A $d=751$ nm, (g) VD38A $d=892$ nm. Fig. 11a gives data for a mixture of 5 samples (460, 602, 672, 721, 892 nm) and fig. 11b for a mixture of all 7 samples.

The latices (a), (d), (f), (g) and (h), as denoted in figure 11 and 12, are kindly supplied by Zsom (AKZO research, the Netherlands) and used without further purification. The latices (b), (c) and (e) are synthesized by us and are described in chapter 5.

A nice feature of the SPOS is that the radius of monodisperse spherical particles can be determined without any external calibration, regardless of their optical properties, because the number of particles is measured directly. The following simple relation holds:

$$C = N \rho \frac{4}{3} \pi a^3 \quad (23)$$

where C is the weight concentration, N the particle number concentration, ρ the density and a the radius of the particles. The weight concentration can be determined gravimetrically.

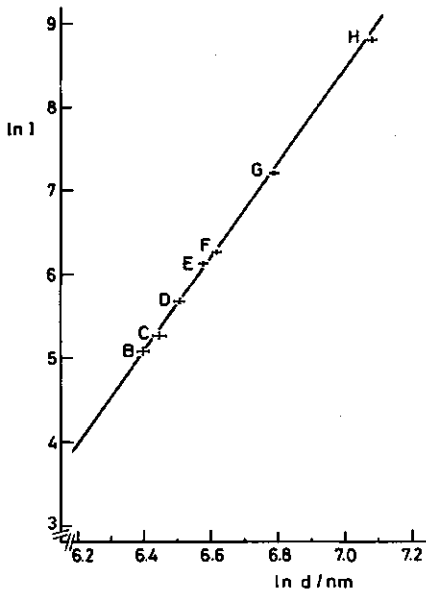


Figure 12. Double logarithmic plot of the light scattering intensity (in arbitrary units) as a function of the particle diameter. The used latices and diameters are: (b) F70 \bar{d} =602 nm, (c) C1N2 \bar{d} =633 nm, (d) VD27A \bar{d} =672 nm, (e) B703 \bar{d} =721 nm, (f) VD23A \bar{d} =751 nm, (g) VD38A \bar{d} =892 nm, (h) WR37A \bar{d} =1200nm.

Table 3 shows particle diameters of a monodisperse sample as obtained from SPOS, electron microscopy and laser beat spectroscopy.

table 3. Particle diameter of B70 latex

technique	diameter in nm
electr. micr.	697
laser beat sp.	707
SPOS	696

Within experimental error (3-5%, depending on the method) excellent agreement

is found.

The instrument has to yield reproducible signals from equally sized particles. The apparent width of the particle size distribution can be influenced by the intensity distribution in the focus, by the spatial stability of the dispersion stream, by presence of dust and by the electrical noise. In order to get an impression of the artificially broadening of the particle size distribution by the instrument, we compare the width of the particle size distribution by various techniques (table 4). The width is expressed as the coefficient of variation CV, which is the relative standard deviation, and is given for the scattering intensity, for the volume, and for the radius.

Table 4. Size distributions of monodisperse particles, as determined with various techniques.

latex	CV in	electron microscopy	SPOS	Coulter counter	Flow Cytometer
polystyrene d=696 nm	scattering intensity		3.8 %		7.8 %
	volume	4.4 %	2.1 %		
	radius	1.6 %	0.64%		
polystyrene d=1305 nm *	radius	1.2 %		2.4 %	

* reference [45].

As can be seen, the SPOS yields the smallest width, hence the error in the size distribution is very small. The Cyto flowmeter (Becton-Dickinson FACS) is not designed for measurement of small particles, hence dust removal is not so efficient as with SPOS. In electron microscopy particles can shrink or melt. Furthermore, determining the size from electron micrographs can introduce an extra error. The Coulter counter gives the largest apparent width. For very small particles one has to rely on electron microscopy.

With the present instrument, the lower limit is 0.2 μm in diameter for polystyrene latices. Below this limit dust particles and electrical noise prohibit the accurate sizing of particles.

In figure 13 we show the number of singlets detected by SPOS as a function of

the real singlet concentration. At high concentration, coincidence events cause a discrepancy between the counted number and the real particle number concentration. In principle two particles in the detection volume emit twice as much scattered light as one particle. Bowen et al [46] claim at high particle concentration a coincidence peak located at twice the singlet intensity. At first hand, this seems rather reasonable. However, the incident light intensity in the focus has a Gaussian distribution in the direction of the flow. Hence, two particles in the detection volume will not always be simultaneously at the maximum of the Gaussian light distribution, but will emit an intensity which is randomly distributed between the position of the singlet intensity and two times this value.

Dust particles can have two effects: they can broaden the size distribution and lead to a higher apparent particle number. By injecting only supernatant, one can determine the signals due to dust particles, so that the particle number can be corrected.

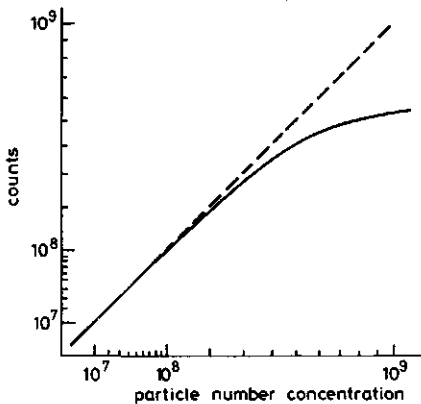


Figure 13. Counted particle concentration versus real particle concentration. Both the vertical and horizontal scale are linear in the square root. At high concentration, the number of counts deviates for real number due to coincidence errors.

4.7.3. Aggregating systems

In figure 14 a particle size distribution of an aggregating monodisperse latex

dispersion is shown. One can clearly distinguish separate aggregates up to heptaplets. The area under each peak is proportional to the number of the aggregates. By measuring such distributions at different times one can obtain information about the kinetics of aggregation.

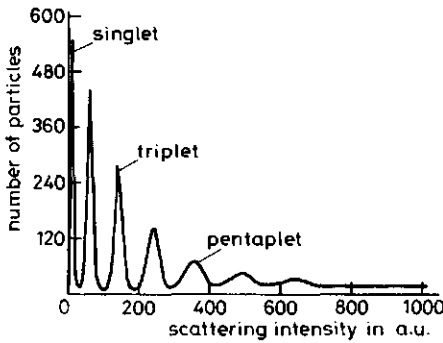


Figure 14. Aggregate size distribution of a monodisperse latex ($d=696$ nm), 200 s after mixing. $N_0 = 2 \cdot 10^{10} \text{ cm}^{-3}$, 0.2 M KNO_3 . The number of particles was counted after dilution by a factor of 400.

In figure 15 we plot the light scattering intensity of the aggregates as a function of the volume of the aggregates.

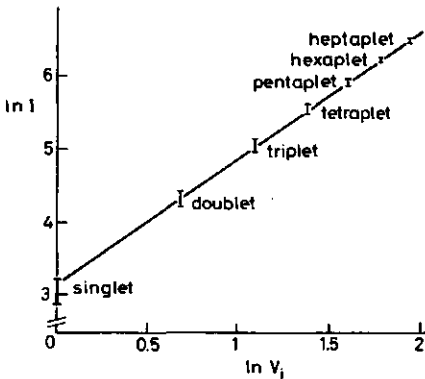


Figure 15. Light scattering intensity (in arbitrary units) as a function of the volume V_i of an aggregate of i singlets, on a double-logarithmic scale. The diameter of a singlet was 696 nm. V_i was taken as iV_1 .

From this graph we obtain:

$$I_i \sim V_i^{1.70} \quad (24)$$

where $I(i)$ is the light scattering intensity and $V(i)$ the volume of an aggregate containing i singlets. The exponent in equation (24) is somewhat lower than for spherical particles (section 4.7.2.) but still not dramatically different from the value of 2 predicted for Rayleigh scattering.

In order to check the influence of the hydrodynamic forces in the instrument on the particle size distribution, we varied the inner water flux by a factor four (between $2.3 \cdot 10^{-2}$ and $9.2 \cdot 10^{-2} \text{ cm}^3/\text{s}$). The system studied was a latex dispersion ($d=696 \text{ nm}$) in 0.5 M KNO_3 with an initial particle concentration of $4 \cdot 10^8$ particles per cm^3 . After 16 minutes we diluted a sample ten times and injected it into the instrument. No influence of the flux of the inner and outer flow on the ratio between singlet number and doublet and triplet number was found. After correction for dust particles (the number of which is proportional to the flux) the absolute particle concentration was the same within experimental error. It is advisable to vary the flow rates in the instrument for each new system to check the independence of the particle size distribution with respect to the hydrodynamic forces.

Bowen et al [46] observed break-up of aggregates at certain flow rates in a Flow Cytometer cell. We derived from their data that the average flow speed of the particles in the detection volume was 150 cm/sec . We are not able to estimate the hydrodynamic forces because the geometry of their cell is unknown to us. But if we consider the velocity of the particles in the detection volume of our instrument (13 cm/sec), it is likely that the flow rate was chosen too high in the Flow cytometer cell.

4.8 Fluorescence detection

4.8.1. Introduction

If particles are fluorescing, they can be counted and sized by SPOS using a fluorescent detection mode. Latex particles can be made fluorescing by incorporating fluorescent molecules. The angular distribution of fluorescence from dyed particles was studied by Lee and Krathovil [47,48]. The interference

effects characteristic for light scattering are completely absent with fluorescence. This observation is consistent with the fact that light scattering is a coherent sum of polarizations within the particle, while fluorescence entails an incoherent sum since the emission of the fluorescent molecules occurs randomly in time. The fluorescent intensity is proportional to the volume of the particles if the number of fluorescent molecules per unit volume is constant for each particle. The main advantage of fluorescence detection is that the measurable particle size range is larger than with light scattering detection. For very large particles deviations may occur due to screening of the fluorescent molecules in the centre of the particles.

4.8.2. Fluorescent particles

Many fluorescent molecules are available [49] which together cover the whole visible light excitation spectrum. However, until now only a small number of these molecules has been incorporated in latex particles. Kaplan et al [50] incorporated a fluorescein derivative in 0.5 μm polymethylmethacrylate spheres. Krathovil and Lee [48,51] used 0.05 μm PMMA particles dyed with dansylallamine. Several particles with fluorescent properties are commercially available but information on the fluorescent molecules used is proprietary [52]. Cummins et al [53] used polystyrene particles ($d=0.6\mu\text{m}$) dyed with perylene and they could distinguish in an aggregation process up to triplets separately. The relative standard deviation of the fluorescent intensity of their particles was 8.2%.

The particles mentioned above must be excited with a mercury lamp, a Helium-Cadmium laser or an Argon laser. We prepared a new type of melamine-formaldehyde particle ($d=4.1\mu\text{m}$) dyed with cresylviolet perchlorate [54]. This particle can be excited with an inexpensive Helium-Neon laser.

Applications of fluorescent particles are, for example, in Flow Cytometry [55], in SPOS measurements and in measurements of self diffusion by means of photobleaching or forced Rayleigh scattering techniques. A possible drawback can be an unwanted surface modification of the particles by the dye.

4.8.3. Size distribution of fluorescent particles

We measured the size distribution of the melamine-formaldehyde particles dyed with cresylviolet perchlorate in the fluorescence detection mode. In figure 16

we represent the particle size distribution of a stable dispersion in water and an aggregating dispersion in 2 M KNO_3 . The fluorescence intensity is proportional to the volume of the particles and therefore the intensity of a doublet is two times that of a singlet. In the stable system some doublets (6% in number) are detected. In 2 M electrolyte solution, the number of doublets increases with respect to the number of singlets and also some triplets are found. The relative standard deviation of the fluorescence intensity of the primary particle is 10.1 %, which corresponds to 3.9 % in particle radius. The width of the distribution can be caused by different sized particles or by the fact that the number of fluorescent molecules for each particle is not perfectly constant. Therefore the resolution in size of the SPOS in fluorescence detection is smaller than with light scattering detection. The particle radius was determined from the total number of primary particles, see section 4.7.2; the result was $d=4.1 \mu\text{m}$.

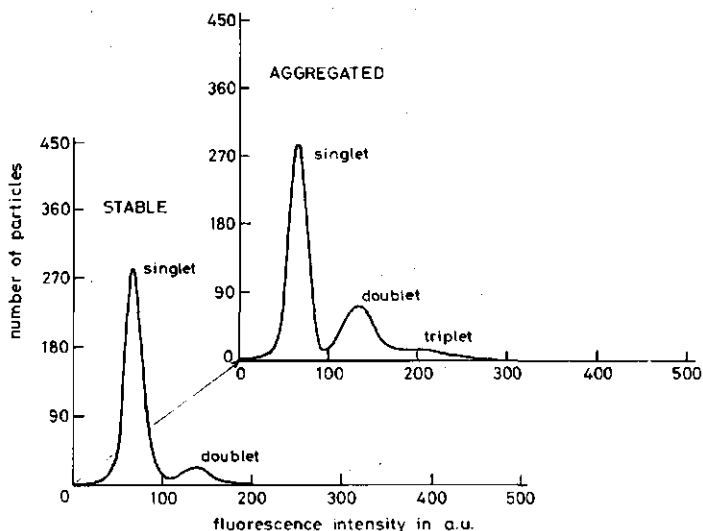


Figure 16. Aggregate size distribution of fluorescent melamine-formaldehyde particles measured in fluorescent detection mode. The aggregating system is measured 200 s after mixing. $N_0=2 \cdot 10^{10} \text{ cm}^{-3}$, 2 M KNO_3 . The number of particles was counted after dilution by a factor of 400.

Although the light scattering intensity is much higher than the fluorescence intensity, the latter can be monitored relatively easily because dust does not interfere. In the experiments, the scattered intensity is effectively blocked with a 665 nm cut-off filter. The light scattering signal after the filter was found to be a factor of 20 smaller than the fluorescent signal. This could be checked by using particles of the same size and type but without the dye. Reflections and light scattering from dust particles are also blocked by the filter.

4.8.4. Discussion

In the light scattering detection mode a lower limit is set to the measurable particle size by the presence of disturbing dust particles. In the fluorescent detection mode, dust particles are, in principle, not monitored and smaller particles can be measured. Two conditions are necessary: the fluorescent signal must be larger than the electrical noise and small monodisperse fluorescent particles have to be available. With the fluorescent particles described so far, the resolution in particle size in the fluorescence detection mode is always smaller than in light scattering detection mode.

4.9. Conclusions

We summarize the most important aspects of the SPOS-instrument, the resolution in particle size, and the influence of the hydrodynamic forces in the instrument.

For stable systems, the resolution in particle size of the SPOS-instrument is superior to electron microscopy, Coulter counters, and Flow cytometers. We obtained such high resolution by minimizing the stray light of the incident light reaching the photomultiplier (see section 4.3.4.), by ensuring a homogeneous light intensity distribution in the detection volume (see section 4.3.3.) and by lowering the number of dust particles in the inner and outer water flow (see section 4.4.4.).

In the present set-up, the latter aspect determines the size of the smallest particle which can be detected unambiguously. A further decrease of dust particles can be reached by using a filtering system in which 99% of the filtered water is fed back to the input gate of the filtering system. In this way the water is effectively filtered 100 times before reaching the flow cell.

Before filtering, the water must be de-gassed, otherwise light scattered by gass bubbles (created on the particle surfaces during particle injection) interferes with the scattering signals of the particles.

For aggregating systems, the number of aggregates types (containing different number of singlets) which can be distinguished separately is not only determined by the resolution in particle size but also by the size distribution of the primary particles. For nearly monodisperse polystyrene latices, up to heptaplets could be distinguished separately.

Shear and extension forces in the flow cell are inevitable if a hydrodynamic focus is created. However, these hydrodynamic forces should not influence the particle size distribution before monitoring, otherwise an incorrect size distribution will be measured for aggregating systems. From detailed calculations on these forces and by estimating binding forces in aggregates, we found that aggregates do not break up appreciably in the instrument, both for Van der Waals type binding forces and in the case of polymer bridging. Also, we demonstrated that orthokinetic aggregation is of minor importance in the instrument. Consequently, a reliable and versatile instrument is now available for the studying coagulation and flocculation kinetics.

References

1. Kogelnik, A., Bell Syst. Tech. J. 44, 455 (1965).
2. Ready, J.F., "Industrial application of lasers", p. 38, Academic Press, New York, 1979.
3. Sears, F.W., "Optics", 3rd ed., p. 107, Addison-Wesley publishing company, Amsterdam, 1974.
4. Born, M., and Wolf, E., "Principles of optics", fifth ed., p. 459, Pergamon Press, Oxford, 1975.
5. "Optics guide 2", p. 27, Melles Griot, Irvine, 1982.
6. Cahill, J., Cummins, P.G., Staples, E.J., and Thompson, L.G., Colloids Surf. 18, 189, (1986).
7. Hershberger, L.W., Callis, J.B., and Christian, G.D., Analytical Chemistry. 51, 1444 (1979).
8. McFadyen, P., and Smith, A.L., J. Colloid Interface Sci. 45, 573 (1973).
9. Gedan, H., thesis, Akademie der Wissenschaften Berlin, D.D.R., (1983).
10. Bird, R.B., Stewart, W.E., and Lightfoot, E.N., "Transport Phenomena", (a) p. 47, (b) p. 49, John Wiley & Sons, 1960.
11. Schiller, L., Z. Ang. Math. Mech. 2, 96, (1922).
12. Boussinesq, J., C. R. Acad. Sci.(Paris), p. 113, 9 (1891).
13. Langhaar, H.L., J. Appl. Mech. 9, A55 (1942).
14. Goren, S.L., J. Colloid Interface Sci. 36, 94 (1971).
15. Cahill, J., Cummins, P.G., Staples, E.J., and Thompson, L., J. Colloid Interface Sci. 117, 406 (1987).
16. Deryaguin, B.V., Trans. Faraday Soc. 36, 203, 730 (1940).
Deryaguin, B.V., and Landau, L.D., Acta Physicochim. 14, 633 (1941).
17. Verwey, E.J., and Overbeek, J.Th.G., "Theory of the stability of Lyophobic Colloids", Elsevier, Amsterdam, 1948.
18. Firth, B.A., and Hunter, R.J., J. Colloid Interface Sci. 57, 248 (1976).
19. Gillespie, T., J. Colloid Sci. 15, 219 (1960).
20. Scheutjens, J.M.H.M., and Fleer, G.J., J. Phys. Chem., 83, 1619 (1979).
ibid, 84, 178 (1980).
21. Visser, J., J. Colloid Interface Sci., 55, 664 (1976).
22. Mühle, K., Coll. Polym. Sci. 263, 660 (1985).
Mühle, K., Colloids Surf. 22, 249 (1987).
23. Hamaker, H.C., Physica. 4, 1058 (1937).

24. Wiese, G.R., and Healy, T.W., Trans. Faraday Soc. 66, 420 (1970)
25. Hogg, R., Healy, T.W., and Fuerstenau, D.W., Trans. Faraday Soc. 62, 1638 (1966).
26. Frens, G., thesis, State University Utrecht, The Netherlands, (1968).
27. Vincent, B., J. Colloid Interface Sci., 42, 270 (1973).
28. Bell, G.M., Levine, S., and McCartney, L.N., J. Colloid Interface Sci. 33, 335 (1970). Equation 44.
29. Overbeek, J.Th.G., J. Colloid Interface Sci. 58, 408 (1977).
30. Pashley, R.M., J. Colloid Interface Sci. 80, 153 (1981).
Pashley, R.M., J. Colloid Interface Sci. 83, 531 (1981).
Pashley, R.M., and Israelachvili, J.N., J. Colloid Interface Sci. 97, 446 (1984).
31. Put van der, A., thesis, Agricultural University Wageningen, The Netherlands, (1980).
32. Bensley, C.N., and Hunter, R.J., J. Colloid Interface Sci. 92, 448 (1983).
33. Lichtenbelt, J., thesis, State University Utrecht, The Netherlands, (1974).
34. Conway, B.E., Ionic Hydration in Chemistry and Biophysics, p. 73, Elsevier, Amsterdam (1981).
35. Norde, W., thesis, Agricultural University Wageningen, The Netherlands, (1976).
36. Honig, E.P., and Mul, P.M., J. Colloid Interface Sci. 36, 258 (1971).
37. Friend, J.P., and Hunter, R.J., J. Colloid Interface Sci. 37, 548 (1971).
38. Scheutjens, J.M.H.M., and Fleer, G.J., Macromolecules. 18, 1882 (1985).
39. Deryaguin, B.V., Kolloid-Z. 60, 155 (1934).
40. Kato, T., Nakamura, K., et al., Polym. J. 13, 1037 (1981).
41. Brandrup, J., and Immergut, E.H., "Polymer Handbook", p. IV-100, Interscience Publishers(Wiley & Sons), New York, 1966.
42. Higashitani, k., Miyafusa, S., Matsuda, T., and Matsuno, Y., J. Colloid Interface Sci., 77, 21 (1980).
43. Gregory, J., in "The effect of polymer on the dispersion properties" (Th.F.Tadros, ed), p. 301, Academic Press, London, 1982.
44. Ven van de, T.G.M., and Mason, S.G., Colloid Polym. Sci. 255, 468 (1977).
45. Spielman, L., and Goren, S.L., J. Colloid Interface Sci. 26, 175 (1968).

46. Bowen, M.S., Broide, M.L., and Cohen, R.J., *J. Colloid Interface Sci.* 105, 605 (1985).
47. Lee, E., Benner, R.E., Fenn, J.B., and Chang, R.K., *Appl. Optics.* 17, 1980 (1978).
48. Kratochvil, J.P., Lee, M.P., and Kerker, M., *Appl. Optics.* 17, 1978 (1978).
49. "Kodak laser products", publication nr jj-169, Eastman kodak company, Rochester, U.S.A. (1982).
50. Kaplan, M.R., Calef, E., Bercovici, T., and Gitler, C., *Biochimica et Biophysica Acta*, 728, 112 (1983).
51. Lee, M., thesis, Clarkson college of technology, U.S.A., (1977).
52. "Polyfacts", nr 17, p. 8, Polysciences, Northampton, England, (1985).
53. Cummins, P.G., Staples, E.J., Thompson, L.G., Smith, A.L., and Pope, L., *J. Colloid Interface Sci.* 92, 189 (1983).
54. Pelssers, E.G.M., and Lerche, K-H., will be submitted to *Colloids and Surfaces*.
55. Fulwyler, M.L., McDonald, C.W., and Haynes, J.L., in "Flow Cytometry and Sorting" (M.R.Melamed, ed), p 653, Wiley, New York, (1979).

CHAPTER 5. PREPARATION OF POLYSTYRENE LATICES AND THEIR COAGULATION BY SALT

5.1. Introduction

In the previous chapter we described the single particle optical sizer, in this chapter we will apply this instrument to study the coagulation kinetics. As indicated in chapter 1, we use the term coagulation for the aggregation caused by salt. In the next chapter we will discuss the kinetics of flocculation kinetics, which we define as the aggregation due to polymer.

Coagulation is a central problem in the field of colloid chemistry. Particles will stick together during collisions if the attraction forces dominate the repulsion forces. These interaction forces are described by the DLVO theory [1,2]. However, this theory does not give information about the kinetics of coagulation.

The kinetic aspect of the colloidal instability, i.e., the aggregation of a colloidal system, was quantified by Von Smoluchowski [3]. In his theory an equation is given for the time dependence of the aggregation process. The process is supposed to be diffusion controlled. Every collision is assumed to create an aggregate if the colliding particles have approached one another within a distance where the attraction forces become dominant. Fuchs [4] incorporated an interaction potential between the particles in the theory. In this case the effectivity of a collision to create an aggregate depends on the attractive and repulsive interactions.

In the Smoluchowski-Fuchs kinetic theory many assumptions are made. The most important are: (i) primary particles are monodisperse, (ii) the rate of coagulation for the different aggregation steps is equal although the size and morphology of the aggregates are different, (iii) only collisions between two particles (aggregates) are considered, (iv) the aggregation process is irreversible, (v) only the steady state process is taken into account. The non-steady state process has been studied by Von Smoluchowski [3] and Roeberson [5]. They concluded that the rate of non-steady state aggregation is larger than that of the steady state process.

The experimentally determined overall rate constant of fast aggregation (i.e., at high salt concentrations) is approximately half the theoretically predicted value of the Von Smoluchowski theory. This deviation has been explained either by hydrodynamic interactions [6-9] or by the reversibility of the process [10,11]. A review on the coagulation process has been given by Overbeek [12].

A quite different approach is the dynamical simulation of aggregation on a computer [13,14]. Such simulations are especially useful for studying the geometrical properties of the clusters. With this simulations it is found that the evolution of the cluster size distribution exhibits a simple scaling behaviour [15]. Possibly, the SPOS technique could be used to test such behaviour experimentally. However, for the present purpose we disregard this application.

Until rather recently, the experimental study of the aggregation process was restricted to the measurement of some qualitative parameter (turbidity, sedimentation, light scattering) for the monitoring the aggregation, or to the determination of the initial rate of the total process from which an overall rate constant could be obtained. For more details we refer to chapter 2. With the single particle optical sizer we are able to measure fast and reliably the aggregate distribution in time and we are now in the position to study the coagulation process in more detail. Furthermore, the number of aggregates (up to heptaplets) can be followed in time without disturbing effects from large aggregates, as experienced, for example, with turbidity measurements. In the study of salt or polymer induced aggregation the SPOS technique yields, at present, more information than any other technique.

Only little information was obtained so far about the values of the rate constants for the different aggregation steps [16-18]. We have performed coagulation experiments to determine the rate constants of the first three coagulation steps (singlet+singlet, singlet+doublet and singlet+triplet). The latex and salt were mixed and after some time diluted to be measured in the SPOS-instrument. In order to study the effect of the mixing on the aggregation process, we used different mixing cells.

For these experiments, we used polystyrene latices, which are widely used in a variety of applications. For example, in industry they are employed as fillers in paper and textiles, or in the well-known latex paint. A more sophisticated application is in diagnostic tests [19,20] and for the calibration of various instruments as Flow Cytometers, sedimentation equipment, and light scattering apparatus. From a scientific point of view, latices constitute one of the most common colloidal model systems.

The latex particles can be prepared very monodisperse in size and refractive index. These properties make the particles especially suited for the study of aggregation with the Single Particle Optical Sizer (SPOS). Furthermore, several data for the overall rate constant have been reported [17,18,21-28],

which can be compared with our results. We first describe the synthesis and characterization of these latices. In sections 5.3.3. and 5.3.4 we present and discuss experimental results on the coagulation.

5.2. Synthesis

5.2.1. Introduction

In order to obtain latices with a clean surface we synthesized emulsifier free polystyrene latices. After synthesis, purification is needed; monomers and salt have to be removed. In the literature one finds various methods of purification [29,30]. We therefore purified our latices in different ways, and determined the surface charge in order to check the result. Size and monodispersity were determined with electron transmission microscopy. Zeta-potential measurements were conducted with a Malvern Zeta-sizer 2.

5.2.2. Polymerization

We carried out the polymerization as described by Goodwin [31] and Furasawa [32] using $K_2S_2O_8$ as initiator and NaCl or $KHCO_3$ as the electrolyte. The temperature was $70^\circ C$ and the styrene concentration 0.87 mol/l. In table 1 we give polymerization conditions and properties of the various prepared samples.

Table 1. Synthesis conditions and properties of the latices

latex	$[K_2S_2O_8]$ mM	$[NaCl]$ mM	$[KHCO_3]$ mM	water ml	d_{63}/d_{30}	diameter nm	σ_0 $\mu C/cm^2$
F70	2.76	14	-	640	1.0004	602	5.4
C3N4	3.74	-	5	170	1.002	629	7.5
C1N2	1.85	-	10	170	1.004	633	4.8
B70	2.76	3	-	640	1.005	696	4.7
B703	2.76	3	-	170	1.004	721	4.9

In this table the uniformity coefficient is defined as d_{63}/d_{30} , where $(d_{xy})^{x-y} = \frac{\sum n_i d_i^x}{\sum n_i d_i^y}$ and d_i is the diameter of the particles in size fraction i . The salt concentrations in table 1 are those in the aqueous phase.

The parameter σ_0 is the surface charge density of the particles.

All materials used were of analytical grade and the water was CO_2 free Millipore super Q quality. All latices were stored in a refrigerator to prevent microbial contamination. Wilkinson [33] reported microbial growth in latices, and we noticed the same for latices stored outside the refrigerator at room temperature. The latices were kept at neutral pH, because the hydrolysis of the charged groups (SO_4^-) on the latex surface is catalysed by both acid and base [34].

5.2.3. Purification

All the latices mentioned in table 1 were purified by distillation under reduced pressure at 40°C and subsequent mixed bed ion exchange, in order to remove monomers and small oligomers. During the distillation also some water is lost, but by supplying water the volume of the latex was kept nearly constant. Many investigators purified their latices by steam stripping [29], but this may have the disadvantage that due to high temperature of the steam the sulphate groups hydrolyse. Steam stripping removes residual monomer very efficiently: Zsom [35] could detect only very little monomer left in the latices after steamstripping ($\approx 0.01\%$ with respect to the particle weight) whereas after distillation in a rotavapor 1-2% monomer was left in the latices. We used teflon between the glass parts of the rotavapor, in order to prevent possible contamination of the latex with grease.

The effect of the purification method on the surface charge of the latex was studied for one sample. Latex F70 was purified by distillation as a first step, followed by four different second purification steps: mixed bed ion exchange [36], serum replacement [29], centrifugation [37] and dialysis [29]. The surface charge density of the latex F70 purified with the former three methods was found to be about the same ($5.7 \mu\text{C}/\text{cm}^2 \pm 6\%$) but the dialysis gave a lower σ_0 ($4 \mu\text{C}/\text{cm}^2$). The dialysis procedure seems to catalyse the hydrolysis of the sulphate groups; in some cases we could detect two types of surface groups by conductometry. Some authors mention polyelectrolyte contamination of the latices purified by the ion exchange method [36] but, by using the mixed bed technique this is minimized. If the surface charge is rather low, aggregation can occur upon centrifugation or serum replacement. A detailed discussion of the synthesis and purification method has been given by Hearn [29].

5.2.4. Characterization

The surface charge density, σ_0 of latices was determined conductometrically [29,38]. The results are presented in table 1 (last column). With a transmission electron microscope (T400 Philips) we measured the particle size and uniformity coefficient, see table 1. For each sample, at least 200 particles were sized from the electron microscope photographs.

The electrophoretic mobility of the cleaned B70 latex particles was measured with a Malvern Zeta-sizer 2 in a KNO_3 solution at pH 6, see figure 1. The equations of O'Brien and White [39] were used for the calculation of the zeta-potential from the electrophoretic mobility data. The maximum in the zeta-potential as function of the salt concentration is rather surprising and cannot be explained in terms of current electrical double layer theory. Other authors have also found this strange behaviour [40,41,42]. In this case the measured mobility is almost proportional to the zeta-potential.

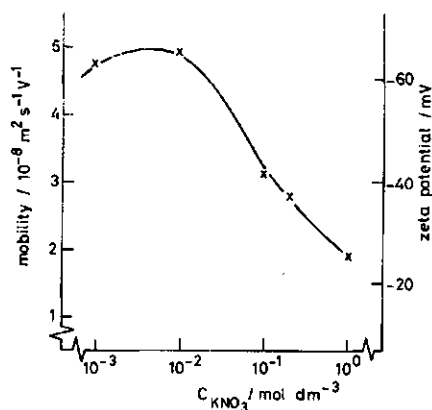


Figure 1. The effect of the ionic strength on the electrophoretic mobility and on the zeta-potential of polystyrene latex B70.

5.3. Coagulation

5.3.1. Introduction

The rapid coagulation of polystyrene latices was investigated by Single Particle Optical Sizing (SPOS). In this way the numbers of singlets, doublets and triplets could be measured as a function of time. It turned out that the reproducibility of the measurement depends on the method of mixing. We used three different mixing cells. The experimental data were analyzed to yield the rate constants for the different steps of the coagulation.

Before discussing our own experiments, we give an overview of literature data.

5.3.2. Overview of literature data

Rapid coagulation occurs when enough electrolyte is added to entirely suppress electrostatic repulsion between interacting particles. Under these conditions, the rate of coagulation is only determined by the Brownian diffusion of the particles and by their hydrodynamic interaction at short separation.

According to Von Smoluchowski [3], the overall rate constant k_s of rapid perikinetetic coagulation, defined by $dN/dt = -k_s N^2$ where N is the total particle concentration, is given by:

$$k_s = \frac{4kT}{3\eta} = 5.43 * 10^{-12} \text{ cm}^3 \text{ sec}^{-1} \quad (\text{water, } T=293^\circ\text{K}) \quad (1)$$

where k is the Boltzmann constant, η the viscosity and T the temperature.

A literature survey yields various experimentally determined rate constants, listed in table 2. As can be seen from this table, they are approximately a factor 2 smaller than the Smoluchowski value. This is presumably due to hydrodynamic interactions. The values for k_s in table 2 represent the values determined at various initial particle concentrations ($N_0 = 5 \cdot 10^6 - 5 \cdot 10^9 \text{ cm}^{-3}$) in the temperature range 293 - 298 K. The third column gives the average values reduced to 293 K and in a much narrower range ($10^8 - 10^9 \text{ cm}^{-3}$) of the initial particle concentration, around $N_0 \approx 5 \cdot 10^8 \text{ cm}^{-3}$. This column makes a useful comparison possible.

Table 2. Literature values of the perikinetetic rate constant k_s for silver iodide (AgI), polystyrene (PS) and haematite (α -Fe₂O₃).

particles	k_s ($10^{12} \text{ cm}^3 \text{ s}^{-1}$)	k_s at $N_0 = 5 \cdot 10^8 \text{ cm}^{-3}$ ($10^{12} \text{ cm}^3 \text{ s}^{-1}$)	reference
AgI	1.6 - 2.55	-	[21]
PS	3.25 - 3.9	3.1	[22]
PS	1.25 - 3.25	2.9	[23]
PS	3.3 - 3.5	3.1	[24]
PS	2.6 - 6	3.4	[25]
PS	1.65 - 3.4	3.0 (N_0 unknown)	[26]
PS	2.1 - 2.45	2.0	[27]
PS	2.6 - 3.8	3.2	[17]
PS	1.5	1.3	[18]
α -Fe ₂ O ₃	0.5 - 2	-	[28]

Hatton et al [25] and Matthews and Rhodes [23] find an increasing rate constant as function of initial particle concentration, in contradistinction to Lips and Willis [24]. Such a dependence can not be explained by the Smoluchowski theory.

In order to study the perikinetetic coagulation, the mixing of the dispersion and the salt must be fast on the time scale of the coagulation process and must produce a homogeneous mixture. Some authors used a Stopped Flow device to mix salt and dispersion [26,27], some injected a small volume of a highly concentrated salt solution [17,23,25,28], others mixed equal volumes of salt and dispersion [18,22] and sometimes no information on the method is given [24]. We used three mixing devices and will compare the results below.

Some aspects of the coagulation process are still poorly understood. For example, the DLVO theory predicts that the rate constant of slow coagulation should depend on particle size, but this is not found experimentally [28,43,45]. Gedan et al [18] and Cahill et al [17] studied slow coagulation looking for evidence of reversible coagulation, but such evidence was not found. Cahill et al [17] also compared their experimental results with theoretically proposed scaling relations for the aggregation [15].

The Smoluchowski theory implies that there is no difference in perikinetetic

rate constant of rapid aggregation for different 1:1 electrolytes, differently charged particles, different charged groups or particles with different size. Gedan [45] discusses data obtained with latices which seem to support this. Other aspects of the coagulation process are the effect of the secondary minimum studied by Reynolds [40], effects of shear and particle concentration (Zollars [46]), and processes leading to gelation (Buscall [47]).

5.3.3. Experimental

The initial particle concentration in the flocculating system was usually $4.1 \cdot 10^8 \text{ cm}^{-3}$ and the KNO_3 concentration was in most cases 0.5 mol/l. Plastic tubes and glassware were thoroughly cleaned and washed with Millipore super Q water. Latex dispersions were sonicated 45 minutes before use, in order to remove any doublets present. The presence of doublets is probably caused by coagulation in a secondary minimum. Some authors [22,23] could not remove doublets by sonicating: in this case possibly persistent doublets occur that had been formed by primary minimum coagulation during the synthesis. Rapid coagulation was induced by mixing 10 ml latex with 10 ml salt solution in a T-shaped cell, see figure 2. Mixing is carried out by pressing both injection syringes simultaneously. The mixing time in the T-shaped cell is well below one second. The plunger of the collecting syringe minimizes the turbulent movements of the mixture.

After carefully removing the plunger of the collecting syringe, we sampled 1 ml aliquots at regular time intervals. We used a finntip with a wide bore to prevent orthokinetic aggregation during sampling. The samples were diluted ten times with water and injected in the SPOS. By this dilution, a particle number concentration in the proper range was obtained for the SPOS measurement. Moreover, the coagulation process is frozen, not only because the particle concentration is ten times lower but also because the salt concentration is reduced to below the critical salt concentration. The change of particle number concentration in the diluted sample was found to be negligible between sampling and monitoring (this cycle takes 200 seconds). Cahill et al [17] suspected some deposition of coagulating latex particles in the syringe of their SPOS instrument over relatively long periods. We avoided this effect by conducting the aggregation experiment outside the SPOS instrument and sampling, rather than allowing the aggregation to proceed within the syringe of the SPOS. Erroneous results due to mixing of consecutive samples in the

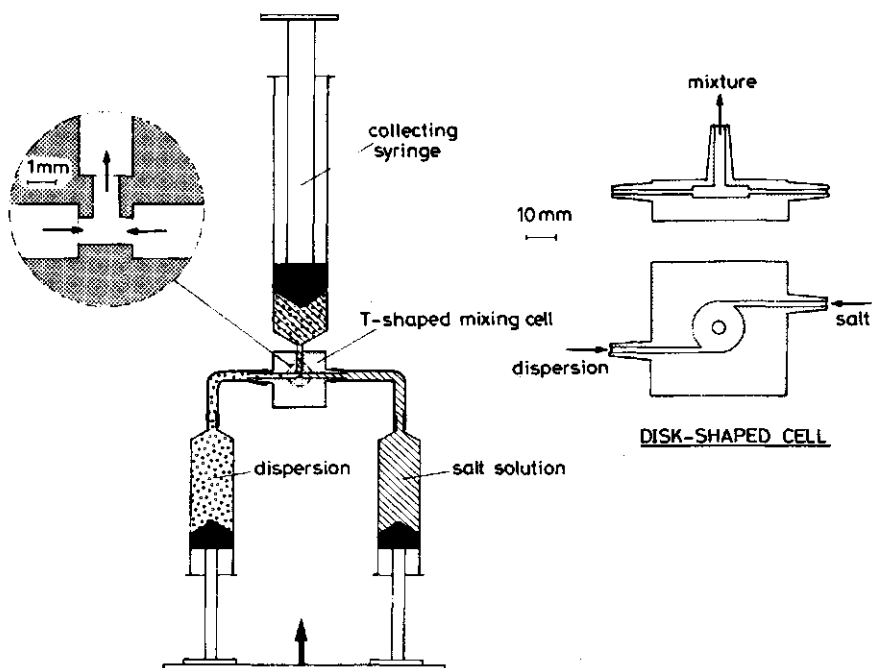


Figure 2. Mixing device, with two types of mixing cells, a T-shaped cell (left) and a disk-shaped cell (right).

SPOS were prevented by rinsing the flowcell with 1.5 ml of each sample before monitoring the particle size distribution. The usual counting period was 60 seconds.

The hydrodynamic forces acting on the dispersion during mixing, sampling, diluting, injecting and monitoring do not influence the rate of aggregation by more than 5%. This aspect was discussed extensively in section 4.6.

In order to study the effect of various mixing procedures we used not only the T-cell, but also two other devices. One was the injection and mixing part of a Durrum-Gibson stopped-flow spectrophotometer. The transmission cell for measuring the turbidity was replaced by a collecting syringe. Samples with a volume of 0.2 ml were taken from this syringe and treated as described above. The second was a disk-shaped cell (figure 2). We discuss these procedures in the next section.

5.3.4. Results

A typical particle size distribution of an aggregated latex dispersion is shown in figure 3.

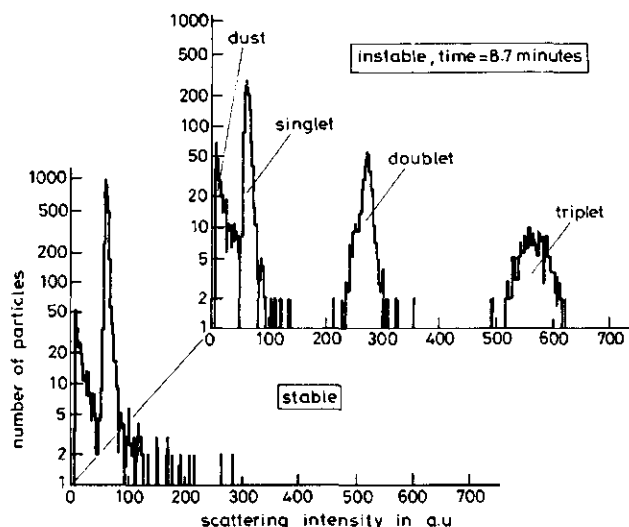


Figure 3. Size distribution of a stable B70-dispersion and of an aggregating dispersion 8.7 min. after mixing. $N_0 = 4.1 \cdot 10^8 \text{ cm}^{-3}$. The final KNO_3 concentration in the aggregating system was 0.5 M. The spectra shown are not corrected for dust.

These data were obtained after mixing in the T-cell. As can be seen some dust particles are present, originating from the carrier water in the SPOS. By measuring only the water we determined the number of dust particles and subtracted these from the spectra as shown in figure 3. To this end, the dead time correction (section 4.5.) had to be applied. In this way we obtain data of the kind shown in figure 4 where concentrations of singlets, doublets and triplets as a function of the coagulation time are shown.

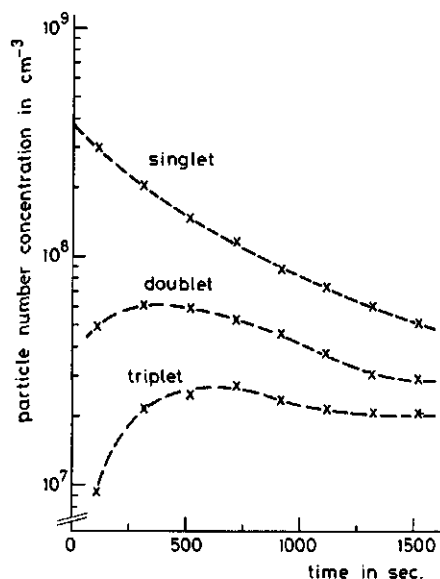
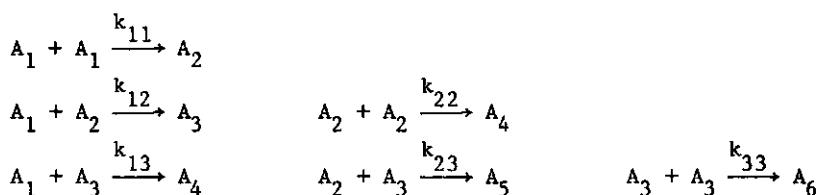


Figure 4. The evolution of the singlet, doublet and triplet particle number concentration as a function of time. $N_0 = 4.1 \cdot 10^8 \text{ cm}^{-3}$, $[\text{KNO}_3] = 0.5 \text{ M}$.

We analyse these data as follows. As in reaction kinetics, the process of coagulation can be treated as a set of consecutive reactions. In the early stages of the coagulation, the following reactions occur:



In this scheme, A_i denotes an aggregate consisting of i singlets. Assuming that in the initial process the concentration of tetraplets and higher aggregates is negligible, the change in the concentration of the singlets, doublets and triplets is described by the following set of differential equations:

$$\frac{dN_1}{dt} = -k_{11}N_1^2 - k_{12}N_1N_2 - k_{13}N_1N_3 \quad (2)$$

$$\frac{dN_2}{dt} = k_{11}N_1^2 - k_{12}N_1N_2 - k_{22}N_2^2 - k_{23}N_2N_3 \quad (3)$$

$$\frac{dN_3}{dt} = k_{12}N_1N_2 - k_{13}N_1N_3 - k_{23}N_2N_3 - k_{33}N_3^2 \quad (4)$$

where N_1 , N_2 , N_3 are the number concentrations of singlets, doublets and triplets, respectively, and t is the time. If the concentration of higher aggregates is not negligible then these equations have to be extended with terms describing the reaction steps of higher aggregates. In fact we used the truncated equations given above.

These non-linear differential equations can not be solved analytically. However the experimental data (N_1, N_2, N_3 as a function of time) can be fitted on a numerical integration of these equations. With an iteration method the fitting parameters ($k_{11}, k_{12}, k_{13}, k_{22}, k_{23}$ and k_{33}) were adjusted to yield the best fit. We used the BMDP Statistical Software [48] on a VAX 8700 computer to calculate the best fitting parameters. The experimental data points were obtained by averaging the number of singlets, doublets and triplets after various coagulation times from six coagulation experiments, all carried out according to the description in the experimental section. We used B70 latex and 0.5 M KNO_3 as salt. In figure 4 the time dependence of the particle number concentration is shown for one of these experiments and in table 3 the determined rate constants are presented. The values of these constants are discussed in the next section.

table 3. The different rate constants at 293°K

k_{ij} in $10^{12} \cdot \text{cm}^3 \cdot \text{sec}^{-1}$					
k_{11}	k_{12}	k_{13}	k_{22}	k_{23}	k_{33}
6.0 ± 0.1	7.2 ± 0.6	10 ± 2	6 ± 5	10 ± 6	-

A much simpler way to determine the rate constant k_{11} is to use the Von Smoluchowski equation for the evolution of the number of primary particles.

Von Smoluchowski assumed all rate constants to be equal to k_{11} . This simplification makes it possible to solve the differential equations analytically, even without truncation, i.e., taking into account the concentrations of all aggregate types.

Von Smoluchowski found for the decrease of the primary particles:

$$N_1 = N_0 (1 + k_{11} N_0 t)^{-2} \quad (5)$$

We know from table 3 that higher rate constants are not exactly equal to k_{11} . As we will see below, the error created by using the Von Smoluchowski equation is only very small.

For the same experiment as presented in figure 4 we plotted $N_1^{-1/2}$ as a function of time, see figure 5.

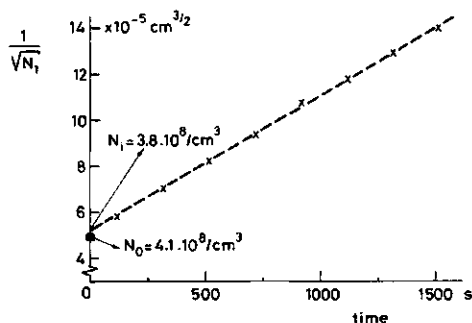


Figure 5. The number of singlets plotted as $N_1^{-0.5}$ versus time. The data are the same as in figure 4. The intercept of the straight line corresponds to a slightly lower particle concentration N_i than the real initial particle concentration N_0 .

According to eq. (5) the intercept should give the initial particle concentration N_0 , and k_{11} is found from the ratio of the slope and intercept.

Two important features of this plot have to be discussed.

Firstly the extrapolation to zero time does not give exactly the initial particle concentration N_0 . Von Smoluchowski and Roeberson reported that in the first seconds after mixing the coagulation process is in a non-steady state, giving a faster rate of the coagulation than in the steady state. Roeberson and Wiersema [5] derived a simple equation for the transition time T between the non-steady state and the steady-state: $T=2.5 \cdot 10^{20} \cdot a^3$, where a is the particle radius in meters and T is found in seconds. At T the rate of coagulation is determined by the non-steady state process for 10% and by the steady state process for 90%. In our experiments T is about 11 seconds and the first data point is taken at 120 seconds after mixing. Therefore the extrapolation to zero time gives a slightly lower apparent initial particle concentration N_1 than the true value N_0 . We are interested in the rate of coagulation in steady state and therefore N_1 instead of N_0 was used in equation (5) to calculate k_{11} .

The second feature of the plot in figure 5 is that the experimental data indeed follow a linear behaviour according to the Von Smoluchowski equation. Apparently the deviations of k_{12} and k_{13} with respect to k_{11} are too small to give rise to non-linear behaviour. But still the value of the slope in figure 5 could be influenced by this differences in the rate constants. To determine this influence we determined for the same data as used above also the rate constant with the Von Smoluchowski equation:

$k_{11}=6.14 \pm 0.14 \cdot 10^{-12} \text{ cm}^3 \text{ s}^{-1}$. We conclude that the value of k_{11} determined with the Von Smoluchowski equation is only about 2% higher than that obtained from the differential equations (see table 3). This difference is smaller than the experimental error.

In order to study the effect of the mixing of salt and dispersion on the aggregation process, we measured the rate constant k_{11} with three different mixing cells, see table 4. Experimental details are described in the previous section experimental. We used equation (5) for the calculation of the rate constants.

Table 4. Coagulation rate constant k_{11} (at 293°K) for different mixing devices.

	N_0 / cm^3	N_1 / cm^3	$k_{11} * 10^{12} \text{ cm}^3 \text{ s}^{-1}$	number of exp.
B70-latex				
T-shaped cell	$4.1 * 10^8$	$3.8 * 10^8$	6.14 ± 0.16	6
Disk-shaped cell	$2.9 * 10^8$	$2.5 * 10^8$	5.74 ± 0.30	5
Stopped flow cell	$4.0 * 10^8$	$3.0 * 10^8$	5.0 ± 1.6	8
F70-latex				
Disk-shaped cell	$2.7 * 10^8$	$2.3 * 10^8$	5.24 ± 0.36	4

The data given in table 4 will be discussed in the next section.

A curious effect was found by mixing a stable latex dispersion with pure water in the Stopped Flow device. We detected some doublets (1.6% in number) in the mixture. Apparently, the very fast mixing induces large hydrodynamic forces which press the particles together so that, in spite of the double layer repulsion, some doublets are formed. Probably this is an example of pressure induced aggregation.

5.3.5. Discussion

We discuss first the rate constants as given in table 3. It is found that $k_{11} < k_{12} < k_{13}$, although the error increases also in this order. For the higher order rate constants k_{22} and k_{23} no unambiguous conclusion is possible because of the large uncertainty. In order to determine these constants with some accuracy, one has to follow the coagulation process for longer time and more data points per unit time have to be collected. However, at longer time higher aggregates could be present and terms involving these aggregates have to be added to the differential equations, which makes it again more difficult to solve these equations.

Both Cahill [17] and Gedon [18] find the same trend for the values of the rate constants. Cahill finds also the same absolute values, within experimental error.

Next we consider literature values for the overall rate constant $k_s = \frac{1}{2}k_{11}$.

For polystyrene latices k_s varies between 1.25 and $6 \cdot 10^{-12} \text{cm}^3 \text{s}^{-1}$. Sometimes the difference originates from the different initial particle concentration. Hatton et al [25] suggest that maybe hydrodynamic interactions between three particles play a role, but no physical interpretation was given. If we select the rate constants determined for PS around an initial particle concentration of $5 \cdot 10^8 \text{cm}^{-3}$ and scale them to 293°K (third column of table 2), we find a rather good agreement between the values in the literature ($k_s = 2.9 - 3.4 \cdot 10^{-12} \text{cm}^3 \text{s}^{-1}$) and our results ($k_s = 3.0 \cdot 10^{-12} \text{cm}^3 \text{s}^{-1}$). We can conclude that different methods yield the same results. Two groups of workers [18,27] found a lower value for the rate constant for polystyrene. Perhaps mixing effects and measuring technique can explain this deviation. Higuchi [22] found lower values for the rate constant for unpurified latices: ($k_s = 0.5 - 2.5 \cdot 10^{-12} \text{cm}^3 \text{sec}^{-1}$). However, Lichtenbelt et al. [26] did not find such a difference in k_s between purified and unpurified latices.

Finally we pay attention to the mixing method, considering the value of k_{11} as given in table 4. The advantage of the stopped flow injection mechanism is the very fast mixing of salt and dispersion. However, in our experiments gas bubbles and small leakages prevented accurate measurements, giving a rather large experimental error. The mixing time of the disk-shaped or T-shaped cell is small ($< 1 \text{ s}$) as compared to the time scale of the coagulation process. The half time $t_{1/2}$ of the coagulation, defined as $2/k_{11}N_0$, was in our experiments more than 850 s. The rate constant found with the disk-shaped cell is somewhat lower than with the T-shaped cell but the difference is hardly significant. The reproducibility of the rate constant with the disk-shaped cell is somewhat lower then with the T-shaped cell. Possibly the mixing is incomplete in the disk-shaped cell. A small difference is found for the rate constant determined with B70 and F70 latex, but again the experimental error is of the same order and no definite conclusions can be drawn.

After mixing the collecting syringe (see figure 2) stops the fluid motion quickly, and the system is left at rest until the first sampling (120 s). Therefore, orthokinetic aggregation can be assumed to be negligible.

5.4. Concluding remarks

The high monodispersity of the polystyrene latices makes them very suitable for the study of coagulation with the SPOS-instrument. Not only can aggregates up to heptaplets be distinguished separately but also the theory of Von

Smoluchowski for the coagulation kinetics of monodisperse particles could be checked.

We found for the overall rate constant of rapid coagulation

$k_g = 3.07 \cdot 10^{-12} \text{ cm}^3 \text{ s}^{-1}$, which is in good agreement with literature data.

Furthermore, we determined the rate constants of three initial aggregation steps (singlet+singlet, singlet+doublet and singlet+triplet) and found that these constants increase slightly in the order $k_{11} < k_{12} < k_{13}$. Although the differences between these constants are not dramatical, the primary assumption of the Von Smoluchowski theory, $k_{11} = k_{ij}$, appears to be not completely valid. Mixing effects are not very important in coagulation studies.

References

1. Deryaguin, B.V., Trans. Faraday Soc., 36, 203, 730 (1940).
Deryaguin, B.V., and Landau, L.D., Acta Physicochim., 14, 633 (1941).
2. Verwey, E.J., and Overbeek, J.Th.G., "Theory of the stability Lyophobic Colloids", Elsevier, Amsterdam, 1948.
3. Von Smoluchowski, M., Phys. Z., 17, 557, 585 (1916).
Von Smoluchowski, M., Z. Phys. Chem., 92, 129 (1917).
4. Fuchs, N., Z. Phys., 89, 736 (1934).
5. Roeberson, G.J., Wiersema, P.H., J. Colloid Interface Sci., 49, 98 (1974).
6. Deryaguin, B.V., and Muller, V.M., Dokl. Akad. Nauk. SSSR (engl. transl.), 176, 738 (1967).
7. Spielman, L.A., J. Colloid Interface Sci., 33, 562 (1970).
8. Honig, E.P., Roeberson, G.J., and Wiersema, P.H., J. Colloid Interface Sci., 36, 97 (1971).
9. Deutch, J.M., and Felderhof, J. Chem. Phys., 59, 1669 (1973).
10. Martynov, G.A., and Muller, V.M., Powerchnostye Sily v Tonkikh Plenkach i Dispersnich Sistemach, Nauka, Moscow, 1972.
11. Frens, G., and Overbeek, J.Th.G., J. Colloid Interface Sci., 38, 376 (1972).
12. Overbeek, J.Th.G., J. Colloid Interface Sci., 58, 408 (1977).
13. Witten, T.A., and Sander, L.M., Phys. Rev. Lett., 47, 1400 (1982).
14. Family, F., and Landau, D.P. (editors), "Kinetics of Aggregation and Gelation", North-Holland, Amsterdam, 1984.
15. Meakin, P., Chen, Z-Y., and Deutch, J.M., J. Chem. Phys., 82, 3786 (1985).
16. Bowen, M.S., Broide, M.L., and Cohen, R.J., J. Colloid Interface Sci., 105, 617 (1985).
17. Cahill, J., Cummins, P.G., Staples, E.J., and Thompson, L.G., Colloids and Surfaces, 18, 189 (1986).
18. Gedan, H., Lichtenfeld, H., Sonntag, H., and Krug, H-J., Colloids and Surfaces, 11, 199 (1984).
19. Malin, S.F., and Edwards, J.R., Nature New Biology, 235, 182 (1972).
20. Singer, J.M., and Plotz, C.M., Amer. J. Med., 21, 888 (1956).
21. Ottewill, R.H., and Rastogi, M.C., Trans. Faraday Soc., 56, 866 (1960).

22. Higuchi, W.I., Okada, R., Stelter, G.A., and Lemberger, A.P., *J. Pharm. Sci.*, 52, 49 (1963).
23. Matthews, B.A., and Rhodes, C.T., *J. Pharm. Sci.*, 57, 557 (1968).
24. Lips, A., and Willis, E.J., *J. Chem. Soc. Faraday Trans. 1.*, 69, 1226 (1973).
25. Hatton, W., McFadyen, P., and Smith, A.L., *J. Chem. Soc. Faraday Trans.1*, 70, 655 (1974).
26. Lichtenbelt, J.W.Th., Pathmamanoharan, C., and Wiersema, P.H., *J. Colloid Interface Sci.*, 49, 281 (1974).
Lichtenbelt, J.W.Th., thesis, State University Utrecht, The Netherlands, (1974).
27. Van der Scheer, A., Tanke, M.A., and Smolders, C.A., *Faraday Discuss. Chem. Soc.*, 65, 264 (1978).
28. Penners, N.H.G., and Koopal, L.K., *Colloid and Surfaces*, 28, 67 (1987).
29. Hearn, J., Wilkinson, M.C., and Goodall, A.R., *Adv. Colloid. Interface Sci.*, 14, 173 (1981).
30. Lerche, K-H., Kretzschmar, G., Richter-Mendau, J., and Becker, G., *Abh. Akad. Wiss., Akademieverlag Berlin DDR*, 1N, 285 (1987).
31. Goodwin, J.W., Hearn, J., Ho, C.C., and Ottewill, R.H., *Br. polym. J.*, 5, 347 (1973).
32. Furasawa, K., Norde, W., and Lyklema, J., *Kolloid Z.Z. Polymere*, 250, 908 (1972).
33. Wilkinson, M.C., Sherwood, R., Hearn, J., and Goodall, A.R., *Br. Polym. J.*, 11, 1 (1979).
34. Kurz, J.L., *J. Phys. Chem.*, 66, 2239 (1962).
35. Zsom, R.L.J., personal communication, AKZO Corporate Research Department, The Netherlands.
36. Van den Hul, H.I., and Vanderhoff, J.W., *J. Colloid Interface Sci.*, 28, 336 (1968).
37. Chondé, Y., and Krieger, I.M., *J. Colloid Interface Sci.*, 77, 138 (1980).
38. Van den Hoven, Th.J.J., thesis, Agricultural University Wageningen, The Netherlands, (1984).
39. O'Brien, R.W., and White, L.R., *Trans. Faraday Soc.*, 68, 907 (1972).
40. Reynolds, P.A., and Goodwin, J.W., *Colloids and Surfaces*, 23, 273 (1987).
41. Brouwer, W.M., and Zsom, R.J.L., *Colloids and Surfaces*, 24, 195 (1987).

42. Tamai, H., Fujii, A., and Suzawa, T., J. Colloid Interface Sci., 118, 176 (1987).
43. Reerink, H., and Overbeek, J.Th.G., Discuss. Faraday Soc., 18, 74 (1954).
Reerink, H., thesis, State University Utrecht, The Netherlands, (1952).
44. Ottewill, R.H., and Shaw, J.N., Discuss. Faraday Soc., 42, 154 (1966).
45. Gedan, H., thesis, Akademie der Wissenschaften Berlin, D.D.R., (1983).
46. Zollars, R.L., and Ali, S.I., Colloids and Surfaces, 24, 183 (1987).
47. Buscall, R., McGowan, I.J., Faraday Discuss. Chem. Soc., 76, 277 (1983).
48. Dixon, W.J.(editor), "BMDP Statistical Software", p. 325, University of California Press, Berkeley, 1985.

CHAPTER 6. EQUILIBRIUM AND NON-EQUILIBRIUM FLOCCULATION BY POLYMER

6.1. Introduction

Flocculation, sensitization and protection of dispersions by polymer are interrelated phenomena which are widely applied in a variety of industrial processes, both in aqueous and non-aqueous media. Examples are water treatment, paper making, mineral processing and sludge dewatering [1]. Reviews concerning the influence of polymer on dispersion stability have been written by Vincent [2], Napper [3], Kitchener [4], Lyklema [5] and La Mer [6].

Since the sixties many theories on the adsorption of flexible linear homopolymer at an interface have been developed [7-11]. The earlier theories suffer from a number of simplifying assumptions about the conformation of the polymer at the interface. More sophisticated calculations could only be done for small oligomers [11]. At the beginning of the eighties Scheutjens and Fleer [12,13] developed a statistical lattice theory, with no a priori assumptions about the conformation of the polymer at the interface. Calculations with this model can now be done up to more than 10^4 statistical chain segments.

All these adsorption theories assume equilibrium between interface and bulk. However, in the case of flocculation two surfaces with polymer interact at very short distances. In that case, the assumption of full equilibrium would seem less obvious. Recently, Scheutjens and Fleer [14] applied their model to the interaction of two adsorbed polymer layers. They calculated the free energy as a function of separation, molecular weight and amount of adsorbed polymer, both for full equilibrium and for restricted equilibrium. In the former case the chemical potentials remain constant during particle approach, implying polymer desorption. In restricted equilibrium there is no time for such a desorption process, and the amount of polymer is assumed to be constant.

The main features of the model have been corroborated by experimental observations, both for adsorption on one surface and for two interacting surfaces. For the latter case, highly elaborate experimental techniques have been developed recently [15-17]. Hence, the equilibrium aspects of polymer adsorption are now rather well understood.

Less, if not very little, information is available about the kinetic aspects of polymer adsorption and flocculation [18-21]. Yet kinetics play an important

role when a dispersion and a flocculant are mixed, particularly when bridging is the dominant flocculation mechanism. Gregory [18] distinguishes two possible cases: equilibrium flocculation and non-equilibrium flocculation. In the former case the adsorbed polymer is in equilibrium at the interface before the particles meet. During non-equilibrium flocculation the polymer at the interface is not yet in its equilibrium state: reconformation and relaxation of the adsorbed layer occur simultaneously with interparticle bridge formation.

In this chapter, we describe experimental data obtained for both types of flocculation. The results for equilibrium flocculation experiments could be compared with the predictions of the Scheutjens-Fleer theory. For the non-equilibrium flocculation experiments no suitable theory is available. Several processes, each with its own rate, take place: transport of polymer to the particles, attachment of polymer, reconformations in the adsorbed layer, and particle collisions during which bridges may be formed.

In our experiments, we used monodisperse negatively charged polystyrene latex (PSL) dispersions as a model system. As described in the previous chapters, the particle size distribution of coagulating and/or flocculating PSL can be studied in detail with the Single Particle Optical Sizer. The latex surface is charged so that double layer repulsion plays a role. By varying the electrolyte concentration, the double layer thickness κ^{-1} and, hence, the ratio between κ^{-1} and the extension of the polymer layer can be modified. We will show that under some conditions equilibrium flocculation occurs, whereas in other cases non-equilibrium flocculation is found.

As the flocculant we used mainly Poly(ethylene) oxide. It is a linear homopolymer and can be purchased in many different molecular weights and also as monodisperse samples. Water is a good solvent for PEO, and the fact that flocculation is induced by an adsorbing neutral homopolymer in a good solvent excludes all other mechanisms than bridging. Literature data [22] for the adsorption of Poly(ethylene) oxide on latex are available.

In this chapter, we will first discuss the present state of knowledge about the kinetic and equilibrium aspects of bridging flocculation. After a description of the adsorption and flocculation experiments, we will interpret the results in terms of a new model for bridging flocculation. In this model, both non-equilibrium flocculation and equilibrium flocculation are incorporated and electrostatic interactions are taken into account.

6.2. Bridging flocculation

Bridging is the adsorption of one polymer on two or more particles, whereby the polymer bridges (i.e., subchains spanning the interparticle gap) lead to an attractive force between the particles [23]. If many of such bridges occur, the particles are held together as flocs.

6.2.1. Dynamic aspects of flocculation.

In bridging flocculation the following rate processes are involved [24].

- a. Mixing of polymer solution and dispersion
- b. Collisions between polymer and particles, leading to attachment.
- c. Reconfiguration of the polymer molecules at the surface of the particles.
- d. Collisions of particles bearing adsorbed polymer with other particles having an exposed area on to which polymer can adsorb to form a bridge.

In figure 1, taken from Gregory [18], these processes are schematically represented. The mixing of polymer and dispersion must be very fast with respect to the rate of the flocculation process, in order to assure that process (a) is not rate determining. Such rapid mixing is done in our experimental set-up.

The rate of process (b) is determined by the transport of the polymer molecules and the particles towards each other. If there are no shear forces (perikinetics) the transport is only due to diffusion, which depends on concentration and size of the polymers and particles. In the presence of shear (orthokinetics) there is an additional component to the transport of polymer to the particles.

Little or no information is available concerning the time scale of process (c), the reconfiguration [21]. In the very first stages of the adsorption, the structure of the polymer is still more or less a random coil with a relatively large extension. Then a reconfiguration follows which makes the polymer layer thinner, until finally the equilibrium conformation (which depends on the adsorbed amount) is reached. If the time required for reconfiguration is greater than the interval between particle collisions, the extended, nonrelaxed polymer layer may lead to long bridges. We call this process non-equilibrium flocculation, see the dashed arrow in figure 1.

Until now no solid evidence for non-equilibrium flocculation was available. We will provide such evidence and discuss the conditions for non-equilibrium

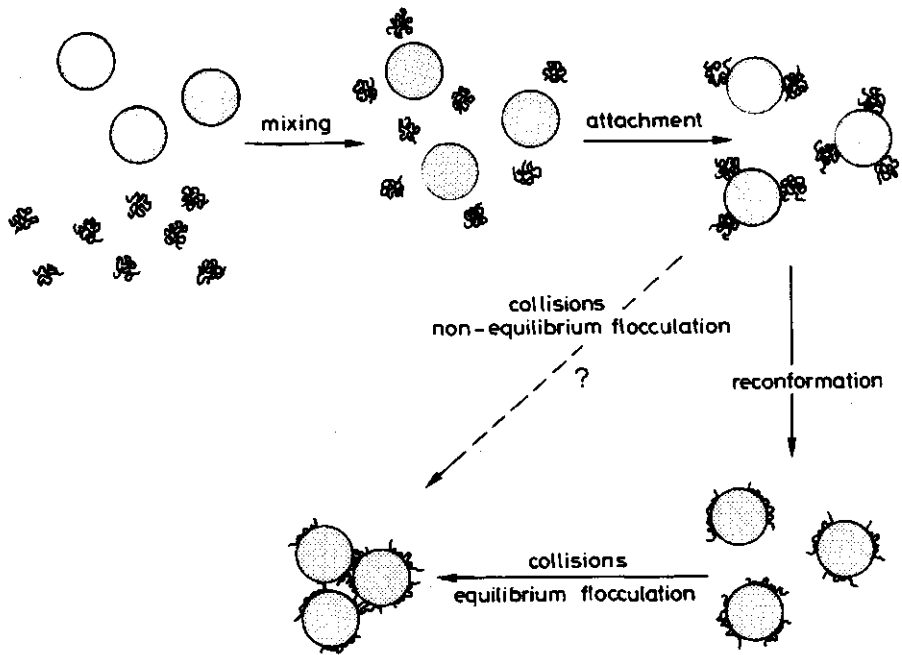


Figure 1. Schematic diagram showing mixing, attachment, reconfiguration and collisions. The dashed arrow indicates a possible alternative flocculation mechanism.

flocculation in section 6.4. It seems reasonable that such an extended polymer layer increases the number of effective collisions of a particle because the polymer reaches further out than the range of electrostatic repulsion and thus enhances the flocculation rate. We note that the reconfiguration rate (c) is independent of the particle concentration, whereas the collision process (d) increases with increasing particle concentration. Therefore it is likely that only at relatively high particle concentration non-equilibrium flocculation occurs. At low particle concentrations the interval between particle collision is greater than the reconfiguration time, and only polymer in its equilibrium conformation will be available for bridging (equilibrium flocculation).

Approximate expressions for the rate constant of the attachment and the collision process have been given in the literature [18]. The rate constant k_{ij} for both processes (b) and (d) can be written as:

$$\text{(perikinetic)} \quad k_{ij} = \frac{2kT}{3\eta} (a_i + a_j)(a_i^{-1} + a_j^{-1}) \quad (1)$$

$$\text{(orthokinetic)} \quad k_{ij} = \frac{4}{3} G (a_i + a_j)^3 \quad (2)$$

where k is the Boltzmann constant, T the temperature, η the viscosity and G the shear rate. In the case of attachment, a_i equals the radius of the particles and a_j the radius of the polymer molecules (approximated as spheres). For the case of collisions between particles or aggregates, a_j and a_i are the radii of the colliding particles.

6.2.2. Equilibrium aspects of flocculation.

Scheutjens and Fleer [14] have calculated the free energy due to polymer adsorption as a function of the separation between two plates. These results are only applicable to systems where the polymer layer at the interface is in internal equilibrium. Nevertheless it seems worthwhile to compare their results with our experimental kinetic results. In figure 9 of chapter 4 we already showed some theoretical results of Scheutjens and Fleer. We can learn from this figure that both at very low and at very high coverage (polymer dose) the bridging flocculation mechanism becomes inoperative, whatever the kinetic mechanism involved. More details are given in section 4.6.3.3.

6.3. Adsorbed amounts

As shown before (section 4.6.3.3.), the amount of polymer is an important factor in the destabilization of latex particles. Therefore we start with a description of the adsorption experiments for PEO on polystyrene latex.

6.3.1 Materials

A detailed description of the synthesis and purification of the lattices is given in chapter 5. Table 1 (top) summarizes the diameter of the particles, the uniformity coefficient d_{63}/d_{30} , and the surface charge density σ_0 . These data are taken from section 5.2.2. where more details can be found. The dispersions are stored in the refrigerators to prevent microbial contamination.

Poly(ethylene) oxide and Polyvinylpyrrolidone were used as flocculants; several properties are listed in table 1. The weight averaged molecular weights M_w and the dispersity index M_w/M_n , if available, are as quoted by the manufacturer. For PVP, M_w and M_n were determined by dr. A.J. Goedhart (AKZO Research, The Netherlands) using Gel Permeation chromatography. The ratio M_w/M_n for the polydisperse samples is unknown but will be of the order of 2.5 to 4 [25a].

We used a Mark-Houwink relation to calculate from the intrinsic viscosity $[\eta]$ (in dl/g), determined with a Ubbelohde viscometer, the viscosity averaged molecular weight M_v (in gmol^{-1}): $[\eta] = K \cdot M_v^a$ where $K = 11.92 \cdot 10^{-5}$ and $a = 0.76$ at 25°C in water [26]. Surprisingly, for PEO $6 \cdot 10^5$ we found $M_v > M_w$: either our value of M_v for this polymer is too large, or the M_w -value quoted by the manufacturer too low.

For an estimate of the rms end-to-end distance h_m of the polymers, we used the Flory equation [27]: $[\eta] = \phi \cdot h_m^3 / M$ where ϕ is a constant given by Tanford [28]. For a good solvent this constant is approximately $2.25 \cdot 10^{21} \text{ mol}^{-1}$. Although this equation is derived for monodisperse polymer, it is often applied for polydisperse samples, substituting M_v for M .

Solutions of polymer were stored in the dark and in a refrigerator. Especially large molecular weight samples of Poly(ethylene) oxide may undergo degradation during storage in solution [25b]. Poly(ethylene) oxide solutions were therefore always used within three days after preparation and the activity as flocculant was tested just before use [see section 6.4.3]. The solid samples of the poly(ethylene) oxide polymer are stored at -5°C Celsius. They were free of water, as checked by micro-elemental analysis.

Potassium nitrate [Merck, pro analyse] solutions were used after filtration ($0.22 \mu\text{m}$ Millipore filter) without further purification. Water was purified by filtration through a Millipore Milli R060 combined with a Super Q system.

Table 1. Latex and polymer samples

Latex	Diameter nm	d_{63}/d_{30}	σ_0 $\mu\text{C}/\text{cm}^2$
F70	602	1.0004	5.4
C3N4	629	1.002	7.5
B70	696	1.005	4.7

Polymer	$M_w(\text{g mol}^{-1})$	$M_v(\text{g mol}^{-1})$	M_w/M_n	h_m (nm)
PEO $2 \cdot 10^4$ (Hoechst)	$2 \cdot 10^4$	$1.7 \cdot 10^4$	-	13
PEO SE-70 (Toyo Soda)	$5.7 \cdot 10^5$	-	1.09	-
PEO $6 \cdot 10^5$ (Aldrich)	$6 \cdot 10^5$	$8 \cdot 10^5$	-	110
PEO $4 \cdot 10^6$ (Aldrich)	$4 \cdot 10^6$	$3 \cdot 10^6$	-	236
PEO $5 \cdot 10^6$ (Aldrich)	$5 \cdot 10^6$	-	-	-
PVP KGO (BASF)	$9.3 \cdot 10^5$	-	5.2	-

6.3.2 Adsorption isotherms

Experimental

Adsorption experiments were carried out in the following way:

An aqueous solution of PEO (2.5 ml, concentration range 50-600 ppm) was added to a latex dispersion (2.5 ml, concentration $5\frac{1}{2}$ % w/w). Prior to use the dispersions were sonicated for 45 minutes. The mixture was rotated end-over-end (25 rpm) for $1\frac{1}{2}$ hour at 20° Celsius. The solution was separated from the latex particles by centrifugation (45 minutes at 40,000 g). The concentration of PEO in the supernatant was determined with the molybdophosphoric acid method as described by Nuysink and Koopal [29].

For the adsorption isotherm of PVP we used a Phase Sep.TOCsinII aqueous carbon analyzer to determine the concentration in the supernatant.

Results

The adsorption isotherms for PEO $2 \cdot 10^4$, PEO $6 \cdot 10^5$ and PEO $4 \cdot 10^6$ on latex B70 from water are shown in Fig. 2a. Fig. 2b gives the isotherm of PEO $4 \cdot 10^6$ on latex C3N4. The surface charge density of B70 latex is $\sigma_0 = 4.7 \mu\text{C}/\text{cm}^2$ and that of C3N4 is $\sigma_0 = 7.5 \mu\text{C}/\text{cm}^2$. The amount of polymer at equilibrium in the bulk is given as $\Gamma^* = CV/A$, where the polymer concentration C is in mg/m^3 , and V is the volume of the sample ($5 \cdot 10^{-6} \text{ m}^3$) and A the surface area of the latex in the sample (2.25 m^2). The isotherms are plotted in this way because then the adsorbed and non-adsorbed amounts are expressed in the same units (mg/m^2).

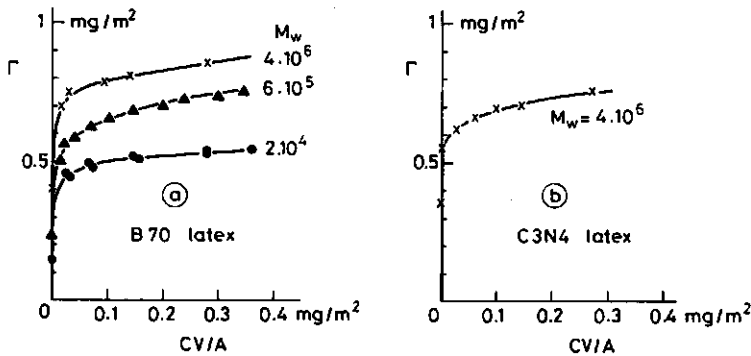


Figure 2. Adsorption isotherms of PEO on latex. The equilibrium amount Γ^* of polymer in solution equals CV/A where C is the polymer concentration. In this case $V = 5 \cdot 10^{-6} \text{ m}^3$ and $A = 2.25 \text{ m}^2$. (a) B70 latex, (b) C3N4 latex. Equilibrium time 1.5 hrs.

Figure 2a demonstrates the effect of molecular weight on the adsorbed amount Γ . As is commonly found, Γ increases with increasing M_w . Polymer molecules have a large affinity for the surface: already at extremely small equilibrium concentrations a large amount is adsorbed. The used polymer samples are polydisperse. With increasing polymer dose (increasing equilibrium concentrations) the smaller polymer chains at the surface are displaced by the larger ones, which shows up as an increase in adsorbed amount. In the semi-plateau region only very long chains are adsorbed. The adsorption isotherm obtained for PEO $2 \cdot 10^5$ is similar to the isotherm measured by Cowell [22]. By comparing the adsorption isotherms of PEO $4 \cdot 10^6$ in figure 2a and 2b, one can

clearly see a decreasing adsorbed amount with increasing surface charge of the latex particles. A possible explanation is that the electronegative oxygen atoms of the polymer molecules are somewhat repelled by the negatively charged surface groups of the latex. In the mixtures of polymer and latex used for constructing the adsorption isotherms we observed, for PEO $4 \cdot 10^6$ at equilibrium concentrations smaller than 10 ppm, flocculation. This can possibly decrease the available surface of the latex, therefore a minor error may be present in the corresponding part of the isotherm.

We also followed the adsorbed amount of PEO $4 \cdot 10^6$ on B70 latex as a function of time and observed hardly any increase in this amount after 30 minutes. Hence, the time chosen for equilibrium ($1\frac{1}{2}$ hours) seems to be justified.

In a separate experiment, we investigated the effect of the sonification of the latex. We found for PEO $4 \cdot 10^6$ on C3N4 latex a decrease of 10% in the adsorbed amount (at $C_p = 15$ ppm) if the sonification step was omitted. This effect is almost certainly caused by a number of doublets (5% in weight) present in the dispersion. With the single particle optical sizer we could clearly detect those doublets and found that they disappeared after 45 minutes of sonication. We always used freshly prepared polymer solutions to construct the adsorption isotherms.

There is a small but significant effect of the ageing on PEO. For a four day old PEO $4 \cdot 10^6$ solution, we measured that the plateau value of the adsorbed amount on B70 latex decreased by about 3.2%. The activity as flocculant of this polymer solution was even decreased by 90% (see section 6.4). Also a small decrease in viscosity of 3% after 20 days could be detected. These effects are presumably caused by the degradation of PEO $4 \cdot 10^6$ in solution.

The adsorbed amount of PEO $6 \cdot 10^5$ on B70 latex was also measured as a function of the NaCl concentration, see table 2. These experiments were carried out by mixing latex with a polymer-salt solution (method (b), see 6.4.1.).

Table 2. Influence of NaCl on the adsorbed amount.

C_{NaCl} (mol/l)	0	10^{-2}	10^{-1}	0.2	0.5
Γ (mg/m ²)	0.65	0.66	0.69	0.69	0.71

Although flocculation was observed at all NaCl concentrations, the adsorbed amount increased slightly as a function of salt concentration. Possible

explanations are that free bulk polymer is captured in the flocs, or that the decreasing solvent quality leads to more adsorption. The latter explanation is more likely since it is generally known that the adsorbed amount from poorer solvents is higher, and that salt worsens the solvent quality of water for PEO [30].

We also determined the adsorbed amount of PEO SE-70, a nearly monodisperse sample with $M_w = 5.7 \cdot 10^5$, on B70 latex. We found 0.79 mg/m^2 at the plateau region (about 100 ppm equilibrium concentration). This value agrees quite reasonably with the isotherms of fig. 3, but is about a factor of 2 lower than that reported by Cohen Stuart et al. [31]. We have no obvious explanation for this discrepancy. Possibly, the surface properties of the latex used by the latter authors were different from those in the present experiments. Also a different value V/A could play a role.

Unfortunately the results obtained with the Carbon Analyzer were rather inaccurate, so that the adsorption measured for PVP was not very reliable. We suspect that small amounts of latex are left in the supernatant. The sulphur present in this residue can deactivate a catalyst used in this instrument. Nevertheless, the adsorption plateau of PVP on B70 latex could be determined. We found $1.1 \pm 0.1 \text{ mg/m}^2$.

6.4. Flocculation of a latex by polymer.

In this section we address a number of topics. First, we pay some attention to the method of mixing latex, polymer and salt. Secondly, we describe the flocculation experiments as a function of polymer dosage, in order to find the optimum polymer dosage for flocculation. For high molecular weight PEO, these experiments show some evidence for non-equilibrium flocculation.

Thirdly, we present the flocculation experiments as a function of initial particle concentration, at the optimum polymer dose. In some cases Von Smoluchowski-type kinetics are observed, but at high molecular weight clear deviations occur. Finally we discuss the flocculation behaviour as a function of time. Various types of rate processes can be observed which can be related to the occurrence of equilibrium and non-equilibrium flocculation.

6.4.1 Methods of mixing

We used three mixing procedures for the flocculation experiments:

a. Latex and polymer.

V ml latex dispersion was added with a Gilson pipette to V ml polymer solution in a 20 ml flask. After addition this flask is shaken by hand for 5 seconds. No salt was added.

b. Latex and polymer/salt mixture.

V ml latex dispersion was added with a Gilson pipette to V ml polymer and salt solution ($2 \cdot 10^{-2} \text{M KNO}_3$) in a 20 ml flask and shaken by hand for 5 seconds.

c. Latex and polymer, followed by salt.

V ml latex dispersion was added with a Gilson pipette to V ml polymer solution in a 20 ml flask. After addition this flask is shaken by hand for 5 seconds and rotated end-over-end (25rpm) during $1\frac{1}{2}$ hours. Hereafter V ml mixture was taken out with a Gilson pipette and added to V ml $2 \cdot 10^{-2} \text{M KNO}_3$ in a 20 ml flask. This flask was shaken by hand for 5 seconds.

The volume V was in the range of 0.1-5 ml. If not specified, $V = 1 \text{ ml}$.

After mixing of polymer and latex according to one of these methods, the sample is rotated end-over-end (25rpm) for $1\frac{1}{2}$ hours, during which adsorption and flocculation could take place. Next, the was diluted to a particle number concentration of about $5 \cdot 10^7 \text{ cm}^{-3}$ and injected into the Single Particle Optical Sizer. A first volume of 1.5 ml was injected to clean the instrument and another 0.5 ml portion was injected for the counting experiment. It is fair to assume that the dilution (gentle agitation, shear rate $\approx 50 \text{ s}^{-1}$) does not change the particle size distribution. The hydrodynamic forces occurring during dilution are certainly not enough to break flocs that are bound by polymer bridges (see section 4.6).

In the first set of experiments we will vary the volumes of the sample to study the effect of mixing and rotation. All experiments are carried out at 20° Celsius .

6.4.2. Results.

6.4.2.1. Influence of mixing methods

In figure 3, we present the degree of flocculation of a mixture of B70 latex and PEO $4 \cdot 10^6$, as a function of the volume of the sample. Mixing method (a) was used, and the results plotted as a function of V. The degree of flocculation is expressed as the ratio N_1/N_0 between the number N_1 of primary

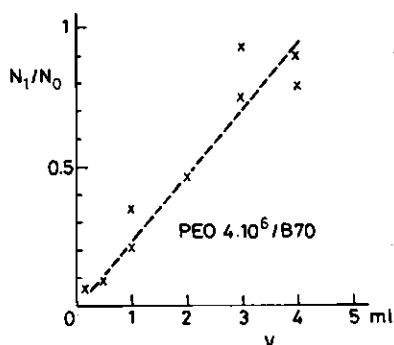


Figure 3. Influence of mixing volumes (mixing method a) of PEO $4 \cdot 10^6$ and B70 latex on the flocculation. $N_0 = 3 \cdot 10^{10} \text{ cm}^{-3}$, PEO-concentration 17 ppm. N_1/N_0 is the ratio of primary particles left in the system after 1.5 hours.

particles left in the sample and the initial number N_0 of primary particles. At first hand, it is rather surprising that at constant final concentration of polymer and latex, the degree of flocculation decreases with increasing volume of the sample. It took us some time to find an explanation for this unexpected effect. A small volume of the mixture is more strongly agitated then a larger volume in a flask of fixed volume (20 ml) during end-over-end rotation at a constant number of revolutions per minute (25 rpm). If the samples are not rotated, no flocculation occurs. Hence the observed flocculation must be due to orthokinetic collisions, polymer/particle and particle/particle, which are more frequent for 0.5 ml mixture in a 20 ml flask than for 8 ml in the same flask. The rates of processes (b) and (c), as described in section 6.2.1., will increase with decreasing V due to shear forces.

Another experiment was done with a lower molecular weight polymer (PEO $6 \cdot 10^5$) and the same latex (B70). Surprisingly, with method (a) no flocculation could be detected, regardless of the mixing volumes V . It is likely that the polymer molecules are too small ($h_m = 110 \text{ nm}$) to outrange the double layer repulsion (at ionic strength of 10^{-5} mol/l , $\kappa^{-1} = 100 \text{ nm}$). Therefore we used method (c), a two step mixing method where salt is added in the second step to suppress the double layer repulsion (ionic strength 10^{-2} mol/l , $\kappa^{-1} = 3 \text{ nm}$). Results are given in figure 4 as a function of the volume V after the second mixing step. A

similar behaviour as in figure 3 is found; also in this case shear forces are necessary for flocculation. Also, we observed that the volume of the first mixing step (latex with polymer) did not influence the degree of flocculation, provided that the final latex and polymer concentrations were not changed. So we assume that in this case the distribution of the polymer over the particles is independent on the mixing volume.

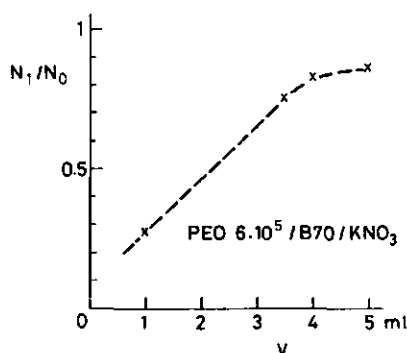


Figure 4. Influence of mixing volumes (mixing method c) of PEO $6 \cdot 10^5$, KNO_3 and B70 latex on the flocculation. $N_0 = 2.3 \cdot 10^9 \text{ cm}^{-3}$, PEO-concentration 2.6 ppm.

6.4.2.2. Flocculation as a function of the polymer dose

It was explained in section 4.6.3.2. that the surface coverage plays a critical role in the process of bridge formation. The coverage, in turn, is entirely determined by the polymer dose. In this section we study the effect of this parameter on the flocculation efficiency. We express the polymer dose in mg added polymer per m^2 of latex surface. Part of this dose will adsorb (Γ) and the other (usually small) part (Γ^*) will remain in the bulk solution as free polymer. This latter fraction may be expressed in the equilibrium concentration C by $\Gamma^* = C V/A$ (mg/m^2). First, we discuss results obtained with relatively low molecular weight polymer (PEO $5.7 \cdot 10^5$, PEO $6 \cdot 10^5$ and PVP $9.3 \cdot 10^5$) which do flocculate the latex only if some electrolyte is present. Second, we turn our attention to longer molecules (PEO $4 \cdot 10^6$ and PEO $5 \cdot 10^6$), that can flocculate latex in the absence of salt.

In fig. 5 we compare the flocculation of latex B70 by PEO $6 \cdot 10^5$ using mixing method c (lower curve) with the coagulation by salt only (upper curve). The bare latex is completely stable against electrolyte up to about $3 \cdot 10^{-2}$ M KNO_3 , whereas PEO induces a flocculation which increases with salt concentration (sensitization). Above $3 \cdot 10^{-2}$ M KNO_3 , the effect of the polymer (i.e., the vertical distance between the two curves of fig. 5) is about constant, beyond 10^{-1} M KNO_3 the flocculation by polymer is nearly complete. For further experiments we used 10^{-2} M KNO_3 , at which concentration no coagulation of the latex occurs as yet.

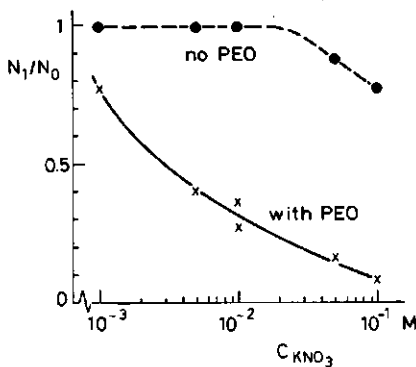


Figure 5. Coagulation of latex B70 by salt (upper curve) and flocculation by PEO $6 \cdot 10^5$. Mixing method c, $N_0 = 2.27 \cdot 10^9 \text{ cm}^{-3}$, PEO-dose 0.83 mg/m^2 . Flocculation time 1.5 hours.

In fig. 6 we show the influence of the polymer dose on the stability, for PEO $5.7 \cdot 10^5$ (monodisperse) and PEO $6 \cdot 10^5$ (polydisperse). Mixing method c is used. At low polymer dose we find almost no flocculation, but at a critical dose of 0.6 mg m^{-2} the stability decreases sharply, after which a levelling off occurs. Theoretical work has shown that at low coverage (i.e. low dose) not only short but also few loops and tails are present [13] and apparently this situation does not lead to flocculation. The monodisperse PEO clearly has the sharper transition between the stability and instability regions. Since the hydrodynamic thickness as given by Cohen Stuart et al. [31] shows a similar sharp transition at a critical coverage, it seems plausible that stability is

governed by the layer thickness. We suggest that the stability transition is so sudden, because it is related to the sharp increase in hydrodynamic thickness of the adsorbed polymer layer. Such an increase in the hydrodynamic thickness would be more gradual with polydisperse polymer, which seems to agree with the more gradual transition observed with the polydisperse PEO. At a polymer dose greater than 0.6 mg/m^2 enough tails and loops are present to destabilize the latex particles. It seems justified here to use arguments based upon equilibrium theories, because flocculation occurs after equilibration of polymer on the latex surface.

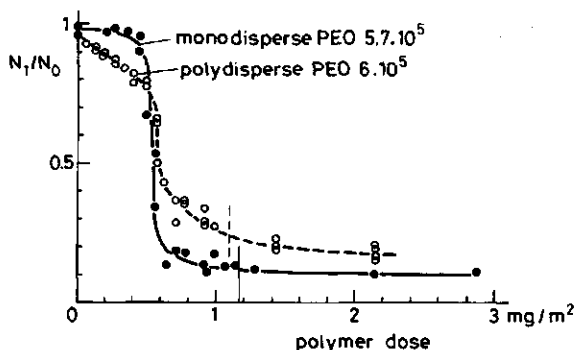


Figure 6. The influence of the PEO-dose on the stability of B70 latex. Mixing method c, $N_0 = 2.27 \cdot 10^9 \text{ cm}^{-3}$, $[\text{KNO}_3] = 0.01 \text{ M}$.

It is often argued that at high polymer dose the particles would again be stabilized by polymer because then no free latex surface is available, preventing bridge formation. However, in figure 6, we do not observe this restabilization phenomenon. A rather simple explanation can be suggested. The vertical lines in figure 6 indicate the polymer dose at which the adsorption plateau region of both polymer is reached (see fig. 2). Upon adding more polymer, very little extra polymer is adsorbed. We conclude that not enough polymer can adsorb in order to restore stability, i.e. even at the plateau region of the isotherm, free surface appears to be available.

The destabilization of latex by PVP is shown in figure 7. In this case a limited restabilization of the dispersion can be observed beyond $\sim 1.2 \text{ mg/m}^2$.

This restabilization dose is consistent with the adsorption plateau of $1.1 \pm 0.1 \text{ mg/m}^2$, found in the adsorption experiments (section 6.3.).

Again, restabilization is restricted by the limited amount of polymer which can adsorb on the surface.

If we assume that also for PVP the latex with the higher surface charge accepts less polymer (as was shown for PEO in fig. 2) we can understand why the restabilization of latex B70 ($\sigma_0 = 4.7 \text{ } \mu\text{C/cm}^2$) is more effective than that of latex F70 ($\sigma_0 = 5.4 \text{ } \mu\text{C/cm}^2$). However, no adsorption isotherm of PVP on latex F70 is available.

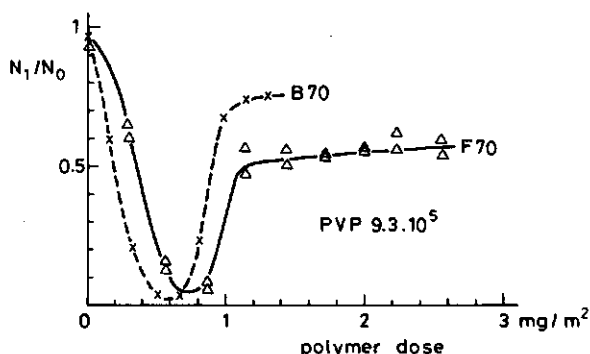


Figure 7. The influence of PVP-dose on the stability of B70 and F70 latex. Mixing method c, $[\text{KNO}_3] = 0.01 \text{ M}$. B70 latex : $N_0 = 1.5 \cdot 10^{10} \text{ cm}^{-3}$, F70 latex : $N_0 = 1.15 \cdot 10^{10} \text{ cm}^{-3}$.

A difference between the destabilization of latex by PVP and that by PEO is that for PVP the transition between stability and flocculation is more gradually. This is to be expected, since PVP is much more polydisperse than PEO. It would be useful to carry out more systematic experiments of this type, so that the transition region as a function of molecular weight with monodisperse samples could be correlated with the hydrodynamic thickness as a function of molecular weight (e.g., as calculated by the SF-theory). We note in passing that the detailed picture shown in figs 6 and 7 could only be obtained with the SPOS, since especially this instrument is capable to measure directly the decrease in the number of primary particles. Other methods, for example turbidity, measure a signal originating from many different aggregates

so that an unambiguous interpretation in terms of particle numbers is impossible.

In contrast with relatively low M_w polymers where salt is needed for flocculation to occur, no addition of salt is necessary to induce flocculation with very long polymer molecules. In this case, we used mixing method (a) with $V = 1$ ml.

As can be seen in figures 8 and 9, destabilization of the latex occurs only over a limited range of the polymer dose. At higher doses, almost complete restabilization is observed for both polymers. For PEO $4 \cdot 10^6$ this happens at a polymer dose of 0.8 mg/m^2 , far below the adsorption plateau region (1.2 mg/m^2 , see figure 2a). Apparently, the obtained coverage is high enough to prevent bridging.

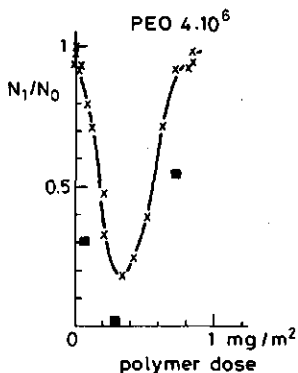


Figure 8. The effect of the dose of PEO $4 \cdot 10^6$ on the stability of B70 latex. $N_0 = 3 \cdot 10^{10} \text{ cm}^{-3}$. The crosses were obtained with mixing method a (no salt), the squares with method b with $[\text{KNO}_3] = 0.01 \text{ M}$.

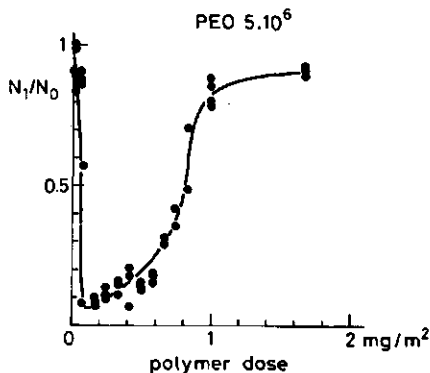


Figure 9. The influence of the dose of PEO $5 \cdot 10^6$ on the stability of B70 latex. $N_0 = 2.6 \cdot 10^{10} \text{ cm}^{-3}$, mixing method a (no salt).

The double layer repulsion separates the particles by a minimum distance, which can be approximated as $2\kappa^{-1}$ which, without added salt, is about 200 nm (ionic strength $\sim 10^{-5} \text{ mol/l}$). This distance has to be overcome by bridges. We may estimate the size of a polymer coil as the rms end-to-end distance h_m

(section 6.3.1.) and find numbers of the same order of magnitude as $2\kappa^{-1}$ for PEO $4 \cdot 10^6$, see table 1. We suppose that bridging occurs before the polymer has found its adsorbed equilibrium conformation. Probably, they are still largely in their solution conformation, whereby a significant fraction of the molecules extend over a distance higher than h_m . We called this mechanism non-equilibrium flocculation (see section 6.2.). However, the fact that flocculation with these large polymers occurs without salt is not yet a direct proof that we are dealing with non-equilibrium flocculation. Such evidence will be given in the following sections.

One could argue that the polymers in their equilibrium state at the latex surface would have such long tails that these would reach beyond the double layer repulsion and would be able to create bridges. This is not very likely, because the dimensions of even the largest tails (in equilibrium) are almost certainly smaller than the dimensions of the complete polymer chain.

When mixing method (b) is used, mixing latex with a polymer/salt solution, the flocculation is more effective, see the square symbols in fig. 8. A more detailed discussion is deferred to section 6.4.

With PEO $5 \cdot 10^6$ the restabilization occurs at a higher dose than with PEO $4 \cdot 10^6$, see fig. 10. This is unexpected if one considers only equilibrium properties: the higher molecular weight has a slightly higher adsorbed amount and would protect the particles somewhat better, at the same equilibrium concentration. Therefore, we invoke kinetic arguments. We assume that the reconfiguration process for PEO $5 \cdot 10^6$ is slower than that for PEO $4 \cdot 10^6$. Consequently, the number of polymer molecules at the surface in the extended non-equilibrium state is higher. The surface coverage is therefore less and the tails are longer, so that bridging may still occur. A similar effect of M_w on the restabilization has also been reported by Gregory and Sheiham [32]. In our opinion, this constitutes one of the very few experimental indications of non-equilibrium flocculation in literature.

We conclude the description of this set of experiments with a general comment related to the application of equilibrium theories. The SF-theory predicts a minimum in the free energy between two adsorbed polymer layers as a function of adsorbed amount. At constant polymer dose, this minimum is predicted to be independent of the molecular weight of the polymers. However, such a picture applies only to equilibrium flocculation. Since we found for high molecular

weights clear evidence for non-equilibrium flocculation, the theory could only be checked using low molecular weight polymers. In such experiments, one would have to measure the flocculation as a function of the adsorbed amount for homodisperse samples of different molecular weights.

6.4.2.3. Flocculation as a function of the initial particle concentration

In this set of experiments we used low molecular weight PVP K90 and high molecular weight PEO ($4 \cdot 10^6$ and $5 \cdot 10^6$) as flocculants. The experiments were done at a constant dose, equal to the optimum polymer dose for flocculation (see figs. 7-9).

In fig. 10, we present the effect of the initial particle concentration of latex F70 with PVP K90. We used mixing method (c) with $V = 1$ ml. In this procedure, the latex is first mixed with polymer solution and subsequently salt is added to this mixture.

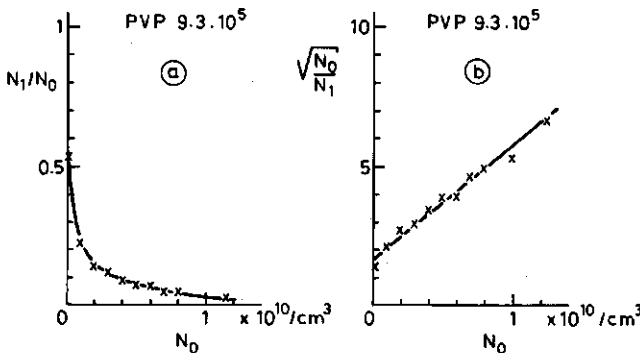


Figure 10. The influence of the initial particle concentration N_0 on the flocculation of latex F70 by PVP $9.3 \cdot 10^5$. Mixing method c, $[\text{KNO}_3] = 0.01$ M, PVP-dose 0.75 mg/m^2 . Time after mixing 1.5 hours. a/ N_1/N_0 versus N_0 b/ $(N_0/N_1)^{0.5}$ versus N_0 .

If the flocculation is a second order rate process, it would follow the kinetics according to Von Smoluchowski [33]:

$$N_1 = N_0 (1 + \frac{1}{2} k_{11} N_0 t)^{-2} \quad (3)$$

where k_{11} is the rate constant for collisions between primary particles. This equation was also used in chapter 5. By plotting $(N_0/N_1)^{\frac{1}{2}}$ versus N_0 one should find a straight line with an intercept of unity and slope $\frac{1}{2} k_{11} t$. In these experiments, t was constant (1.5 h). Such a plot is given in fig. 10b. The intercept in this figure is slightly above unity. We suspect that non-steady state flocculation, in the second mixing step (salt addition to the mixture of polymer and latex) is responsible for this deviation (see also section 5.3.3). Nevertheless the straight line in fig. 10b shows that the flocculation of latex with PVP is essentially a second order rate process. The salt concentration is well below the critical coagulation concentration, so that the destabilization must be caused by bridging. Since the loops and tails of the polymer are in equilibrium at the surface we have again an example of equilibrium flocculation. For this case (low M_w), the interpretation of the flocculation results is rather straightforward. We will see that the situation is more complex for high molecular weights.

In figure 11 we have plotted the relative number of singlets N_1/N_0 and of doublets N_2/N_0 as a function of N_0 , for latex B70 with PEO $4 \cdot 10^6$ as flocculant. We used mixing method (a), mixing latex with polymer without salt, to induce flocculation. The results are completely different from those with PVP (fig. 10a).

At low concentrations, up to 10^{10} cm^{-3} , almost no flocculation occurs, although a small fraction of doublets is present. The number of doublets will be discussed further in section 6.4.2.5. However, at $1.1 \cdot 10^{10} \text{ particles/cm}^3$ a sudden transition between a stable and unstable region is observed. In terms of the absolute number of primary particles, the flocculation process after the transition seems to stop at an approximately constant value of N_1 : $N_0(N_1/N_0) = 2.2 \cdot 10^9 \text{ cm}^{-3}$. Between N_0 -values of $2.2 \cdot 10^8$ and $1.1 \cdot 10^{10} \text{ cm}^{-3}$, N_1 is higher, increasing from approximately $2.2 \cdot 10^9$ tot $8 \cdot 10^9 \text{ cm}^{-3}$. Apparently the flocculation rate at these initial concentrations is too low to reach (nearly) complete flocculation within $1\frac{1}{2}$ hours. Surprisingly, at smaller initial concentrations than $2.2 \cdot 10^9$ also some flocculation is observed.

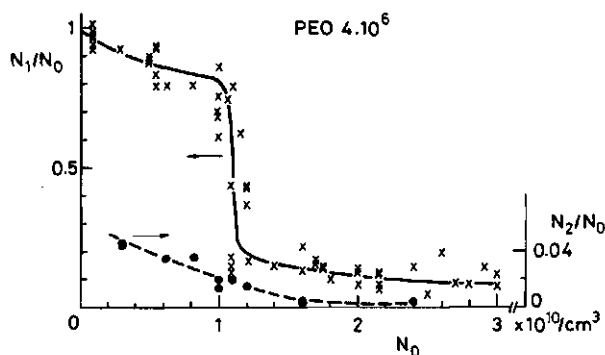


Figure 11. The influence of the initial particle concentration N_0 on the flocculation of 870 latex by PEO $4 \cdot 10^6$. Mixing method a, no salt, PEO-dose 0.34 mg/m^2 . Time after mixing 1.5 hours. The crosses (left hand scale) give N_1/N_0 , the circles (right hand scale) N_2/N_0 .

As before, this is probably caused by an initial non-steady state effect or by an inhomogeneous mixing in the first seconds after the addition of latex to polymer solution. We will not pursue this minor point any further, but concentrate on the main trends. According to Gregory [18] both the attachment and the inter-particle collisions can be approximated by second order rate processes. It is clear that the observed sharp transition cannot be described in terms of a second order rate process.

We propose that a competition between attachment, reconfiguration and inter-particle collisions is responsible for the observed transition. Polymers can only form bridges if they extend beyond the distance of closest approach of the particles (determined by the double layer repulsion). During reconfiguration, the thickness of the polymer layer decreases and therefore the reconfiguration changes the polymers from active (extended, polymer thickness $> 2\kappa^{-1}$) to inactive (equilibrium state, polymer thickness $< 2\kappa^{-1}$). For efficient flocculation to occur, two conditions must be satisfied: Firstly a certain minimum coverage with active polymer is needed, so that there is enough potential for bridge formation. Secondly, particle collisions must be fast enough to ensure that the bridges are actually formed before the polymer becomes inactive due to the reconfiguration. The first condition is met if the

attachment process is fast enough to cover the surface to the required degree before the first attached polymer molecules are already inactivated. The rates of the attachment process and the particle collision process both increase with increasing particle concentration but the reconfiguration process is presumably independent of particle concentration. Therefore, as a function of particle concentration a transition exists between the occurrence of particles with active polymer during collisions and particles with inactive polymer. The times needed to attach, to flatten by reconfiguration, and to collide, for a given system of particles and polymer, will vary around an average. If the distributions around this average values are small then the transition will be rather sharp.

We observed that below a certain concentration of primary particles the flocculation comes to a halt. Apparently at this concentration the reconfiguration process is again faster than the attachment process or the collision process, probably because the particle number becomes too low. At decreasing particle concentration both the time interval between particle collisions and the time interval between particle-polymer collisions increases.

In fig. 12a we present a similar experiment as shown in fig. 11, with the only difference that we used mixing method (b) (mixing latex with a polymer/salt solution), at a final salt concentration of 10^{-2} M KNO_3 . Because the double layer repulsion is now suppressed, also polymers in the equilibrium state are able to create bridges, i.e. particles remain 'active' and we expect again a second order rate process. We can see clearly that now also at low particle concentration flocculation occurs, and it is tempting to check the order by plotting $(N_0/N_1)^{1/2}$ against N_0 . This is done in fig. 12b. For N_0 up to about $8 \cdot 10^9 \text{ cm}^{-3}$ a straight line is found, corroborating a second order rate process. Although in this concentration region some flocculation may occur due to extended polymers, the decrease in primary particles is probably mainly determined by polymers in an equilibrium conformation (equilibrium flocculation). Around a particle concentration of $1.1 \cdot 10^{10} \text{ cm}^{-3}$ a transition can be seen in fig. 12b; at this point flocculation by extended polymers begins to enhance the flocculation rate. At these higher N_0 values there is no time for the polymers to flatten before the particles collide, and also non-equilibrium flocculation occurs.

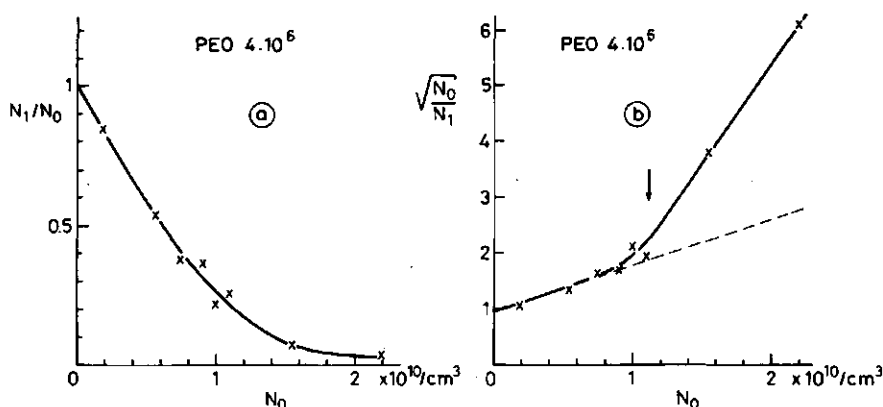


Figure 12. The influence of the initial particle concentration N_0 on the flocculation of B70 latex by PEO $4 \cdot 10^6$. Mixing method b, $[\text{KNO}_3] = 0.01 \text{ M}$, PEO-dose 0.34 mg/m^2 . Time after mixing 1.5 hours. a/ N_1/N_0 versus N_0 , b/ $(N_0/N_1)^{0.5}$ versus N_0 . The dashed line corresponds to purely second order rate process.

In fig. 13a we give data on the influence of the initial particle concentration on the stability of B70 latex with PEO $5 \cdot 10^6$ as a flocculant. This polymer has a slightly higher molecular weight than the previous one and hence, we expect a slower reconfiguration and, consequently, non-equilibrium flocculation. We used mixing method (a), mixing without salt i.e. the same experiment as shown in fig. 11. At first sight, the result looks as if equilibrium flocculation occurs. The sharp decrease of N_1/N_0 and the slowing down of the flocculation rate observed in fig. 11 seem to be absent here. However, plotting the data as $(N_0/N_1)^{1/2}$ versus N_0 does not give the straight line which would correspond to equilibrium flocculation (figure 13b). It is therefore likely that non-equilibrium flocculation contributes to the total rate. However, from this result alone we cannot decide whether we are dealing with non-equilibrium flocculation or not. It is also possible that, for this long polymer, the equilibrium conformation of the polymer is still sufficiently extended to be able to create bridges, despite the double layer repulsion limiting the distance of closest approach. Below (figure 17) we will describe experiments as function of time which are in line with our expectation that this long polymer gives rise to non-equilibrium flocculation.

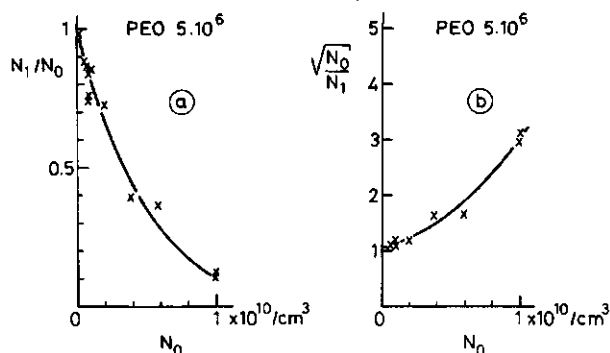


Figure 13. The influence of the initial particle concentration N_0 on the flocculation of B70 latex by PEO $5 \cdot 10^6$. Mixing method a, no salt, PEO-dose 0.17 mg/m^2 . Time after mixing 1.5 hours.

a/ N_1/N_0 versus N_0 , b/ $(N_0/N_1)^{0.5}$ versus N_0 .

Fig. 14, the last experiment in this set, is again for PEO $4 \cdot 10^6$. In this experiment we employed a two-portion method, mixing 1 ml of bare B70 latex with an equal amount of B70 latex covered with polymer, to such an extent that the covered particles are sterically stabilized. We prepared the latter portion by mixing method (a) at a polymer dose of 0.88 mg/m^2 . From previous results we know that the covered latex is stable (see fig. 8). This is indeed observed, see the triangles in fig. 14. The adsorbed polymers were allowed to equilibrate before mixing the two portions and therefore we expect that bridging is not possible: The distance of closest approach is larger than the thickness of the polymer layer. Mixing uncovered particles and covered particles should thus not lead to flocculation. The experimental results (filled circles) are given in fig. 14. Surprisingly, flocculation is observed and even a sudden decrease in primary particle concentration occurs at $1.1 \cdot 10^{10} \text{ cm}^{-3}$. This result seems to be at variance with our conclusions so far. From fig. 2 one can see that for PEO at polymer dose of 0.88 mg/m^2 , 0.78 mg/m^2 will be adsorbed, so that about 0.1 mg/m^2 is present as free polymer in the solution. Perhaps this free polymer interacts with both uncovered and covered particles, creating an initial bridge, which might trigger exchange of

polymer from the covered to the uncovered particle. The kinetics of the exchange of polymer between surface and bulk and between covered and uncovered particles is still very poorly understood.

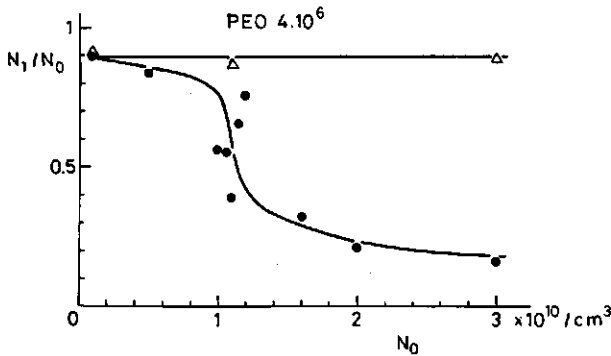


Figure 14. The influence of the initial particle concentration N_0 on the flocculation of B70 latex by PEO $4 \cdot 10^6$. The triangles give the result for a one portion method a, no salt added, PEO-dose 0.88 mg/m^2 . The circles are for a two portion method, mixing bare latex and latex covered with PEO (initial dose 0.88 mg/m^2). Time after mixing 1.5 hours.

6.4.2.4. Flocculation as a function of time

We determined the decrease of primary particles as a function of time for B70 and F70 latex with PEO $6 \cdot 10^5$ and PVP $9.3 \cdot 10^5$, respectively. These polymers may be denoted as 'small' in the context of the flocculation experiments. Mixing method (c), with salt, was used to induce flocculation. The time of end-over-end rotation was varied between 1000 and 5000 s. The results are presented in figures 15 and 16. For both polymers the flocculation appears to follow second order kinetics: the plot of $(N_0/N_1)^{1/2}$ vs t produces a straight line, as should be expected from eq. 3. From the slope we calculated the flocculation rate constant, k_{11} . For PEO $6 \cdot 10^5$ we found a rate constant of $k_{11} = 1.2 \cdot 10^{-13} \text{ cm}^3 \text{ s}^{-1}$ and for PVP $9.3 \cdot 10^5$ $k_{11} = 3.3 \cdot 10^{-13} \text{ cm}^3 \text{ s}^{-1}$. Apparently, the bridging process is more effective with the larger polymer. The rate constant for rapid coagulation is about a factor of 15 larger (see section 5.3.3.).

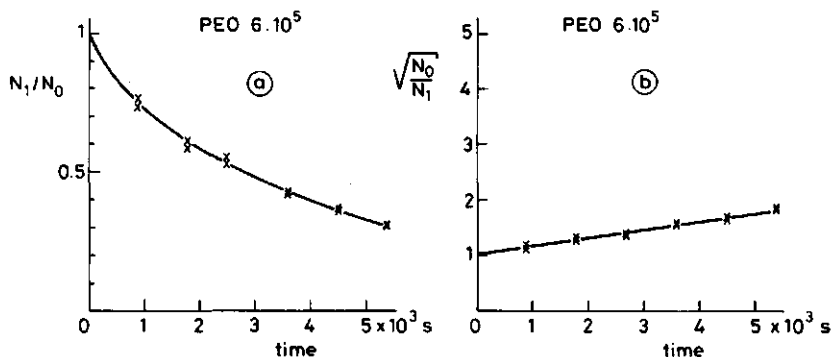


Figure 15. The ratio between the number of primary particles N_1 and to the initial particle concentration N_0 as a function of time. Mixing method c, PEO $6 \cdot 10^5$, dose 0.83 mg/m^2 , B70 latex with $N_0 = 2.3 \cdot 10^9 \text{ cm}^{-3}$, $[\text{KNO}_3] = 0.01 \text{ M}$. a/ N_1/N_0 versus t , b/ $(N_0/N_1)^{0.5}$ versus t .

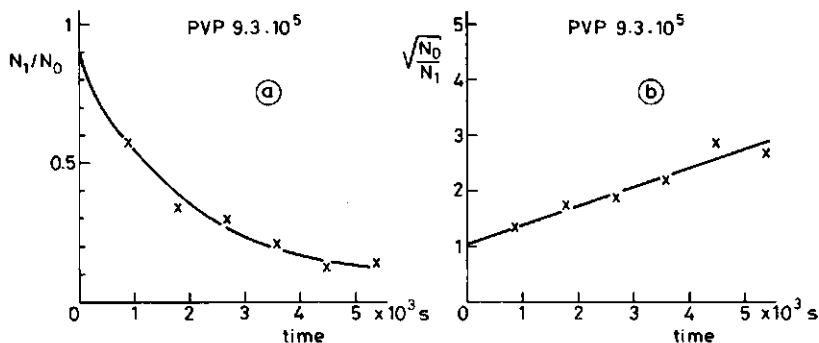


Figure 16. The influence of the flocculation time on the number of primary particles. Mixing method c, PVP $9.3 \cdot 10^5$, dose 0.75 mg/m^2 , F70 latex with $N_0 = 2.0 \cdot 10^9 \text{ cm}^{-3}$, $[\text{KNO}_3] = 0.01 \text{ M}$. a/ N_1/N_0 versus t , b/ $(N_0/N_1)^{0.5}$ versus t .

We carried out a similar experiment with B70 latex and PEO $5 \cdot 10^6$ as the flocculant, but now without salt using mixing method (a), for two initial particle concentrations. The result is given in fig. 17. The number of doublets displayed in fig. 17 will be discussed in the next section. We can see that the (non-equilibrium) flocculation is very fast and that the process stops abruptly at a certain level of particle concentrations. This clearly indicates that the attached polymers become inactive at a certain critical particle concentration (about 10^9 cm^{-3}). Apparently, below this concentration the reformation process is faster than the attachment and/or collision process, so that not enough polymers are available in the extended active state during particle collisions.

We consider this result as a clear indication of non-equilibrium flocculation. For equilibrium flocculation one does not expect that the rate drops to zero below a certain particle concentration. We should mention here that, with PEO $5 \cdot 10^6$, we found no effect of the volume of the latex/polymer mixture during rotation on the degree of flocculation. This is in agreement with the fact that the flocculation process is already finished after the first sampling (5 minutes after mixing) so that orthokinetics (section 6.4.2.1.) probably play a minor role.

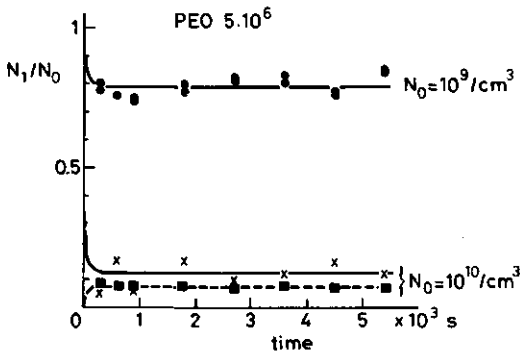


Figure 17. The influence of the flocculation time on the flocculation of B70 latex by PEO $5 \cdot 10^6$. Mixing method a, no salt added. The circles and crosses represent N_1/N_0 at two N_0 -values, the squares are N_2/N_0 at $N_0 = 10^{10} \text{ cm}^{-3}$.

6.4.2.5. Particle size distribution during flocculation

So far, we have only discussed the decrease of primary particles in the flocculation process. However, with SPOS also doublets, triplets and larger aggregates (up to heptaplets) can be observed. As shown in Ch. 5 (fig. 4), a regular evolution in time of doublets and triplets occurs for coagulation by salt.

However, we found that with polymer as the flocculant almost no small aggregates are detected. A typical example is given in fig. 11. The dashed curve represents the number of doublets normalized with respect to the initial particle concentration. Few doublets are observed, of the order of at most 4%. This is representative for all the experiments done, except for the highest molecular weight (PEO $5 \cdot 10^6$). With the latter polymer we detected a reasonable number of doublets ($\sim 8\%$), see the dashed curve in fig. 17. In this case the flocculation is very fast and stops after the first few minutes. In order to explain these observations, we consider perikinetic and orthokinetic effects. In all experiments we rotated the sample end-over-end before counting, introducing orthokinetic collisions. This enhances the flocculation process. According to eq. (2), the orthokinetic rate constant for collisions between two particles i and j with radii a_i and a_j , respectively, is proportional to $(a_i + a_j)^3$. On the basis of this equation, k_{12} for collisions between singlets ($i=1$) and doublets ($i=2$) is greater than k_{11} . Similarly, k_{22} will be larger than k_{12} etc. The values of the rate constant for the formation of aggregates increases with the size of the aggregates. Hence, doublets disappear faster than singlets, and triplets faster than doublets. This is why almost no small aggregates are observed during orthokinetic aggregation. Once the flocculation has started, large aggregates are formed quickly. Indeed did we observe visually large flocs in the flocculation experiments. One might wonder why for PEO $5 \cdot 10^6$ more doublets are found. We assume that in this case the flocculation rate is so high, that the flocculation is nearly complete, before the rotation was started, i.e., in the first seconds after mixing. Then the process is mainly determined by perikinetics $\{k_{ij} \sim (a_i + a_j)(a_i^{-1} + a_j^{-1})$, see eq.(1)}. The rate is nearly independent of the aggregate size, implying a more even distribution of aggregates of different sizes. By way of example, we calculated from eqs.(1) and (2) the ratios of several rate constants for the peri- and orthokinetic case, see table 3.

For the calculations we assumed more or less arbitrarily the effective radius of a doublet and a triplet to be $1.5 a_1$ and $2a_1$, respectively.

Table 3. Ratio of rate constants

	k_{12}/k_{11}	k_{13}/k_{11}	k_{22}/k_{11}	k_{23}/k_{11}	k_{33}/k_{11}
perikinetic	1.04	1.13	1	1.02	1
orthokinetic	1.95	3.38	3.38	5.36	8

On the basis of these numbers it is easily explained why in perikinetic flocculation, as with PEO $5 \cdot 10^6$, more doublets are found than in processes when the orthokinetic contribution is considerable. In our experiments, we counted also some higher aggregates than doublets. The numbers are small and not very accurate. So far we have not attempted to analyze the data fully.

6.5. A new model for polymer flocculation

In the results discussed in section 6.4., a clear distinction between two mechanism of flocculation could be made, namely equilibrium and non-equilibrium flocculation.

In the case of equilibrium flocculation (figs 10, 15 and 16), the decrease of primary particles goes on gradually until all are incorporated in larger aggregates. The final average size of the aggregates will depend on shear forces, binding forces and the amounts of polymer and latex used. Furthermore, at not too high particle concentrations, the decrease of primary particles obeys second order kinetics according to the Von Smoluchowski theory, at least in the observed time scale.

In non-equilibrium flocculation (figures 11 and 17) the number of singlets decreases with time until a certain residual concentration of particles is reached. At this concentration level, the processes leading to bridge formation have become so slow that they can no longer compete with the reconformation process; the polymer goes from the active (extended) state to the inactive equilibrium conformation before enough polymer is adsorbed or before particle collision occurs. In some cases, a sudden transition between a stable and unstable dispersion occurs as function of the particle

concentration. The occurrence of such a transition depends on the molecular weight of the polymer.

We have schematically represented these flocculation mechanisms in fig. 18, and will discuss the conditions for them to be operative. We assume that mixing yields a homogeneous mixture within a time that is small compared to the time of flocculation. In this scheme we therefore start with a homogeneous mixture of latex and polymer (upper left corner). The particles are charged and the double layer thickness κ^{-1} is indicated as the dashed circle around the particles. We will have to compare the extension of the polymer with $2\kappa^{-1}$, the distance of closest approach. The polymer molecules are random coils in solution with a Gaussian density distribution. The flocculation process starts with attachment of polymer on the particles. The rate of this process is determined by the concentration of polymer and particles, and by the migration speed of both species in solution. This migration speed is determined by Brownian diffusion (perikinetics) and, in case of shear forces, also by fluid motion (orthokinetics). A semiquantitative expression for the rate of attachment has been given in section 6.2.1.

A certain minimum degree of polymer coverage is needed so that potentially enough bridges can be formed during particle collision to get an effective binding. We consider two possibilities: 1) the attachment is slow with respect to the reformation process and 2) the attachment is faster than this reformation.

In case (1) the first attached polymers flatten to an extension below $2\kappa^{-1}$, before the required coverage is reached. Hence no flocculation occurs (left hand route in fig. 18).

In case (2) enough polymer is attached and still available in the extended state so that potentially effective bridging is possible. However, whether or not a stable bridge between the particles is formed depends on the particle collision rate. Also for this situation, eqs. (1) and (2) can be used to get a semiquantitative estimate. At too slow a collision rate the extended polymers will have flattened before a collision occurs: also in this case no flocculation occurs (middle column of fig. 18). Only in the case of a fast attachment and a fast collision process enough active polymer is available during collisions for bridging to take place: non-equilibrium flocculation is found (top row in fig. 18). As the flocculation proceeds, the rates of attachment and collision decrease due to the decreasing particle concentration. Therefore the flocculation will stop at a certain particle

concentration.

In the case of a slow adsorption process and/or a slow collision process, flocculation can be induced by salt addition. Due to this addition, κ^{-1} becomes smaller and polymers in the equilibrium conformation may create effective bridges and therefore equilibrium flocculation occurs (bottom right in fig. 18).

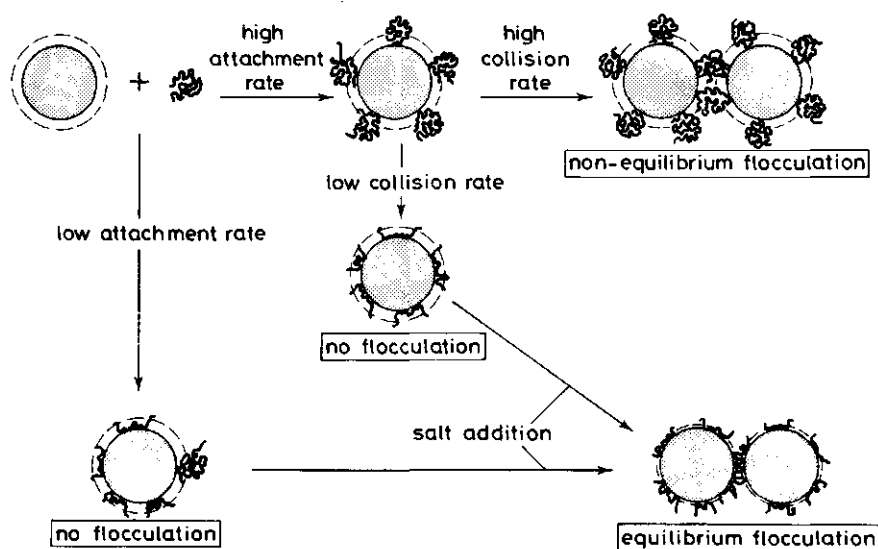


Figure 18. Schematic representation of the mechanisms of bridging flocculation in charged systems.

When salt is added to a dispersion in which both the adsorption and collision processes are fast, we may have both mechanisms operating. In the initial stages there will be mainly non-equilibrium flocculation but as the number of particles decreases, the mechanism changes gradually to equilibrium flocculation.

Finally, in fig. 19 we present an overview of the various observed and expected flocculation phenomena. From left to right the double layer thickness (κ^{-1}) decreases. This distance is compared with the end-to-end distance h_m of the polymer coil and with the equilibrium thickness δ_h of the polymer layer on the surface. From top to bottom the length of the polymer increases and,

consequently, the reconformation rate decreases.


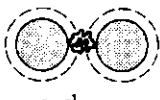

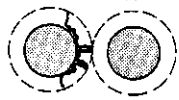
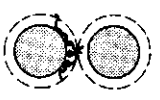
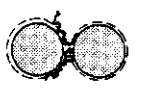
In case (A) (second column) even the size of the extended polymer is smaller than $2\kappa^{-1}$ and therefore flocculation is impossible. For short polymers this situation is experimentally accessible but for long polymers h_m is always larger than $2\kappa^{-1}$, even at very low ionic strengths.

In case (B) (third column), the size of the extended polymer is larger than the distance of closest approach but the thickness of the equilibrium polymer layer is smaller. Therefore, if flocculation occurs this is only possible due to the extended polymers. Short polymers have a very fast reconformation process and the particle concentration where the attachment and collision process could compete with this process is experimentally inaccessible. For medium length polymers the reconformation process is slower, and this competition is possible at 'normal' particle concentrations. At high N_0 non-equilibrium flocculation occurs, at low N_0 no flocculation occurs. With long polymers, the reconformation process is much slower and therefore even at rather low particle concentrations non-equilibrium flocculation takes place.

In case (C) (right hand column), also the equilibrium thickness of the polymer is larger than the distance of a closest approach. For short polymers equilibrium flocculation occurs at all particle concentrations. Extended polymers are not available due to the fast reconformation process. For medium length polymers at high particle concentrations, the attachment and collision processes are faster than the reconformation process and non-equilibrium flocculation is found. At lower N_0 bridging takes place only due to polymer in equilibrium at the surface (equilibrium flocculation). For long polymers initially only non-equilibrium flocculation occurs, even at low particle concentrations, at very low concentrations followed by equilibrium flocculation.

6.6. Estimation of the reconformation time

As discussed before, the type and efficiency of the flocculation depends on the relative time scales t_{att} for the polymer attachment, t_{rec} for the reconformation of the adsorbed polymer and t_{col} for the collision between the particles. Here, t_{att} is the average time needed to attach enough (active) polymer to form sufficient bridges, t_{rec} the time required for flattening of the adsorbed polymer to less than $2\kappa^{-1}$, and t_{col} the average time between two two particle collisions. From the data plotted in fig. 11 it is possible to

<div> <div> <div>→</div> <div>increasing salt concentration</div> </div> <div> <div>↓</div> <div>increasing M of polymer</div> </div> </div>	case A	case B	case C
	 $2\kappa^{-1} > h_m$	 $2\kappa^{-1} < h_m$	 $2\kappa^{-1} \ll h_m$
	 $2\kappa^{-1} \gg \delta_h$	 $2\kappa^{-1} > \delta_h$	 $2\kappa^{-1} < \delta_h$
Short polymer	NF	reconformation fast NF	reconformation fast EF.
Medium length polymer	experimentally inaccessible	reconformation slower low N_0 : NF. high N_0 : NEF, because of high attachment and collision rate	reconformation slower low N_0 : EF. high N_0 : first NEF, followed by EF
Long polymer	experimentally inaccessible	reconformation slow NEF	reconformation slow first NEF at very low N_0 , followed by EF

NF means no flocculation, EF means equilibrium flocculation and NEF means non-equilibrium flocculation.

Figure 19. Flocculation of charged particles by polymers of various molecular weights at different ionic strengths. κ^{-1} is the Debye length, h_m the rms end-to-end distance of a polymer coil, δ the polymer layer thickness at equilibrium, and N_0 the initial particle concentration.

obtain a semiquantitative estimate of t_{rec} , provided that approximate values of t_{att} and t_{col} are available. Since t_{att} and t_{col} are determined by collision processes, they can be estimated, following Gregory [18], from the rate constants as given in eqs. (1) and (2). Whereas t_{rec} is independent of

the particle concentration N_0 , t_{att} and t_{col} are a function of N_0 .

For low N_0 in fig. 11, polymer attachment and particle collisions are slow with respect to the reconfiguration: $t_{att} > t_{rec}$ and/or $t_{col} > t_{rec}$, giving no flocculation. For high N_0 , non-equilibrium flocculation occurs and both t_{att} and t_{col} are smaller than t_{rec} . At the transition concentration in fig. 11, we expect that t_{rec} is about equal to the largest value of t_{att} and t_{col} , because both $t_{rec} > t_{att}$ and $t_{rec} > t_{col}$ are sufficient conditions for flocculation to occur.

For an estimation of t_{att} we first calculate the rate constant k_{lp} for a collision between a singlet and a polymer coil. From eqs. (1) and (2) we find, using $a_1 = 348$ nm, $a_p = 118$ nm (see table 1), and $G = 400$ s⁻¹ (gentle end-over-end rotation), the values for k_{lp} listed in table 4, for both perikinetik and orthokinetic conditions and for a combination of the two. Gregory (18) estimated t_{att} from

$$t_{att} = - [\ln(1 - f)] / k_{lp} N_0 \quad (4)$$

where f is the fraction of initially present polymer molecules that needs to be adsorbed for efficient bridging. This expression was derived under the assumption that k_{lp} is independent of surface coverage and that N_0 does not change during attachment. We assumed $f = 0.9$, but this choice is not very critical: taking $f = 0.5$ decreases t_{att} by only a factor of 3. With $N_0 = 1.1 \cdot 10^{10}$ cm⁻³, t_{att} is obtained immediately, see table 4.

Table 4. Rate constants k_{lp} and k_{ll} , and the corresponding time scales t_{att} and t_{col} at the transition concentration $N_0 = 1.1 \cdot 10^{10}$ cm⁻³.

k_{lp}	k_{ll} (10 ¹² cm ³ s ⁻¹)	t_{att} (10 ¹² cm ³ s ⁻¹)	t_{col} (s)	(s)
peri	15.7	10.8	13.3	16.8
ortho	47.6	181.3	4.4	1.0
peri+ortho	63.3	192.1	3.4	0.95

Similarly, t_{col} follows from the rate constant k_{11} for a collision between singlets. In eqs. (1) and (2) we now substitute $a_1 = a_2 = 349 \text{ nm}$ and $G = 400 \text{ s}^{-1}$. The values found for k_{11} are again given in table 4. The time t_{col} follows from k_{11} through $t_{col} = 2/k_{11}N_0$, and is also given in table 4.

Now we can conclude from table 4 that the time t_{rec} in which PEO $4 \cdot 10^6$ rearranges itself to such an extent that the layer thickness becomes less than $2\kappa^{-1} \approx 200 \text{ nm}$ is 3-4 seconds. Obviously, this is not the time in which the polymer layer changes from fully extended to fully relaxed. As shown by Cohen Stuart [21] the latter time scale may be, for PVP of molecular weight $7 \cdot 10^5$, of the order of minutes. For very high molecular weight PEO, this could be even longer.

6.7. Concluding remarks

We summarize the most important features of aggregation of colloidal particles by polymer.

Polymer adsorption is characterized by an initial attachment followed by a reconfiguration process during which the polymer layer thickness decreases. We can distinguish two limiting cases for the mechanism of bridging flocculation:

- a. bridging due to relaxed polymers, denoted as equilibrium flocculation,
- b. bridging due to extended polymers, indicated as non-equilibrium flocculation.

Equilibrium flocculation may take place when the dispersion remains stable during the adsorption process. This flocculation can be induced by adding salt, thereby reducing the double layer repulsion. In this mechanism the adsorption process is completed before the flocculation starts.

Non-equilibrium flocculation can occur if the distance of closest approach, determined by the double layer repulsion, is smaller than the size of the extended non relaxed polymer on the surface. The attachment and collision processes must be fast enough to give flocculation before the reconfiguration has decreased the polymer layer thickness considerably. Because both the rates of attachment and of collision depend on the particle number concentration, the occurrence of this mechanism is predominantly found at relatively high particle concentrations. For very long polymer chains, non-equilibrium flocculation may be found at low concentrations of the dispersion.

Experiments with poly(ethylene) oxide of various molecular weight on latex show that, depending on molecular weight and salt concentration, one or both

mechanisms are operative.

If only non-equilibrium flocculation occurs, the reconformation time, i.e. the average time needed to change the polymers from active to inactive polymers can be estimated from the particle concentration at which the flocculation starts. For PEO $4 \cdot 10^6$ we found 3-4 seconds.

We found that, within our experimental conditions, shear forces were necessary to induce flocculation both in the case of equilibrium and non-equilibrium flocculation (except for the longest polymer, PEO $5 \cdot 10^6$). In the case of only Brownian motion, the rate of the equilibrium flocculation is very slow and non-equilibrium flocculation does not occur because the attachment and collision processes (see table 4) are too slow to compete with the reconformation process.

In the case of orthokinetic non-equilibrium flocculation the decrease in primary particles as a function of the initial particle concentration does not follow second order kinetics. Also as a function of time such a behaviour is not found. A very conspicuous feature is that below a certain concentration of monomers the flocculation comes to a halt.

References

1. Kuz'kin, S.K., and Nebera, V.P., Synthetic Flocculants in De-watering Processes, Moscow (1963) (Trans. Nat. Lending Library, Boston, G.B., 1966)
2. Vincent, B., and Everett, D.H., (Senior reporter), "Colloid Science Vol.I." The Chemical Society, London (1973).
Vincent, B., Adv. Colloid Interface Sci. 4, 193 (1974).
3. Napper, D.H., and Hunter, R.J., in "M.T.I. International Review of Science, Physical Chemistry, Surfaces Chemistry and Colloids" (M. Kerker, Ed), Ser. 1, Vol. 7. Butherworths, London (1972).
4. Kitchener, J.A., Br. Polym. J. 4, 217 (1972).
5. Lyklema, J., Adv. Colloid Interface Sci. 2, 65 (1968).
6. La Mer, V.K., and Healy, T.W., Rev. Pure Appl. Chem. 13, 112 (1963).
7. Silberberg, A., J. Chem. Phys., 48, 2835 (1968).
8. Hoeve, C.A.J., J. Chem. Phys., 44, 1505 (1966).
9. Roe, R.J., J. Chem. Phys., 60, 4192 (1974).
10. Dimarzio, E.A., and Rubin, R.J., J. Chem. Phys., 55, 4318 (1971).
11. Ash, S.G., Everett, D.H., and Findenegg, G.H., Trans. Faraday Soc., 66, 708 (1970) ; *ibid.*, 67, 2122 (1971).
12. Scheutjens, J.M.H.M., and Fleer, G.J., J. Phys. Chem. 83, 1619 (1979).
13. Scheutjens, J.M.H.M., and Fleer, G.J., J. Phys. Chem. 84, 178 (1980).
14. Scheutjens, J.M.H.M., and Fleer, G.J., Macromolecules 18, 1882 (1985).
15. Klein, J., Adv. Colloid Interface Sci., 16, 101 (1982).
16. Klein, J., and Luckham, P.F., Nature (London) 308, 836 (1984).
17. Israelachvili, J.N., Tirrell, M., Klein, J., and Almoy, Y., Macromolecules 17, 204 (1984).
18. Gregory, J., Conference Polymers in Colloidal Systems, Eindhoven (1987). To be published in Colloids and Surfaces.
19. Csempesz, F., and Rohrsetzer, S., Conference Polymers in Colloidal Systems, Eindhoven (1987). To be published in Colloids and Surfaces.
20. Ash, S.G., and Clayfield, E.J., J. Colloid Interface Sci. 55, 645 (1976).
21. Cohen Stuart, M.A., and Tamai, H., accepted Macromolecules.
22. Cowell, C., and Vincent, B., in "The effect of polymer on dispersion properties"(Th.F. Tadros, Ed), p. 263, Academic Press, London (1982).
23. Ruehrwein, R.A., and Ward, D.W., Soil Sci. 73, 485 (1952).
24. Akers, R.J., Flocculation, I. Chem. E., London (1975).

25. Bailey, F.E., and Koleske, J.V., Poly(Ethylene Oxide), (a) p. 46, (b) p. 53, Academic Press, New York (1976).
26. Nabi, G., Pak. J. Sci. 20 (3), 136 (1968).
27. Flory, P.J., Principles of Polymer Chemistry, p. 611, Cornell University Press, Ithaca (1953).
28. Tanford, C., Physical Chemistry of Macromolecules, p. 401, Wiley, New York (1961).
29. Nuysink, J., and Koopal, L.K., Talanta, 29, 495 (1982).
30. Florin-Robertson, E., Thesis, The Royal Institute of Technology, Stockholm (1983).
Kjellander, R., and Florin, E., J. Chem. Soc., Faraday Trans. 1, 77, 2053 (1981).
31. Cohen Stuart, M.A., Waajen, F.H.W.H., Cosgrove, T., Vincent, B., and Crowley, T.L., Macromolecules, 17, 1825 (1984).
32. Gregory, J., and Sheiham, I., Br. Polym. J. 6, 47 (1974).
33. Von Smoluchowski, M., Phys. Z., 17, 557, 585 (1916).
Von Smoluchowski, M., Z. Phys. Chem., 92, 129 (1917).

Appendix A

The sample and hold electronics circuit

The function of the electronics circuit is to determine the peak height of an electrical pulse (time base 225 μ s) originating from the photomultiplier, and delivering an electrical pulse of the same height but with a much smaller time base (7 μ s) to the multichannel analyzer (pca2048, The nucleus). The latter instrument can only accept pulses up to 20 μ s correctly. Pulses of longer duration would be sampled more than once, leading to erroneous data collection.

In addition we built in several other functions: disturbing signals are filtered out, and only pulses above a certain level and with a certain time base are processed. We will discuss these functions with the help of figure 1, which gives an overall scheme of the electronics circuit.

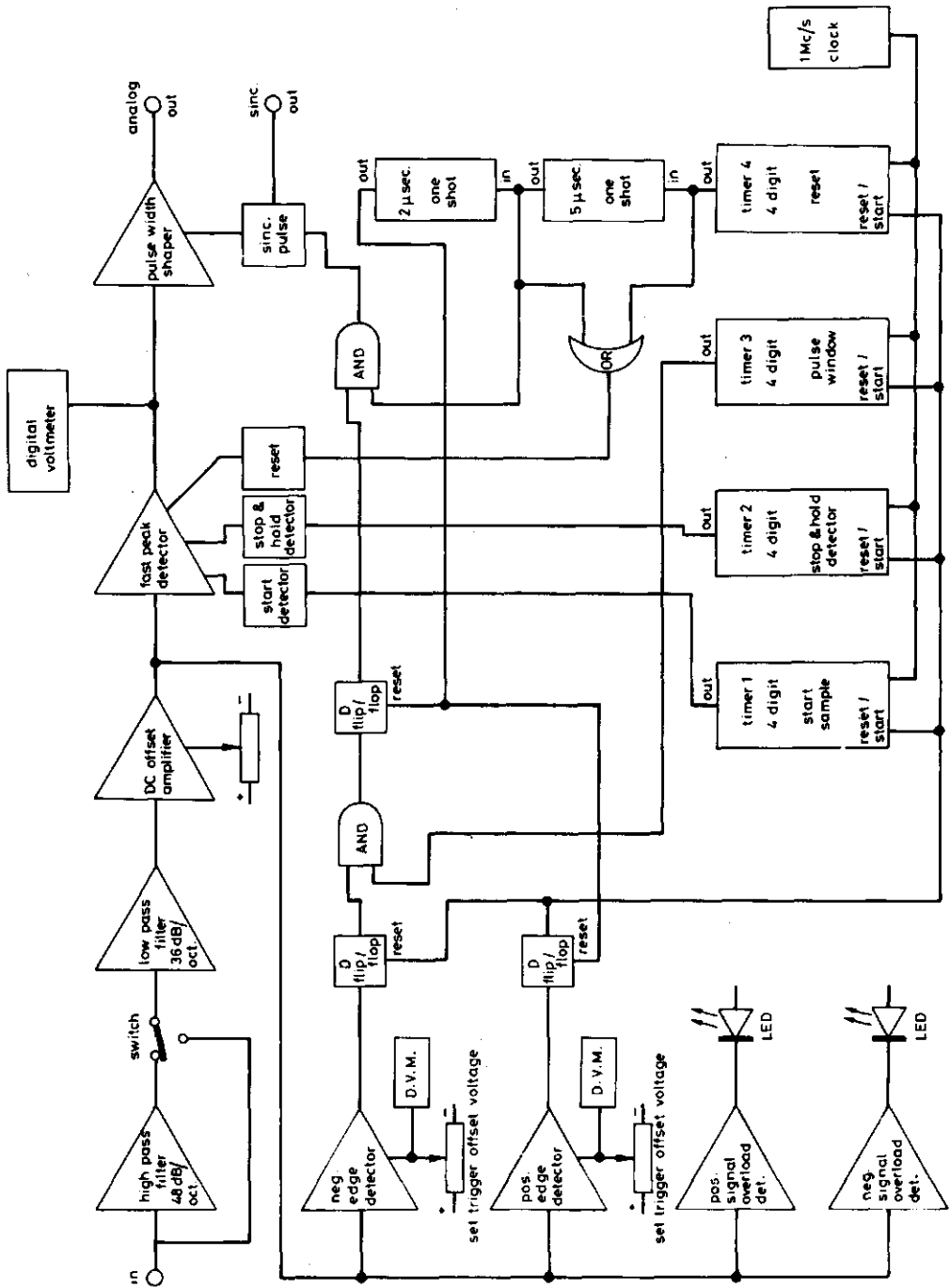
Starting at the upper left corner, a high pass filter, a low pass filter and a DC offset amplifier are indicated. The high pass filter can be switched off; in most cases we did not use this filter. This first part of the circuit is used to filter out small signals of high frequency, superimposed on our signals that have a relatively low frequency. We suspect that these high frequency signals originate from the fact that the intensity distribution across the laser focus is not a perfectly Gaussian distribution (see section 4.3.2.) but still very small light intensity variations are present. From basic physics we know that an electronic filter is a differentiator. Therefore, after the filter also negative pulses are present. After passage through a low pass filter these negative pulses are very wide and shallow. With many of these pulses (as in our case) the total effect is a decrease of the DC-zero level. This is compensated by the DC-offset amplifier. The differentiating effect of a high pass filter would be short and relatively strong negative pulses, which cannot be corrected by a DC-offset amplifier. This is the main reason for not using this filter.

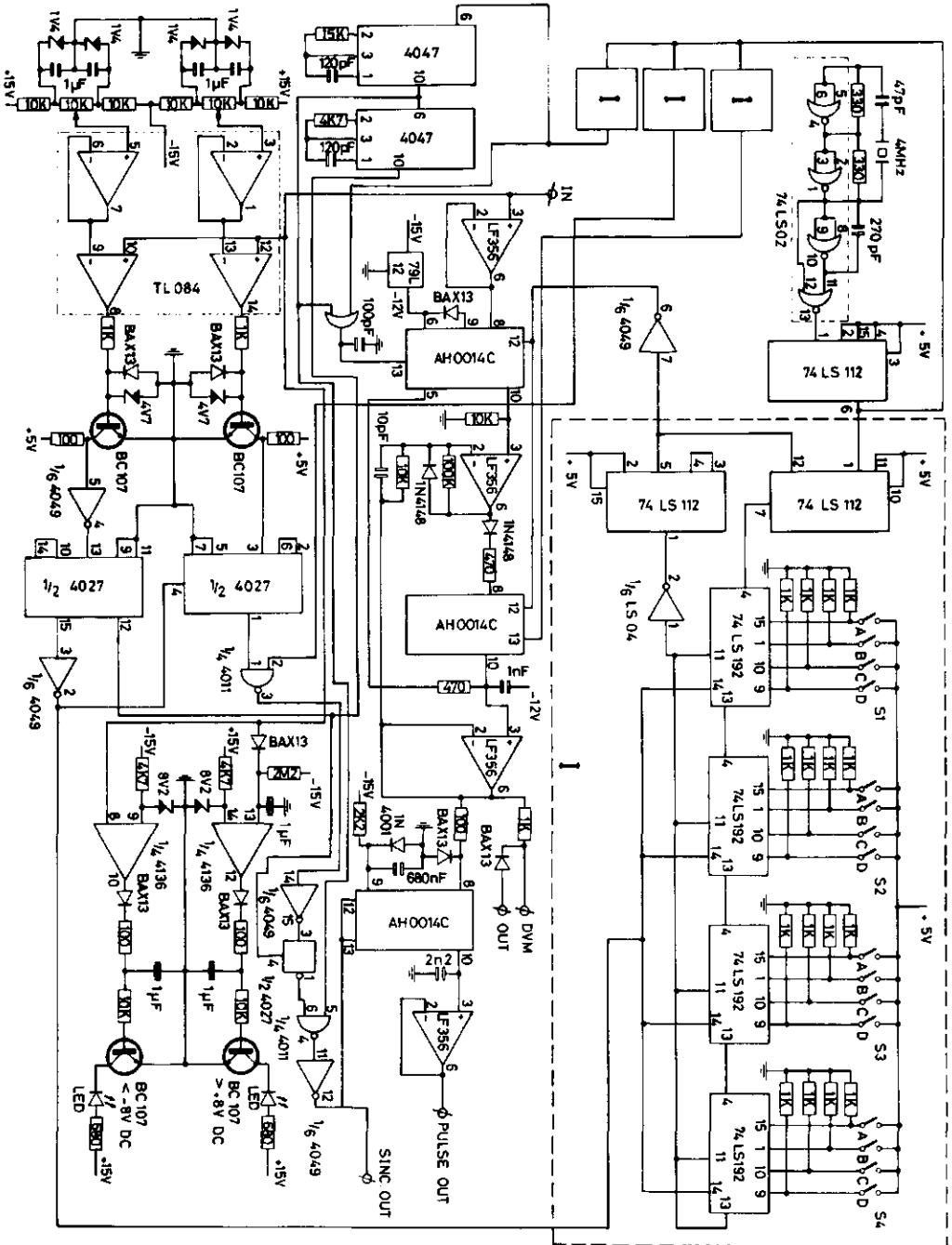
The fast peak detector is activated as the electrical incoming pulse reaches a certain trigger level value, an internal clock starts running. Hence weak signals generated by small dust particles or other sources of noise are not recorded. After time t_1 (usually 1 μ s) the output signal of the sample and hold circuit equals the value of the input value. Therefore pulses with a time base smaller than t_1 are ignored. The output signal is maintained at the

maximum level of the input signal even if this input signal decreases. After time t_2 (usually 450 μ s) the output signal is kept constant even if the input signal increases above this level. In this way, noise with a small time base just after the particle pulse is disregarded. After time t_3 (usually 700 μ s) the input signal is compared with a trigger end value. If the input signal is still higher, the output signal is reset to a negative value the multichannel analyzer receives no signal. Therefore very big dust particles or very big aggregates or two particles passing just after each other are not recorded if the signal has a time base above t_3 .

The output signal is fed to a pulse width shaper (top right in fig. 1) which blocks the connection between the sample and hold output gate and the input gate of the multichannel analyzer. After time t_4 (usually 701 μ s) the sample and hold circuit puts out a synchronisation pulse, which instructs the pulse width shaper to connect the output signal to the multichannel analyzer during 7 μ s. After t_4 the circuit is reset and can accept a new pulse. In principle, the dead time per particle pulse is given by t_4 . With these time windows we tried to avoid signals of very small and very large dust particles. However, many "skips" of these particles could influence the total dead time. We checked that this was not the case by varying the values of the time windows. We want to acknowledge mr. Wegh of our electronic workshop who designed the electronics circuit. Figure 2 and 3 give technical details of the frequency cut-off filter and the sample and hold circuit, respectively.

Figure 1. The overall scheme of the electronics circuit of the filter and the 'sample and hold'.





Summary

The subject of this thesis is the development of a Single Particle Optical Sizer (SPOS) which is capable of measuring in detail discrete particle size distributions in the colloidal size range. With this instrument we studied the aggregation of latices induced by polymer and salt, and found evidence for non-equilibrium flocculation.

Chapter 2 is an inventory of the existing methods of measuring aggregation. A comparison is made with our SPOS instrument. The techniques are classified into three groups: classical, multi particle detection and single particle detection methods. Only very global information is obtained about the aggregation process with the classical methods. In the case of turbidity, only the initial rate of the total aggregation process can be obtained. Multi-particle detection methods are able to determine accurately a particle size in monodisperse samples (laser beat spectroscopy). For large spherical particles ($d > 1 \mu\text{m}$) a particle size distribution can be measured (laser diffraction spectroscopy). With small angle light scattering an initial rate of the aggregation can be determined. Single particle detection methods are able to measure discrete particle size distributions. With electron microscopy very small particles can be individually sized. However this technique is rather tedious and unsuitable for the study of aggregation kinetics. With SPOS, also a single particle detection method, fast and reliable particle size and aggregate distribution can be measured as a function of time.

The SPOS instrument operates on the principle of low angle light scattering. In order to determine the measurable size range of the SPOS, we present in chapter 3 numerical results of the light scattering intensity as a function of size, type, solvent and detection angle, as obtained with the Mie theory.

In chapter 4, the design of the SPOS is described and several test experiments on the operation of the instrument are presented. In the instrument the particles are hydrodynamically focused into a very narrow stream, and they pass one-by-one through an elliptical laser focus. Upon passage, each of them emits a flash of light which is detected by a photomultiplier and converted into an electronic pulse which is stored according to its intensity in a multichannel analyzer. The number of signals of each size can be displayed and renders a complete particle size distribution.

Much attention is paid to the possible influence of the hydrodynamic forces in the instrument on the disruption of aggregates. We conclude that only for very

weakly bond aggregates de-aggregation may occur before monitoring.

In chapter 5 the instrument is used to study the coagulation process (aggregation induced by salt) of latex dispersions. We describe the preparation of the latices and determine the rate constants of three initial aggregation steps (singlet+singlet, singlet+doublet and singlet+triplet). This enables us to check the primary assumption of the Von Smulochowski theory which states that all these rate constants are the same. We measured a difference between the value of the determined rate constants. Furthermore we used three different mixing cells to study the effectivity of mixing and the influence on the aggregation rate.

In chapter 6 we use the SPOS method to study the aggregation induced by polymer. The experimental results are on first sight rather surprising. In many cases the flocculation does not obey second order kinetics. Nevertheless, the data can be well understood if the dynamical aspects of the polymer adsorption are taken into account. From our experiments a clear distinction in behaviour was found between polymers in a relaxed or a non-relaxed state on the latex surface, leading to equilibrium or non-equilibrium flocculation, respectively. In the latter case the rates of polymer attachment and particle collision are faster than the rate of reformation of adsorbed polymer. We propose a new model for polymer induced bridging flocculation which incorporates these two mechanisms and predicts the occurrence of these mechanisms as a function of particle concentration, molecular weight of the polymer, shear forces and double layer repulsion.

Samenvatting

In dit proefschrift wordt de ontwikkeling van een "Single Particle Optical Sizer" (SPOS) beschreven, welk apparaat de mogelijkheid biedt om discrete grootteverdelingen van kolloidale deeltjes te bepalen. Met dit instrument is een studie verricht naar de vlokking van latices onder invloed van zout en polymeer.

Hoofdstuk 2 geeft een inventaris van de bestaande methoden om vlokking te bestuderen en een vergelijking met het door ons ontwikkelde apparaat. Deze technieken worden geklassificeerd in drie categorieën, respectievelijk de klassieke methoden, de detectiemethoden voor meerdere deeltjes tegelijkertijd, en de methoden gebaseerd op de detectie van afzonderlijke deeltjes. Klassieke methoden geven alleen kwalitatieve informatie over de vlokking. Zo kan met turbiditeitsmetingen de initiële vloksnelheid gemeten worden. Toepassing van detectiemethoden voor meerdere deeltjes, zoals dynamische lichtverstrooiing, geeft de mogelijkheid de deeltjesstraal van monodisperse monsters nauwkeurig te bepalen. Voor grote deeltjes ($d > 1 \mu\text{m}$) kan soms een deeltjesgrootteverdeling gemeten worden (laser diffractie spectroscopie). Met lichtverstrooiing onder kleine hoek kan de initiële vloksnelheid bepaald worden.

Met behulp van methoden gebaseerd op de detectie van afzonderlijke deeltjes, kan een discrete deeltjesgrootteverdeling gemeten worden. Met elektronenmicroscopie kunnen zeer kleine deeltjes bestudeerd worden, maar deze techniek is omslachtig en niet geschikt voor kinetisch onderzoek van aggregatie processen. Met SPOS, de meest geavanceerde vertegenwoordiger van deze groep, kan snel en betrouwbaar de grootteverdeling van deeltjes en aggregaten als functie van tijd gemeten worden.

Het SPOS-instrument is gebaseerd op lichtverstrooiing aan afzonderlijke deeltjes onder een kleine hoek. Om het meest geschikte meetbereik van de SPOS te analyseren, worden in hoofdstuk 3 numeriek berekende resultaten gegeven van de intensiteit van de lichtverstrooiing, als functie van de grootte en het type deeltjes, van het soort oplosmiddel, en van de detectiehoek. Deze resultaten werden verkregen door gebruik te maken van de theorie van Mie.

In hoofdstuk 4 wordt de constructie van het SPOS-instrument in detail beschreven. Tevens worden test-experimenten besproken, die de mogelijkheden van het apparaat aangeven. In het apparaat worden de deeltjes hydrodynamisch gefocusseerd tot een zeer smalle dispersiestraal, waarbij de deeltjes één voor

één een elliptisch gefocusseerde nauwe laserbundel passeren. Tijdens elke passage emitteert een deeltje een lichtflits welke omgezet wordt in een elektrische puls door een fotomultiplicatorbuis. De elektrische pulsen worden naar grootte gesorteerd en opgeslagen in een 'multichannel analyzer'.

Veel aandacht werd besteed aan de mogelijke invloed op de aggregaatverdeling van de hydrodynamische krachten in het instrument. Het blijkt dat alleen zeer zwak gebonden aggregaten worden opgebroken door deze krachten. In de meeste gevallen zal dus de correcte verdeling van de grootte van aggregaten gemeten worden.

In hoofdstuk 5 wordt de vlokking onder invloed van zout, zoals gemeten met SPOS, besproken. We beschrijven de synthese van de latices en de waarde van de vloksnelheidsconstanten van drie initiële vlokreacties: singlet+singlet, singlet+doublet en singlet+triplet. De primaire veronderstelling van de Von Smoluchowski theorie dat alle vloksnelheidsconstanten gelijk zijn, blijkt niet volledig juist. Verder zijn verschillende mengcellen gebruikt om de invloed van de menging op de vloksnelheid te bestuderen.

In hoofdstuk 6 volgt de beschrijving hoe SPOS gebruikt kan worden om de vlokking van latex onder invloed van polymeer te bestuderen. Op het eerste gezicht zijn de experimentele resultaten nogal verrassend. In veel gevallen blijkt de kinetiek niet van tweede orde te zijn, zoals verwacht mag worden bij processen die bepaald worden door botsingen van twee deeltjes. Desalniettemin kunnen de resultaten goed begrepen worden als de dynamische aspecten van polymeeradsorptie in rekening gebracht worden. Uit onze experimenten blijkt een duidelijk verschil in het gedrag van vlokkende latices tussen systemen waarbij het polymeer in een gerelaxeerde dan wel niet-gerelaxeerde toestand aanwezig is op het oppervlak van de deeltjes. In het eerste geval spreken we van evenwichtsvlokking, in het tweede geval van niet-evenwichtsvlokking. Bij niet-evenwichtsvlokking zijn de snelheden van de aanhechting van polymeer en van de botsingen tussen de deeltjes sneller dan de snelheid van reconformatie van het geadsorbeerde polymeer. Afgeleid kan worden dat het enkele seconden duurt voordat het aangehechte polymeer minder ver uitstrekt dan tweemaal de dubbellaagdikte ($\kappa^{-1} \sim 100$ nm). Wij poneren een nieuw model voor de vlokking door middel van brugvorming. Zowel evenwichtsvlokking als niet-evenwichtsvlokking zijn in het model verwerkt. Voorspeld kan worden wanneer deze beide mechanismen voorkomen, als functie van de deeltjes concentratie, het molecuulgewicht van het polymeer, van afschuifkrachten en van dubbellaagrepulsie.

Levensloop



Een moment opname

De schrijver van dit proefschrift werd geboren op 2 februari 1958 te Geleen. Na het behalen van het diploma Atheneum B aan de Albert Schweitzer Scholengemeenschap te Geleen in 1976 begon hij in dat jaar met de studie Scheikunde aan de Rijksuniversiteit van Utrecht. In augustus 1983 werd het doctoraal Scheikunde afgelegd met als hoofdvak fysische en colloïdchemie en als bijvak biochemie. Op 1 september 1983 trad hij in dienst van de Landbouwniversiteit te Wageningen als medewerker bij de vakgroep Fysische en Kolloïdchemie, waar het in dit proefschrift beschreven onderzoek werd uitgevoerd.

Dankwoord

Boven in het kraaiennest, lijkt een schip zeer hevig te slingeren. Telkens als er een golf komt, lijkt de ondergang nabij maar gelukkig is de mast tussen kraaiennest en schip stevig geconstrueerd.

Beste Pa en Ma, als eerste denk ik aan jullie en aan de fijne jeugd die ik heb gehad. Jullie hebben mij gestimuleerd om dat te studeren wat ik zelf wilde, al was dat in het verre Utrecht.

Knappe Thea, in meer dan een opzicht, met meer dan wie dan ook, heb ik met jouw lief en leed gedeeld. Wat denk je van een vakantie in rustig vaarwater rond een zonovergoten eiland.

Beste Gerard Fleeer, als ik je mag vergelijken met een zeeman dan ben je de machinist die onvermoeibaar het schip op stoom houdt en de schoorsteen laat roken. Met volle kracht voorruit laat je het Kolloidschip opstomen door weer en wind. Je zorgt dat je 'crew' optimaal kan werken en ik wil je hartelijk bedanken voor de vele hulp bij het schrijven van mijn 'logboek'.

Enthousiaste Martien Cohen Stuart, jouw serieuze belangstelling voor mijn problemen zijn een grote steun geweest. Jouw stijl van onderzoek is van hoge kwaliteit en dynamisch bewonderenswaardig. Ook jou wil ik bedanken voor de 'logboek' activiteiten.

Beste Erik Buiskool, Bert Koops, Geert Verhoeven, Jacco Wijkmans en Leo Verbene, jullie zijn mij zeer ten dienste geweest tijdens jullie stage periode. Leo heeft er hard aan getrokken om de 'software' voor de data verwerking op tijd af te hebben. Bert heeft veel werk verricht aan de synthese en de karakterisering van de latices. Jacco, Geert en Erik hebben elk hun eigen unieke bijdrage geleverd aan de belangrijke polymeer-experimenten. Erik, in de lange periode dat wij hebben samengewerkt, heb je getuigt van grote inzet en goed inzicht.

Beste Jan Scheutjens, in mijn volgende leven kom ik bij jou een vak doen om van jouw kienheid en kennis nog meer te leren. Beste Hennie van Beek, jij kan als geen ander de draaibank laten draaien, ik ben jou veel dank verschuldigd voor al die mooie onderdelen van 'mijn' SPOS. Maar ook jij Louis Verhagen wil ik bedanken voor het nauwgezette werk wat je voor mij gedaan hebt. En Gerrit Buurman, een beste jongen, de plaatjes zijn met een woord professioneel! Ronald Wegh en Rob Vullings, jullie electronica is vakmanschap. Het ziet er zo vreselijk eenvoudig uit als Ronald de meest ingewikkelde schakelingen ontwerpt.

Maar ook de welwillendheid van Ab van der Linden om mij in de geheimen van de latex synthese in te wijden en de laatste loodjes die Anton Korteweg nauwgezet voor mij heeft uitgevoerd, zijn voor mij van grote waarde geweest. En dan is er Bert Bouman, die werkelijk altijd goedgeluimd, voor iedereen alles regelt van dropjes tot tekstverwerking, dank je wel. José Zeevat, Willy Kleijne en Yvonne Toussaint, bedankt voor juist die vanzelfsprekendheid waarmee jullie mij geholpen hebben. Beste Willem van Maanen en Ben Spee, glaswerk en chemicaliën waren nooit een probleem. Beste Maarten Bakkenes (wat een panoramisch uitzicht), Mara Vink, Frans Geurts en Henk van der Deen, daar in het transitorium wordt heel wat overgedragen, bedankt.

Beste Arie van Hoek (Moleculaire Fysica), je bent een laser-specialist bij uitstek. Jouw interesse en degelijke adviezen waren van grote waarde. Elke keer weer sta ik vol bewondering naar jouw laser-opstelling te kijken. Maarten de Gee (Wiskunde), jouw snelle aktie wat betreft de dataverwerking stel ik zeer op prijs. Ook John de Swart (ITAL) wil ik bedanken voor het lenen van apparatuur en voor de inleiding betreffende de "multichannel analyzer". Rob Szom (AKZO) wil ik bedanken voor de adviezen wat betreft de latex synthese.

I want to express my sincere thanks to Hans Sonntag and Heinz Lichtenfeld (Academie der Wissenschaften, Berlin) and to Lauri Thompson and John Cahill (Unilever, Port Sunlight) for their kind help and useful advise about the development of the SPOS.

En nu denk ik aan dat stelletje (ex)promovendi, die bepaald niet stil zitten, ik wens jullie allen veel succes. Hans Fraaye, ik heb veel plezier met je beleefd, jij gigantische smeltkroes van ideeën, emoties en verstand. Beste Albert Philipse (ECN), bedankt voor het uitvoeren van de dynamische lichtverstrooiings experimenten maar vooral ook voor jouw relativerend vermogen.

Tenslotte denk ik aan André Evertse, Erwin de Hamer en Caroline Meidam (zij noemt mij Wardtje). Als ik moe was van al die golven over mij heen, dan kon ik altijd terecht voor een gesprek over de middeleeuwen waarin vaak Trappisten voorkwamen of voor een aktie van spierpijn tot set 'm up.

Nu mijn koffertje gepakt staat naast dat van mijn eerbiedwaardige collega Frans Leermakers, kruip ik voor de laatste maal in het kraaiennest. Ik heb wel wat geleerd en ik wens jullie allen een behouden vaart.